Effect of Purge Gas Flow Rate and Oxygen Impurity on Heel build-up and Prediction of Heel build-up Using Machine Learning

by

Keivan Rahmani

A thesis submitted in partial fulfillment of the requirements for the degree of

Master of Science

in

Environmental Engineering

Department of Civil and Environmental Engineering

University of Alberta

Abstract

Heel buildup, i.e., the accumulation of non-desorbed/non-desorbable adsorbates and their by-products on an adsorbent, during cyclic adsorption/regeneration of volatile organic compounds (VOCs) onto activated carbon decreases its adsorption capacity and lifetime. In this this study, the effect of purge gas glow rate and oxygen impurity on heel build-up were investigated and machine learning was used to predict heel build-up.

In the first part, the simultaneous effect of purge gas flow rate and oxygen impurity during successive adsorption/regeneration cycles on adsorption capacity of and heel buildup on activated carbon during cyclic adsorption-desorption of TMB was investigated. Nine thermal desorption scenarios were investigated by varying nitrogen purge gas oxygen impurity level (< 5 ppmv, 10,000 ppmv, and 21%) and flow rate (0.1, 1 and 10 L/min or 1, 10 and 100% of adsorption flowrate) during thermal regeneration. The results show that increasing purge gas flow rate during thermal desorption improves adsorption capacity recovery and mitigates adverse effects of purge gas oxygen impurity. By increasing the purge gas flow rate from 0.1 to 10 SLPM, fifth cycle adsorption capacity increased from 30 to 40 wt% when 10,000 ppmv O_2 was used as purge gas and from 10 to 37 wt% when dry air (21% O_2) was used. Cumulative heel increased with increasing the purge gas oxygen impurity and decreasing its flow rate. In the least effective regeneration scenario (0.1 L/min N_2 with 21% O_2), 32.8 wt% cumulative heel was formed on BAC after 5 adsorption-desorption cycles whereas that of the best-case scenario (10 L/min N_2 with <5 ppmv O_2) was 0.3 wt%. Comparing the pore size distributions of virgin and used BAC indicated that heel is firstly built in narrow micropores (<8.5Å) and then starts to engage mesopores. Thermogravimetric analysis (TGA) of regenerated samples revealed that oxygen impurity leads to

formation of high boiling point and/or strongly bound heel species. TGA confirmed that in presence of oxygen, higher purge gas flow rates could reduce the amount of heel but promote chemisorbed heel formation. These results can be used for optimizing the regeneration conditions to boost activated carbon's long-term performance in cyclic adsorption.

In the second part, two machine learning (ML) algorithms (XGBoost and deep neural network (DNN)) were applied to predict volatile organic compounds (VOCs) cyclic heel buildup on activated carbons (ACs). A dataset consisting of 411 experimental tests of cyclic adsorption/desorption of different VOCs on ACs with distinct properties was used. Our study revealed that cyclic heel buildup can be predicted with acceptable accuracy using both ML algorithms by considering the adsorbent characteristics, adsorbate properties and regeneration conditions. The DNN algorithm showed better performance in prediction of cyclic heel buildup ($R^2 = 0.94$) than XGBoost ($R^2 = 0.81$). To verify the ML algorithms results and gain some insight into heel buildup relation to adsorbent's nature characteristics, partial dependency plots were generated using adsorbate properties and regeneration conditions, partial dependency plots were generated. The proposed ML-based heel prediction methods can be used to: (i) optimize adsorption/desorption operating conditions to minimize heel buildup on activated carbon in cyclic adsorption processes and (ii) quickly screen various adsorbents for efficient adsorption of a particular family of VOCs.

Preface

This MSc dissertation contains the result of a research conducted by me, Keivan Rahmani, in the Department of Civil and Environmental Engineering at the University of Alberta. Chapters 3 and 4 have been submitted or ready for the submission to peer-reviewed journals. My co-authors from the Air Quality Characterization Laboratory in the Department of Civil & Environmental Engineering at the University of Alberta and collaborators from our industrial sponsor, Ford Motor Company, were responsible for conducting part of laboratory tests and/or reviewing the manuscript drafts.

Chapter 3 is ready for the submission to a peer-reviewed journal.

Chapter 4 has been submitted (under review) as K. Rahmani, A.H. Mamaghani, Z. Hashisho, D. Crompton, J. E. Anderson (2021). Prediction of Activated Carbon Performance Degradation Using Machine Learning Algorithms (XGBoost and Deep Neural Network). Chemical Engineering Journal.

Dedications

Dedicated to grandma in heaven.

Acknowledgements

I cannot give enough thanks to my amazing academic advisor, Professor Zaher Hashisho. His positive outlook and confidence in my research inspired me and gave me confidence. I will forever be grateful for the support and encouragement you gave me when I needed it.

I would like to thank Ford Motor Company, Natural Sciences and Engineering Research Council (NSERC) of Canada, Lehigh Hanson Materials, and the University of Alberta for funding throughout my MSc. Without their generous support of this research, it could not have occurred.

In addition, I would like to thank my lovely parents, Habib and Maryam, and sister, Kimia, for their wise counsel and sympathetic ear. You are always there for me. I would like to thank my girlfriend and best friend Marjan, thank you for all your love and support. Also, I would like to thank my second family, my friends, Vahab and Amin.

I appreciate my colleagues and friends in the Air Quality Characterization Lab for their valuable help, contributions, and, more importantly, their friendship: Alireza Haghighat, Arman Peyravi, Mohammad Feizbakshan, Yang Yu, Sina Esfandiarpour, and Morteza Davarpanah.

TABLE OF CONTENTS

LIST OF TABLES

LIST OF FIGURES

1 Background

According to US Environmental Protection Agency (EPA), Volatile organic compounds (VOCs) are any organic chemical except carbon monoxide and dioxide, carbonic acid, metallic carbides or carbonates, and ammonium carbonate which participate in photochemical reactions in the atmosphere (e.g., photochemical smog reaction)[1].

VOCs emission to the atmosphere originates from anthropogenic and biogenic sources (from soil and vegetation) as well as forest wildfire. In 2019, 1675 kilotons of VOCs were emitted in Canada, where the oil and gas sector, paint and solvent industry, and transportation accounted for ~ 39, 18, and 9% of VOC emissions, respectively [2]. One of the important sources contributing to VOCs emission is automotive paint booths that use solvent-based paints in their spray booth operations. The solvents used in solvent-based paints include esters, ketones, alcohols, glycolethers, aromatic and aliphatic hydrocarbons [3].

The emission of VOCs is of concern since prolonged exposure to some VOCs brings about eye, nose, and throat irritations, headache, dizziness, nausea, memory loss, and damages to the central nervous system, liver, and lungs [4]. Besides, VOCs facilitate the formation of photochemical smog, including tropospheric ozone, through photochemical reactions with NO_x in the atmosphere [5]. Therefore, considerable scientific and industrial attention has been directed towards the abatement of VOCs.

1.1 VOCs treatment techniques

Several methods, including physical, chemical, and biological treatments, can be applied for VOCs removal. However, removal techniques can generally be classified into two main categories, namely(i) recovery-based and (ii) destruction-based methods [6].

In destruction-based techniques, VOCs are converted mainly into carbon dioxide and water. The destruction process includes oxidation and biofiltration [7]. The oxidation process is applied where energy recovery rather than VOC recovery is the primary concern, and it can be subcategorized into thermal oxidation (also known as fume incinerators) and catalytic oxidation. While up to 85 and 70% energy recovery can be achieved through thermal and catalytic oxidation, respectively, the efficiency of both processes is highly dependent on operating conditions, and additional control equipment may be required downstream [6, 8]. On the other hand, bio-filtration, which is a cost-effective technique for VOC removal, is a slow process and produces biomass as the secondary pollutant [9].

Recovery methods are applied when retrieved VOCs can be re-used in the system and/or are economically valuable. Condensation [10], absorption [11] , adsorption [12], and membrane separation [13] are commonly applied methods for VOC recovery. However, there are certain limitations associated with some methods. For example, more than 85% removal efficiency is not feasible with condensation, while absorption requires rigorous maintenance and may require pre-treatment of VOC. Membrane separation is an expensive process [6].

Among recovery-based techniques, adsorption is commonly applied due to its high removal efficiency, low maintenance cost, and low required energy. Among different adsorbents, activated carbon (AC) is a widely used adsorbent to capture VOCs due to its low cost, high removal efficiency, and ability to be regenerated [14-16]. As a common practice in the industry, following the

adsorption process, the used adsorbent (i.e., loaded with VOCs) is regenerated to restore its adsorption capacity and recover the adsorbates.

The adsorption process can occur reversibly (i.e., physisorption), irreversibly (i.e., chemisorption or non-desorbed physisorption), or a combination of both [17]. Regarding VOCs removal with adsorption, an obstacle is heel buildup, i.e., the accumulation of non-desorbed/non-desorbable adsorbates and their by-products on the surface/pores of the adsorbent. Heel buildup decreases recovered VOC and reduces activated carbon's lifetime and adsorption capacity after each adsorption/regeneration cycle [18]. Accumulation of heel species and consequently loss of activated carbon micropores, in turn, increases the cost associated with the treatment process due to the necessity for more frequent replacement of adsorbent [19].

1.2 Research Objectives

This study has two main goals regarding heel buildup:

1. To investigate the simultaneous effect of purge gas oxygen impurity and flow rate on irreversible adsorption (heel buildup).
2. To predict heel buildup on activated carbon using machine learning (Deep learning and XGBoost).

In the first study, nine different regeneration scenarios, consisting of a combination of three different purge gas flow rates and three different purge gas oxygen impurities, were applied to regenerate VOC latent beaded activated carbon (BAC) to study the following objectives:

- to systematically identify the simultaneous effect of flow rate and oxygen impurity of the desorption purge gas on heel formation mechanism(s) and heel buildup
- to study whether using a higher purge gas flow rate can mitigate the presence of oxygen impurity in the desorption purge gas in terms of adsorption capacity recovery and heel buildup

In the second study, a data set including 411 experimental tests of cyclic adsorption/desorption of VOCs on activated carbon was collected from the literature, including the adsorption/desorption cycles generated in the first study. Two machine learning (ML) algorithms, namely, XGBoost and deep neural network (DNN), were applied to predict cyclic heel buildup given the adsorbent characteristics, adsorbate properties, and regeneration conditions.

1.3 Thesis outline

This thesis is divided into five chapters. Chapter 1 gives a general introduction of the topic and its objectives. Chapter 2 includes a general literature review about adsorption, regeneration, heel formation, machine learning, and its application in adsorption. Chapter 3 investigates the simultaneous effect of purge gas oxygen impurity and flow rate in regeneration on heel buildup. Chapter 4 provides two machine learning algorithms to predict cyclic heel buildup based on adsorbent characteristics, adsorbate properties, and regeneration parameters. Finally, in chapter 5 conclusion of the research as well as recommendation for future works are included.

1.4 References

1. USEPA. Technical Overview of Volatile Organic Compounds; https://www.epa.gov/indoor-air-quality-iaq/technical-overview-volatile-organic-compounds.

2. *Canada's Air Pollutant Emissions Inventory*; Open Data Canada; https://open.canada.ca/data/en/dataset/fa1c88a8-bf78-4fcb-9c1e-2a5534b92131.

3. Kim, B. VOC Emissions from Automotive Painting and Their Control: A Review. *Environmental Engineering Research* **2011,** *16* (1), 1-9; 10.4491/eer.2011.16.1.001.

4. Molhave, L. Volatile Organic Compounds, Indoor Air Quality and Health. *Indoor Air* **1991,** *1* (4), 357-376; 10.1111/j.1600-0668.1991.00001.x.

5. Aydin Berenjian; Natalie Chan; Hoda, J.M. Volatile Organic Compounds Removal Methods: A Review. *American Journal of Biochemistry and Biotechnology* **2012,** *8* (4); 10.3844/ajbbsp.2012.220.229.

6. Khan, F.I.; Kr. Ghoshal, A. Removal of Volatile Organic Compounds from Polluted Air. *Journal of Loss Prevention in the Process Industries* **2000,** *13* (6), 527-545; https://doi.org/10.1016/S0950-4230(00)00007-3.

7. Parmar, G.R.; Rao, N.N. Emerging Control Technologies for Volatile Organic Compounds. *null* **2008,** *39* (1), 41-78; 10.1080/10643380701413658.

8. J.C William and P.E Lead VOC Control Strategies in Plant Design. *Chemical Processing: Project Engineering Annual* **1997**.

9. Ottengraf, S.P.; Van Den Oever, A. H. Kinetics of Organic Compound Removal from Waste Gases with a Biological Filter. *Biotechnology and Bioengineering* **1983,** *25* (12), 3089-3102; 10.1002/bit.260251222.

10. Gupta, V.K.; Verma, N. Removal of Volatile Organic Compounds by Cryogenic Condensation Followed by Adsorption. *Chemical Engineering Science* **2002,** *57* (14), 2679-2696; https://doi.org/10.1016/S0009-2509(02)00158-6.

11. Li, Y.; Chang, H.; Yan, H.; Tian, S.; Jessop, P.G. Reversible Absorption of Volatile Organic Compounds by Switchable-Hydrophilicity Solvents: A Case Study of Toluene with N,N-Dimethylcyclohexylamine. *ACS Omega* **2021,** *6* (1), 253-264; 10.1021/acsomega.0c04443.

12. Zhu, L.; Shen, D.; Luo, K.H. A Critical Review on VOCs Adsorption by Different Porous Materials: Species, Mechanisms and Modification Methods. *Journal of Hazardous Materials* **2020,** *389*, 122102; https://doi.org/10.1016/j.jhazmat.2020.122102.

13. Verstraete, S.; Hermia, J.; Vigneron, S. VOC Separation on Membranes: A Review. *Studies in Environmental Science* **1994,** *61*, 359-373; https://doi.org/10.1016/S0166-1116(08)72068-5.

14. Tefera, D.T.; Hashisho, Z.; Philips, J.H.; Anderson, J.E.; Nichols, M. Modeling Competitive Adsorption of Mixtures of Volatile Organic Compounds in a Fixed-Bed of Beaded Activated Carbon. *Environmental Science & Technology* **2014,** *48* (9), 5108-5117; 10.1021/es404667f.

15. Jahandar Lashaki, M.; Atkinson, J.D.; Hashisho, Z.; Phillips, J.H.; Anderson, J.E.; Nichols, M. The Role of Beaded Activated Carbon's Surface Oxygen Groups on Irreversible Adsorption of Organic Vapors. *Journal of Hazardous Materials* **2016,** *317*, 284-294; 10.1016/j.jhazmat.2016.05.087.

16. Tefera, D.T.; Jahandar Lashaki, M.; Fayaz, M.; Hashisho, Z.; Philips, J.H.; Anderson, J.E.; Nichols, M. Two-Dimensional Modeling of Volatile Organic Compounds Adsorption onto Beaded Activated Carbon. *Environmental Science & Technology* **2013,** *47* (20), 11700-11710; 10.1021/es402369u.

17. Jahandar Lashaki, M.; Hashisho, Z.; Phillips, J.H.; Crompton, D.; Anderson, J.E.; Nichols, M. Mechanisms of Heel Buildup During Cyclic Adsorption-Desorption of Volatile Organic

Compounds in a Full-Scale Adsorber-Desorber. *Chemical Engineering Journal* **2020,** *400*, 124937; https://doi.org/10.1016/j.cej.2020.124937.

18. Magne, P.; Walker, P.L. Phenol Adsorption on Activated Carbons: Application to the Regeneration of Activated Carbons Polluted with Phenol. *Carbon* **1986,** *24* (2), 101-107; 10.1016/0008-6223(86)90102-8.

19. Tanthapanichakoon, W.; Ariyadejwanich, P.; Japthong, P.; Nakagawa, K.; Mukai, S.R.; Tamon, H. Adsorption–Desorption Characteristics of Phenol and Reactive Dyes from Aqueous Solution on Mesoporous Activated Carbon Prepared from Waste Tires. *Water Research* **2005,** *39* (7), 1347-1353; 10.1016/j.watres.2004.12.044.

2 Literature review

2.1 Adsorption

Adsorption is a process whereby gas or liquid molecules are collected on the internal surface of a solid. Adsorption on solids is attributed to unbalanced forces which attract adsorbate molecules on the solid surface. Adsorption can be divided into two categories: physical adsorption and chemical adsorption [1, 2].

Physical adsorption is reversible and occurs where intermolecular forces (i.e., van der Waals forces) are the primary attractive forces between adsorbate species and the adsorbent surface. In addition, a fast adsorption rate and low heat of adsorption (< 2- or 3-times latent heat of evaporation) are the other properties of physical adsorption. Since intermolecular forces are weak, the adsorbate molecules' structure will remain unchanged after physical adsorption, and by applying proper regeneration conditions, they can be recovered again[3, 4].

On the other hand, chemical adsorption or chemisorption is based on the forming chemical bonds and changes in adsorbate molecules' structure, making it irreversible. Chemical bonds are highly specific and release a relatively high heat of adsorption (> 2- or 3-times latent heat of evaporation) [2, 4].

2.2 Regeneration

During adsorption, the adsorbate species are increasingly accumulated on the adsorbent; hence, the adsorption capacity of the adsorbent is continuously decreased until the adsorbent reaches the saturation point. Regeneration of the adsorbent, rather than disposal, can be conducted to recover adsorption capacity, reuse adsorbent, and recover adsorbates. Different regeneration methods such

as thermal [5], chemical [6], vacuum [7], and bio-regeneration [8] can be applied to regenerate exhausted adsorbents.

2.2.1 Thermal regeneration

Thermal regeneration includes increasing the adsorbent's bed temperature while a purge gas or steam passes through the adsorbent bed [9]. The regeneration heat can be provided to the adsorbent bed with a hot purge gas or steam [9], conductive heating [10, 11], microwave [10, 11], ultrasound [12], or resistive heating [13]. In conductive heating regeneration, the activated carbon bed is heated up using conductive heating while a purge gas is introduced to the adsorbent bed to carry desorbed species away. An inert gas (mainly nitrogen) is used in conductive heating regeneration to prevent any potential reaction between purge gas and desorbed species [9].

2.2.2 Chemical regeneration

Chemical regeneration includes three main mechanisms: extraction, reaction, and pH changes. Depending on the adsorbate properties, more than one mechanism might be involved in a chemical regeneration method [14]. According to the mechanisms mentioned above, the most common chemical regeneration methods are solvent, NaOH, supercritical and oxidative regeneration. Solutions of NaCl or NaNO in pure water [15] and boiling [16] or pressurized [17-19] liquid water can also be applied for the chemical regeneration of carbonous adsorbents.

NaOH can be used to recover specific adsorbates from activated carbons, and depending on adsorbate type, chemical reaction or pH change might account for the regeneration mechanism. [17, 21]

Solvent regeneration can be applied to remove adsorbate species that are difficult to desorb. In addition, solvent regeneration outperforms thermal regeneration in terms of ease of adsorbates recovery, mass loss, and potential damage to adsorbents pores [20-24]. However, some important

drawbacks such as a drastic increase in regeneration cost due to employment of organic solvents and high toxicity of solutions produced in the regeneration step limit their application to only specific cases [25].

In supercritical regeneration, the extraction mechanism occurs by introducing a supercritical fluid to the adsorbent bed. The high diffusivity of supercritical fluids alongside their low viscosity and low dielectric constant makes them a promising solvent for organic adsorbates [26]. Water [27] and CO_2 [28] are the agents usually applied in supercritical regeneration. Depending on the adsorbate type, supercritical regeneration can result in high adsorbate removal efficiency (RE = ~100%) and increases in adsorbent pores and surface area after regeneration, especially when supercritical water is applied as the regeneration agent. However, different adsorbates have shown different solubility in critical agents and consequently different removal efficiency. For example, in regeneration with supercritical CO_2, some organic compounds such as phenol (RE = ~36%) [29] and naphthalene (RE = ~75%) [30] have shown less solubility compared to others such as benzene (RE = ~100%) or toluene (RE = ~100%) [31]. In addition, it should be noted that the severe condition required for supercritical agents, which is at least and Pc = 74 bar, Tc = 31°C for CO_2 and P_c =221 bar and T_c = 374°C for water, is not feasible in many cases especially when supercritical water is desired. Furthermore, supercritical CO_2 has shown poor performance in removing strongly adsorbed adsorbates and adsorbates with heavy molecular weights such as pesticides [30], herbicides [32], or insecticides [33].

In oxidative regeneration, adsorption capacity is recovered through the reaction between oxidative agent and adsorbate species and degradation of the adsorbate. The extraction mechanism is also involved in the oxidative regeneration process. The oxidative regeneration process can be categorized into oxidative regeneration with O_2 as the oxidative agent and with other oxidants such

as $S_2O_8^{2-}$ and H_2O_2 as the oxidative agent [14]. It should be noted that the high reactivity of O_2 can damage adsorbents' pore structure [34] and produce non-desorbable by-product species through thermal oxidative reactions with adsorbate species [35].

2.3 Heel buildup

A challenge associated with the adsorption of VOCs on activated carbon is the accumulation of adsorbate species that remain non-desorbed or transform into non-desorbable species during regeneration [36]. Successive heel buildup decreases adsorption capacity and shortens adsorbent lifetime. Therefore, it increases the cost associated with the treatment process due to the necessity for a more frequent replacement of adsorbent to meet the required removal efficiency or the minimum adsorption capacity to recover concentrated VOCs during regeneration.

The following mechanisms are reported to contribute to heel buildup so far [36]:

- non-desorbed physisorption,
- chemisorption of adsorbates,
- adsorbates' reaction by-products,
- adsorbate decomposition (i.e., char formation)

Many studies have been conducted to identify the parameters affecting heel buildup quantitively and qualitatively. The effective parameters can be categorized into three different classes:

Adsorbent properties (e.g., BET surface, micropore volume)

Adsorbate properties (e.g., molecular weight, boiling point)

Adsorption/desorption conditions (e.g., adsorption and regeneration temperate, purge gas oxygen impurity)

Regarding adsorbent properties, different studies have been conducted, as summarized here. Jahandar Lashaki et al. [37] studied the role of beaded activated carbon's pore size distribution on heel buildup. Their experimental data indicate that heel is mainly formed in beaded activated

carbon (BAC) micropores, while BAC mesopores contribute to organic vapor adsorption but not heel formation. They also reported a linear correlation (R^2= 0.91) between heel buildup and BAC micropore volume among their study samples. Following Jahandar Lashaki's findings, Fezibakhshan et al. [38] also observed high heel buildup in samples with high microporosity and inadequate meso/macropores and concluded that hierarchical pore structure mitigates heel buildup by facilitating desorbed species diffusion to the fluid phase. In another study on the role of beaded activated carbon's surface oxygen groups on heel buildup, Jahandar Lashaki et al. [39] reported higher heel buildup for BACs with higher surface oxygen groups.

From the perspective of adsorbate's properties, molecular weight and boiling points are known to directly affect heel buildup. Specifically, higher heel buildup is observed for heavier VOCs (high boiling point and/or molecular weight) [40].

The extent of regeneration parameters' impact on heel buildup depends on the regeneration method. For an adsorption system with conductive heating as the regeneration method, logically, the applied temperature must be greater than the adsorbate's boiling point to achieve complete desorption at atmospheric pressure [41]. Purge gas oxygen impurity can increase the heel buildup on BAC by reacting with adsorbate species or adsorbent surface [41-43].

Jahandar Lashaki et al. [44], in a study on the effect of adsorption and regeneration temperature on heel buildup on activated carbon, reported a 30% increase in heel buildup by changing the adsorption temperature from 25°C to 45°C. In addition, they observed that a higher regeneration temperature accelerates the regeneration process and decreases heel buildup as it could facilitate mass transfer and diffusion in micropores, specifically for adsorbates with high affinity when high temperature is applied. However, it should be noted that the study was conducted in the absence of oxygen. In contrast, increasing regeneration temperature in the presence of oxygen facilitates

reactions between purge gas oxygen and the adsorbate; hence, increases heel buildup. In a study on the simultaneous effect of regeneration temperature and oxygen impurity on heel buildup, Fezibakhshan et al. [41] showed the adverse effect of increasing regeneration temperature on heel buildup in the presence of oxygen for the first time.

Purge gas flow rate and heating rate are other regeneration parameters playing a role in heel buildup. It has been demonstrated in a study conducted by Niknaddaf et al.[45] that decreasing heating rate and/or increasing purge gas flow rate decreases heel buildup. They supported their results by arguing that increasing purge gas flow rate and decreasing heating rate shortens desorbed species residence time in adsorbents micropores and the duration for which the adsorbate species are exposed to high temperature. However, in that study, carbon fibers were regenerated with resistive heating and in absence of oxygen. No study has been conducted so far to study the effect of purge gas flow rate on heel buildup in an adsorption system with conductive heating regeneration method.

Selecting the optimal adsorption/regeneration condition requires a cost/performance trade-off since regeneration parameters change the operational cost drastically. For example, introducing pure nitrogen reduces heel formation due to oxygen impurity; however, the nitrogen purification process is relatively energy-consuming and costly; consequently, it increases the process's operational cost. In addition, the required energy to purify nitrogen exponentially increases with the purity level. For example, in a typical pressure swing adsorption process, power consumption increases 2.5-fold in order to improve the N_2 purity from 95 to 99.99%[46].

2.4 Machine learning and adsorption

Machine learning (ML) is one of the most powerful tools to learn, elaborate, and predict non-linear and complex models. Many well-developed ML algorithms such as artificial neural network

(ANN), extreme gradient boosting (XGBoost), gaussian process regression, decision tree, random forest (RF), gradient boosting trees, and support vector machines (SVM) are applied to chemical and environmental engineering problems such as adsorption. The mathematical details of applied ML methods are provided in the Methods section in chapter 4.

The ML studies conducted in adsorption have mainly focused on the optimization of adsorption condition [47], performance prediction or construction of adsorption models [48, 49], and inverse design of adsorbent materials [50]. Nagesh Pai et al. [51] applied different ML algorithms to predict and optimize the separation of CO_2 from N_2 with zeolite 13X in the vacuum swing adsorption (VSA) process. They were able to provide a fast and accurate predictive model (Gaussian process regression based with $R^2 = 0.98$) based on the data collected from an experimentally verified computational model. Furthermore, they performed process optimization by (i) prediction of process performance using the trained ML algorithm in different practical conditions and (ii) using the predicted optimized condition by ML algorithm as the initial input for the detailed computational model to shorten the converging time, which resulted in 23- and 6-times decrease in computer load respectively.

ANN algorithm has been used to learn and optimize a hydrogen purification pressure swing adsorption (PSA) process in another study [52]. For the first step, ANN was applied to the data set generated by an experimentally verified ASPEN model (average $R^2 = 0.88$). Then by combining the validated ML algorithm with the sequence quadratic program (SQP) algorithm, multi-objective optimization of the weighted linear combination of hydrogen productivity, recovery, and purity was achieved.

In a study conducted by Burns et al. [53], RF has been applied to classify Metal−organic frameworks (MOFs) based on whether they meet the US Department of Energy requirements of 95% CO_2

purity and 90% CO_2 recovery target (95/90-PRTs) in an optimized four-step VSA system. This study used an experimentally validated process simulator to generate more than 5 million data points by varying operating conditions and MOFs. The trained RF method was able to predict MOFs capability to meet the 95/90-PRTs with an accuracy of 91% based on adsorption metrics (e.g., CO_2 working capacity), composite metrics (e.g., adsorption performance score [54], i.e., the product of CO_2 working capacity and the CO_2/N_2 selectivity), and MOF's geometric features (e.g., maximum pore diameter).

Finally, regarding the application of machine learning in the inverse design of adsorbent materials, generative machine learning methods found their way in adsorption studies, such as the study conducted by Kim et al. [50] on the inverse design of pure silica zeolites for methane adsorption using generative adversarial network (GAN). GAN consists of a generator and a discriminator. The former is assigned to generate realistic fake data points to deceive the latter, which is responsible for distinguishing between real and generated data. This study used 31,713 known zeolites and their attributed properties, including energy (or methane potential) grid and oxygen and silicon positions grid, to train the GAN. It should be mentioned that Gaussian functions (μ = 1, σ = 0.5) were used to represent silicon on oxygen atom positions in the material grid. Furthermore, the Lennard-Jones (LJ) 12-6 potential model was applied to compute the interaction energy level in each grid node. After applying the post-clean-up procedure, they were able to generate eight zeolite structures, one of which had not been reported in any literature before. In addition, they targeted zeolites with the heat of adsorption value between 18 and 22 kJ/mol for methane and were able to generate six new zeolites, two of which were not included in the dataset.

Although an increasing number of studies have been conducted about different applications of machine learning algorithms in adsorption, no single study has been carried to investigate and predict heel buildup. As mentioned earlier, heel buildup substantially deteriorates adsorbents long-term performance in the cyclic adsorption/desorption process and causes unsustainable adsorption process requiring frequent replacement of/discarding exhausted adsorbent. Hence developing a machine learning algorithm that predicts heel buildup has important practical implications.

2.5 Reference

1. Hu, H.; Xu, K. Chapter 8 - Physicochemical Technologies for HRPs and Risk Control, In *High-Risk Pollutants in Wastewater,* Ren, H.; Zhang, X., Eds.; Elsevier: 2020; pp. 169-207.

2. Wilcox, J. Adsorption, In *Carbon Capture,* Wilcox, J., Ed.; Springer: 2012; pp. 115-175.

3. Schirmer, W. *Physical Adsorption: Forces and Phenomena.* De Gruyter Oldenbourg: 1999.

4. Ruthven, D. *Principles of Adsorption and Adsorption Processes.* John Wiley & Sons: 1984.

5. Hemphill, L.; Okla,Robert S.Kerr Environmental Research Laboratory, Ada, *Thermal Regeneration of Activated Carbon.* National Technical Information Service: 1978.

6. Rydberg, J. *Principles and Practices of Solvent Extraction.* Dekker: 1992.

7. Ruthven, D.M.; Farooq, S.; Knaebel, K.S. *Pressure Swing Adsorption.* VCH: 1994.

8. Cecen, F.; Aktas, Ö Activated carbon for Water and Wastewater Treatment; Integration of Adsorption and Biological treatment. *Reference & Research Book News* **2011**.

9. Friday, D.K.; LeVan, M.D. Hot purge gas Regeneration of Adsorption Beds with Solute Condensation: Experimental studies. *AIChE Journal* **1985,** *31* (8), 1322-1328; https://doi.org/10.1002/aic.690310811.

10. Ania, C.O.; Parra, J.B.; Menéndez, J.A.; Pis, J.J. Microwave-Assisted Regeneration of Activated Carbons Loaded with Pharmaceuticals. *Water Research* **2007,** *41* (15), 3299-3306; https://doi.org/10.1016/j.watres.2007.05.006.

11. Fayaz, M.; Shariaty, P.; Atkinson, J.D.; Hashisho, Z.; Phillips, J.H.; Anderson, J.E.; Nichols, M. Using Microwave Heating to Improve the Desorption Efficiency of High Molecular Weight

VOC from Beaded Activated Carbon. *Environmental Science & Technology* **2015,** *49* (7), 4536-4542; 10.1021/es505953c.

12. Lim, J.; Okada, M. Regeneration of Granular Activated Carbon Using Ultrasound. *Ultrasonics Sonochemistry* **2005,** *12* (4), 277-282; https://doi.org/10.1016/j.ultsonch.2004.02.003.

13. Niknaddaf, S.; Atkinson, J.D.; Shariaty, P.; Jahandar Lashaki, M.; Hashisho, Z.; Phillips, J.H.; Anderson, J.E.; Nichols, M. Heel Formation During Volatile Organic Compound Desorption from Activated Carbon Fiber cloth. *Carbon* **2016,** *96*, 131-138; https://doi.org/10.1016/j.carbon.2015.09.049.

14. Salvador, F.; Martin-Sanchez, N.; Sanchez-Hernandez, R.; Sanchez-Montero, M.J.; Izquierdo, C. Regeneration of Carbonaceous Adsorbents. Part II: Chemical, Microbiological and Vacuum Regeneration. *Microporous and Mesoporous Materials* **2015,** *202*, 277-296; https://doi.org/10.1016/j.micromeso.2014.08.019.

15. Di Natale, F.; Erto, A.; Lancia, A. Desorption of Arsenic from Exhaust Activated Carbons Used for Water Purification. *Journal of Hazardous Materials* **2013,** *260*, 451-458; https://doi.org/10.1016/j.jhazmat.2013.05.055.

16. Martin, R.J.; Ng, W.J. Chemical Regeneration of Exhausted Activated Carbon—II. *Water Research* **1985,** *19* (12), 1527-1535; https://doi.org/10.1016/0043-1354(85)90398-7.

17. Salvador, F.; Merchan, M.D. A Simple Apparatus for Studies of Thermoprogrammed Desorption in Solution. *Langmuir* **1992,** *8* (4), 1226-1229; 10.1021/la00040a034.

18. Merchán, M.D.; Salvador, F. Characterization of Solids by Thermal Desorption in Solution. *Studies in Surface Science and Catalysis* **1994,** *87*, 391-400; https://doi.org/10.1016/S0167-2991(08)63100-6.

19. Salvador, F.; Merchán, M.D. Study of the Desorption of Phenol and Phenolic Compounds from Activated Carbon by Liquid-Phase Temperature-Programmed Desorption. *Carbon* **1996,** *34* (12), 1543-1551; https://doi.org/10.1016/S0008-6223(96)00105-4.

20. Tamon, H.; Saito, T.; Kishimura, M.; Okazaki, M.; Toei, R. Solvent Regeneration of Spent Activated Carbon in Wastewater Treatment. *Journal of Chemical Engineering of Japan* **1990,** *23* (4), 426-432; 10.1252/jcej.23.426.

21. Sutikno, T.; Himmelstein, K.J. Desorption of Phenol from Activated Carbon by Solvent Regeneration. *Industrial & Engineering Chemistry Fundamentals* **1983,** *22* (4), 420-425; 10.1021/i100012a011.

22. Cooney, D.O.; Nagerl, A.; Hines, A.L. Solvent Regeneration of Activated Carbon. *Water Research* **1983,** *17* (4), 403-410; 10.1016/0043-1354(83)90136-7.

23. McLaughlin, H.S. Regenerate Activated Carbon Using Organic Solvents. *Chemical Engineering Progress* **1995,** *91* (7).

24. Guo, D.; Shi, Q.; He, B.; Yuan, X. Different Solvents for the Regeneration of the Exhausted Activated Carbon Used in the Treatment of Coking Wastewater. *Journal of Hazardous Materials* **2011,** *186* (2), 1788-1793; https://doi.org/10.1016/j.jhazmat.2010.12.068.

25. Martin, R.J.; Ng, W.J. The Repeated Exhaustion and Chemical Regeneration of Activated Carbon. *Water Research* **1987,** *21* (8), 961-965; 10.1016/S0043-1354(87)80014-3.

26. Salvador, F.; Sánchez-Montero, M.J.; Salvador, A.; Martín, M.J. Study of the Energetic Heterogeneity of the Adsorption of Phenol onto Activated Carbons by TPD Under Supercritical Conditions. *Applied Surface Science* **2005,** *252* (3), 641-646; 10.1016/j.apsusc.2005.02.090.

27. Salvador, F.; Martin-Sanchez, N.; Sanchez-Montero, M.J.; Montero, J.; Izquierdo, C. Regeneration of Activated Carbons Contaminated by Phenol Using Supercritical Water. *The Journal of Supercritical Fluids* **2013,** *74*, 1-7; 10.1016/j.supflu.2012.11.025.

28. Chihara, K.; Oomori, K.; Oono, T.; Mochizuki, Y. Supercritical CO2 Regeneration of Activated Carbon Loaded with Organic Adsorbates. *Water Science and Technology* **1997,** *35* (7), 261-268; https://doi.org/10.1016/S0273-1223(97)00139-X.

29. Humayun, R.; Karakas, G.; Dahlstrom, P.R.; Ozkan, U.S.; Tomasko, D.L. Supercritical Fluid Extraction and Temperature-Programmed Desorption of Phenol and Its Oxidative Coupling Products from Activated Carbon. *Industrial & Engineering Chemistry Research* **1998,** *37* (8), 3089-3097; 10.1021/ie970936p.

30. Madras, G.; Erkey, C.; Akgerman, A. Supercritical Fluid Regeneration of Activated Carbon Loaded with Heavy Molecular Weight Organics. *Industrial & Engineering Chemistry Research* **1993,** *32* (6), 1163-1168; 10.1021/ie00018a022.

31. Tan, C.S.; Liou, D.C. Supercritical Regeneration of Activated Carbon Loaded with Benzene and Toluene. *Industrial & Engineering Chemistry Research* **1989,** *28* (8), 1222-1226; 10.1021/ie00092a015.

32. Taylor, P.N.; Lester, J.N. Rapid Extraction of Isoproturon and Diuron from Granular Activated Carbon. *Chemosphere* **1996,** *33* (7), 1227-1240; 10.1016/0045-6535(96)00261-5.

33. Macnaughton, S.J.; Foster, N.R. Supercritical Adsorption and Desorption Behavior of DDT on Activated Carbon Using Carbon Dioxide. *Industrial & Engineering Chemistry Research* **1995,** *34* (1), 275-282; 10.1021/ie00040a029.

34. Sabio, E.; González, E.; González, J.F.; González-García, C.M.; Ramiro, A.; Gañan, J. Thermal Regeneration of Activated Carbon Saturated with P-Nitrophenol. *Carbon* **2004,** *42* (11), 2285-2293; 10.1016/j.carbon.2004.05.007.

35. Hashemi, S.M.; Jahandar Lashaki, M.; Hashisho, Z.; Phillips, J.H.; Anderson, J.E.; Nichols, M. Oxygen impurity in nitrogen desorption purge gas can increase heel buildup on activated carbon. *Separation and Purification Technology* **2019,** *210*, 497-503.

36. Jahandar Lashaki, M.; Hashisho, Z.; Phillips, J.H.; Crompton, D.; Anderson, J.E.; Nichols, M. Mechanisms of Heel Buildup During Cyclic Adsorption-Desorption of Volatile Organic Compounds in a Full-Scale Adsorber-Desorber. *Chemical Engineering Journal* **2020,** *400*, 124937; https://doi.org/10.1016/j.cej.2020.124937.

37. Jahandar Lashaki, M.; Atkinson, J.D.; Hashisho, Z.; Phillips, J.H.; Anderson, J.E.; Nichols, M. The Role of Beaded Activated Carbon's Pore Size Distribution on Heel Formation During Cyclic Adsorption/Desorption of Organic Vapors. *Journal of Hazardous Materials* **2016,** *315*, 42-51; 10.1016/j.jhazmat.2016.04.071.

38. Feizbakhshan, M. Heel Build-up During Thermal Desorption of VOCs in Presence of Oxygen. University of Alberta, 2020.

39. Jahandar Lashaki, M.; Atkinson, J.D.; Hashisho, Z.; Phillips, J.H.; Anderson, J.E.; Nichols, M. The Role of Beaded Activated Carbon's Surface Oxygen Groups on Irreversible Adsorption of Organic Vapors. *Journal of Hazardous Materials* **2016,** *317*, 284-294; 10.1016/j.jhazmat.2016.05.087.

40. Fayaz, M. Adsorption and Microwave Regeneration for Controlling Volatile Organic Compounds Emissions from Automotive Paint Booths. University of Alberta, 2016.

41. Feizbakhshan, M.; Amdebrhan, B.; Hashisho, Z.; Phillips, J.H.; Crompton, D.; Anderson, J.E.; Nichols, M. Effects of Oxygen Impurity and Desorption Temperature on Heel Build-up in Activated Carbon. *Chemical Engineering Journal* **2021,** *409*, 128232; 10.1016/j.cej.2020.128232.

42. Mojtaba Hashemi, S.; Jahandar Lashaki, M.; Hashisho, Z.; Phillips, J.H.; Anderson, J.E.; Nichols, M. Oxygen Impurity in Nitrogen Desorption Purge Gas Can Increase Heel Buildup on Activated Carbon. *Separation and Purification Technology* **2019,** *210*, 497-503; 10.1016/j.seppur.2018.08.035.

43. Jahandar Lashaki, M.; Atkinson, J.D.; Hashisho, Z.; Phillips, J.H.; Anderson, J.E.; Nichols, M.; Misovski, T. Effect of Desorption Purge Gas Oxygen Impurity on Irreversible Adsorption of Organic Vapors. *Carbon* **2016,** *99*, 310-317; 10.1016/j.carbon.2015.12.037.

44. Jahandar Lashaki, M.; Fayaz, M.; Wang, H.; Hashisho, Z.; Philips, J.H.; Anderson, J.E.; Nichols, M. Effect of Adsorption and Regeneration Temperature on Irreversible Adsorption of Organic Vapors on Beaded Activated Carbon. *Environmental Science & Technology* **2012,** *46* (7), 4083-4090; 10.1021/es3000195.

45. Niknaddaf, S.; Atkinson, J.D.; Gholidoust, A.; Fayaz, M.; Awad, R.; Hashisho, Z.; Phillips, J.H.; Anderson, J.E.; Nichols, M. Influence of Purge Gas Flow and Heating Rates on Volatile Organic Compound Decomposition during Regeneration of an Activated Carbon Fiber Cloth.

Industrial & Engineering Chemistry Research **2020,** *59* (8), 3521-3530; 10.1021/acs.iecr.9b06070.

46. Compressed Air Best Practices, The Energy Costs Associated with Nitrogen Specifications.; http://www.airbestpractices.com/system-assessments/air-treatment/n2/energy-costs-associated-nitrogen-specifications.

47. Foroughi, M.; Ahmadi Azqhandi, M.H.; Kakhki, S. Bio-inspired, High, and Fast Adsorption of Tetracycline from Aqueous Media Using Fe3O4-g-CN@PEI-β-CD Nanocomposite: Modeling by Response Surface Methodology (RSM), Boosted Regression Tree (BRT), and General Regression Neural Network (GRNN). *Journal of Hazardous Materials* **2020,** *388*, 121769; 10.1016/j.jhazmat.2019.121769.

48. Zhang, K.; Zhong, S.; Zhang, H. Predicting Aqueous Adsorption of Organic Compounds onto Biochars, Carbon Nanotubes, Granular Activated Carbons, and Resins with Machine Learning. *Environmental Science & Technology* **2020,** *54* (11), 7008-7018; 10.1021/acs.est.0c02526.

49. Sigmund, G.; Gharasoo, M.; Hüffer, T.; Hofmann, T. Deep Learning Neural Network Approach for Predicting the Sorption of Ionizable and Polar Organic Pollutants to a Wide Range of Carbonaceous Materials. *Environmental Science & Technology* **2020,** *54* (7), 4583-4591; 10.1021/acs.est.9b06287.

50. Kim, B.; Lee, S.; Kim, J. Inverse Design of Porous Materials Using Artificial Neural Networks. *Science Advances* **2020,** *6* (1), eaax9324; 10.1126/sciadv.aax9324.

51. Pai, K.N.; Prasad, V.; Rajendran, A. Experimentally Validated Machine Learning Frameworks for Accelerated Prediction of Cyclic Steady State and Optimization of Pressure Swing Adsorption Processes. *Separation and Purification Technology* **2020,** *241*, 116651; 10.1016/j.seppur.2020.116651.

52. Xiao, J.; Li, C.; Fang, L.; Böwer, P.; Wark, M.; Bénard, P.; Chahine, R. Machine learning–Based Optimization for Hydrogen Purification Performance of Layered Bed Pressure Swing Adsorption. *International Journal of Energy Research* **2020,** *44* (6), 4475-4492; 10.1002/er.5225.

53. Burns, T.D.; Pai, K.N.; Subraveti, S.G.; Collins, S.P.; Krykunov, M.; Rajendran, A.; Woo, T.K. Prediction of MOF Performance in Vacuum Swing Adsorption Systems for Postcombustion CO2 Capture Based on Integrated Molecular Simulations, Process Optimizations, and Machine Learning Models. *Environmental Science & Technology* **2020,** *54* (7), 4536-4544; 10.1021/acs.est.9b07407.

54. Daglar, H.; Keskin, S. Computational Screening of Metal–Organic Frameworks for Membrane-Based CO2/N2/H2O Separations: Best Materials for Flue Gas Separation. *Journal of Physical Chemistry. C* **2018,** *122* (30), 17347-17357; 10.1021/acs.jpcc.8b05416.

3 Simultaneous effect of oxygen impurity and flow rate of purge gas on adsorption capacity of and heel buildup on activated carbon during cyclic adsorption-desorption of VOC

3.1 Introduction

Volatile organic compounds (VOCs) have been extensively used as solvents in chemical industries involving paints and are used in lubricants and liquid fuels [1-3]. In automotive manufacturing, vehicle painting operations are the main source of VOCs emissions due to their use of solvent-based paints [4]. Adsorption onto activated carbon (AC) is widely used for capture of VOCs due to its low cost, high removal efficiency, and ability to recover the adsorbate and regenerate the adsorbent for reuse [5, 6].

Adsorption is strongly influenced by the adsorbent's characteristics including surface area, surface functional groups, and pore size distribution, as well as the adsorbate's properties such as polarity, molecular size, molecular weight and boiling point [7-10]. Depending on the type of interaction between the adsorbent and adsorbate, adsorption process can occur reversibly (i.e. physisorption), irreversibly (i.e. chemisorption or non-desorbed physisorption), or a combination of the two [11].

Both physiosorbed and chemisorbed adsorbates can undergo transformation (i.e. decomposition/pyrolysis, polymerization) and become permanent heel [11]. Heel buildup not only decreases the amount of recovered VOC but also reduces activated carbon's lifetime and its adsorption capacity after each adsorption/regeneration cycle [12, 13]. This can, in turn, increase the cost associated with the abatement process due to the need for more frequent replacement of adsorbent [14].

Thermal regeneration is an effective approach for regenerating activated carbon. Several studies have focused on determining the parameters that can affect heel formation on activated carbon during thermal regeneration [5, 11, 15, 16]. For instance, Jahandar Lashaki et al. [15] found that raising the adsorption temperature from 25 to 45 °C increased the heel buildup on activated carbon beads by 30%, while increasing the regeneration temperature from 288 to 400 °C could reduce the heel

buildup by 61%. Using activated carbons with different pore size distributions, Jahandar Lashaki et al. [16] observed that heel was mainly formed in AC micropores, and demonstrated that heel buildup can be linearly correlated with activated carbon micropore volume. They also highlighted that carbon's mesopores primarily are involved in physisorption (i.e. reversible adsorption) of VOCs and tend not be susceptible to heel formation. The presence of surface oxygen groups on activated carbon is another important factor contributing to heel buildup [5]. Formation of covalent bonds between the adsorbate and surface oxygen groups can lead to chemisorption. Jahandar Lashaki et al. [5] reported that for activated carbon samples with low surface oxygen content heel buildup is greatly suppressed and mainly stems from non-desorbed physisorption. From the perspective of adsorbate properties, VOCs with high molecular weight and large kinetic diameter are more difficult to desorb and more likely to result in heel formation [2, 17].

Presence of oxygen in the purge gas (usually nitrogen) used during regeneration can also increase the heel buildup on AC due to the formation of chemical bonds between O_2 and adsorbates/adsorbent at high temperatures [18-21]. Jahandar Lashaki et al. [19] observed that increasing the oxygen concentration in the desorption purge gas increased cumulative heel build in cyclic adsorption/desorption of a mixture of VOCs on activated carbon. In accordance with Jahandar Lashaki's findings [19], Hashemi et al. [18] also found an adverse impact of oxygen impurity in the purge gas. Nevertheless, it needs to be mentioned that generating purge gas with low impurity can be energy consuming and costly. For instance, in a typical pressure swing adsorption process, compressor power consumption increases 2.5-fold in order to improve the N_2 purity from 95 to 99.99% [22].

In addition to oxygen impurity, the flow rate of the desorption purge gas can also affect heel buildup and adsorbent lifetime. However, no study has investigated the simultaneous effect of

purge gas impurity and flow rate. Hence, the objectives of the present study are (i) to systematically identify the simultaneous effect of flow rate and oxygen impurity of the desorption purge gas on heel formation mechanism(s) and heel buildup and (ii) to study whether using a higher purge gas flow rate can mitigate for presence of oxygen impurity in the desorption purge gas in terms of adsorption capacity recovery and heel buildup. A broader understanding of the parameters playing roles in heel formation can give insight into how heel buildup can be mitigated to enhance activated carbon performance during cyclic adsorption/desorption. Furthermore, reducing the amount of heel formed on activated carbon can lead to significant energy/cost savings for regeneration or replacement of the adsorbent.

3.2 Material and methods

3.2.1 Adsorbent and adsorbate

Virgin petroleum pitch-derived beaded activated carbon (BAC; G-70R; Kureha Corporation) is the adsorbent studied in this work. This BAC is a highly microporous (~87%) material with narrow pores from 0.6 to 8.4 nm in diameter. Before each experiment, BAC was preheated at 288 °C for 2h to remove potentially adsorbed impurities. 1,2,4-trimethylbenzene (TMB, 98%, Acros Organics) was used as adsorbate as it is a common component of automotive paint solvents. In addition, TMB has high tendency to form heel on BAC [15, 23] because of its relatively large kinetic diameter (0.61 nm) [24] and high boiling point (171 °C) among solvent compounds commonly used in automotive paints [2].

3.2.2 Experimental set-up and methods

A schematic of the adsorption/regeneration set-up is presented in Fig. 3-1. The adsorption/regeneration experiments were conducted in a stainless-steel tube containing 4.000±0.002 g of BAC supported by glass wool at both ends. During the adsorption, 10 standard

liter per minute (SLPM) dry air with a concentration of 500 ppmv TMB was introduced into the adsorption tube. Liquid TMB was injected at a rate of 28.0 µl/min using a syringe pump (KD scientific) onto glass wool in the injection port to avoid concentration fluctuations during the experiment. The temperature was maintained at 24±1 °C during adsorption. Flame ionization detector (FID; Baseline-Mocon Inc. series 9000) was used to measure the VOC inlet and outlet concentrations.

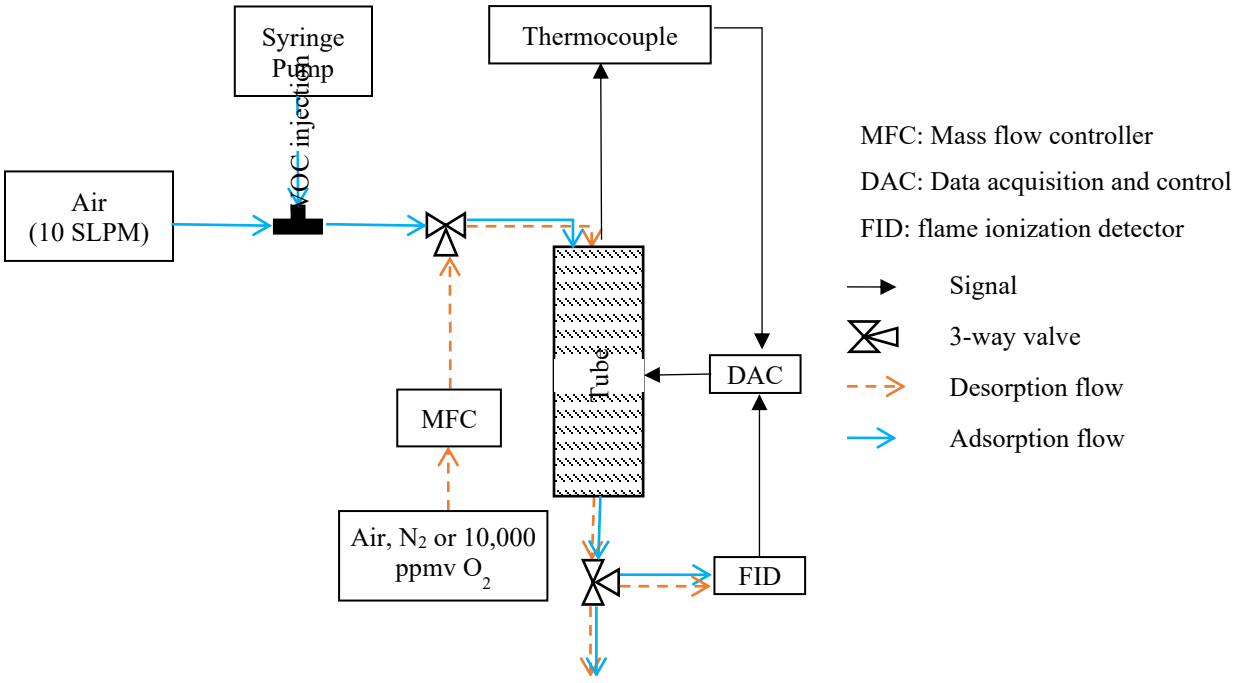

Fig. 3-1. Schematic diagram of the adsorption-desorption setup

All adsorption experiments were conducted for 2h. Regeneration was conducted at 288 °C (550 °F), in the range of temperatures used in industrial applications, in order to desorb the adsorbate while minimizing the energy consumption and damage to BAC pore structure [25]. A constant flow rate of the purge gas passed through the adsorbent bed during desorption. Heating was provided to maintain the BAC temperature at 288 °C in the first 3h, followed by a cooling step for 50 min. For regeneration, heating tape and insulation tape were respectively wrapped around the stainless-

steel tube to provide the required heat and minimize the heat loss. The BAC temperature was measured and controlled during regeneration using a K type thermocouple connected to a data acquisition and control (DAC) system. The DAC consisted of a data logger (National Instruments, Compact DAQ) and a LabVIEW program (National Instruments) to record the bed temperature and control heating. In order to investigate the effect of purge gas flow rate and oxygen content on heel buildup, three flow rates (0.1, 1, and 10 SLPM corresponding to 1, 10 and 100% of adsorption flowrate) and three levels of oxygen impurity (<5 ppmv, 10,000 ppmv, and 21%) were used, creating nine different regeneration scenarios. The flow of the purge gas was set using a 100 SCCM, 1 SLPM, or 20 SLPM mass flow controller (Alicat Scientific). Ultra-high purity nitrogen (99.9984%, Praxair), mixed nitrogen (containing 10,000 ppmv oxygen, Praxair) or air (99.999%, Praxair) was used as the purge gas, containing <5 ppmv, 10,000 ppmv and, 21% oxygen, respectively.

Heel buildup and adsorption capacity are determined based on gravimetric analysis and the results are reported as percentages relative to the weight of the virgin BAC. The amount of adsorbed VOC in each cycle is calculated by subtracting BAC's weight before adsorption from its weight after adsorption in that cycle. The amount of heel buildup in each cycle is defined as the difference between BAC weight before adsorption and after regeneration in that cycle. Cumulative heel in each cycle is determined by subtracting preheated BAC weight from its weight after regeneration in that cycle. Therefore, fifth cycle cumulative heel buildup represents the difference between preheated BAC weight and its weight after regeneration in the fifth (final) cycle.

$$\text{Adsorption capacity (wt\%)} = \frac{\text{weight of BAC after adsorption} - \text{weight of BAC before adsorption}}{\text{weight of preheated BAC}} \times 100$$

Mass balance cumulative heel (wt%)

$$= \frac{\text{weight of BAC after last regeneration cycle} - \text{weight of BAC before adsorption}}{\text{weight of preheated BAC}} \times 100$$

Adsorption/desorption experiments were duplicated, and average values are reported. Virgin and used BAC samples (i.e. after the fifth adsorption-regeneration cycle) were characterized in a micropore surface analysis system to obtain the pore size distribution (PSD) and surface area (iQ2MP, Quantachrome). After degassing the samples for 5h at 120 °C, nitrogen adsorption was conducted at -196 °C while its relative pressure (p/p_0) varied from 10^{-7} to 1. Relative pressures ranging from 0.01 to 0.07 and 0.2 to 0.5 were used to obtain specific surface area and micropore volume by BET method and V-t model, respectively. The p/p0 = 0.975 was used to determine the total pore volume. Pore size distribution was determined using the quenched solid density functional theory (QSDFT).

Surface elemental compositions (C, O, and N) of samples were determined with X-ray photoelectron spectroscopy (XPS). High resolution scans of binding energy with signal to noise ratio of greater than 10 were collected by an AXIS 165 spectrometer (Kratos Analytical). An energy analyzer at a pass energy of 20 V and a step of 0.1 eV was used to obtain the scans with the binding energy within the range of 0 eV to 1100 eV. XPS data were then processed using CasaXPS Software and the final results were obtained as atomic concentrations.

After completion of five successive adsorption/regeneration cycles, the BAC samples were analyzed with thermogravimetric analysis (TGA/DSC 1, Mettler Toledo). For the TGA test, a heating rate of 2 °C/min was used to increase BAC sample temperature from 25 to 800 °C in a 50 SCCM N_2 flow.

3.3 RESULTS AND DISCUSSION

3.3.1 5-cycle adsorption breakthrough curve and capacity

5-cycle breakthrough curves and adsorption capacities during cyclic adsorption/desorption experiments for regeneration scenarios are shown in Fig. 3-2 and Fig. 3-3 A, respectively. All the experiments were replicated, with the differences in adsorption capacity of replicates being within 4 wt%. In successive adsorption/regeneration cycles, the 5% breakthrough time (i.e. time at which the outlet concentration reaches 5% of the inlet concentration) shifts to earlier times and\or the area above the breakthrough curve decreases, meaning that the adsorption capacity has declined. In experiments where higher oxygen impurity and/or lower purge gas flow rate were used, the reduction in breakthrough times was greater. For example, using 0.1 SLPM air (21% O_2) as purge gas, the breakthrough time in the first cycle was 52 minutes while that of fifth cycle decreased to 6 minutes. Increasing purge gas flow rate instead of reducing its oxygen impurity also mitigates the adverse effect of oxygen on BAC regeneration. For instance, for the 0.1 SLPM air purge flow case above, the difference between the first and fifth cycle breakthrough times was 46 minutes ($\Delta T_{1,5}$ =46 min); however, by increasing the flow rate to 10 SLPM air (10 SLPM 21% O_2) or decreasing purge gas oxygen concentration to < 5 ppmv (0.1 SLPM N2 containing < 5 ppmv O_2), the breakthrough time reduction decreased to only 6 minutes ($\Delta T_{1,5}$ = 6 min).

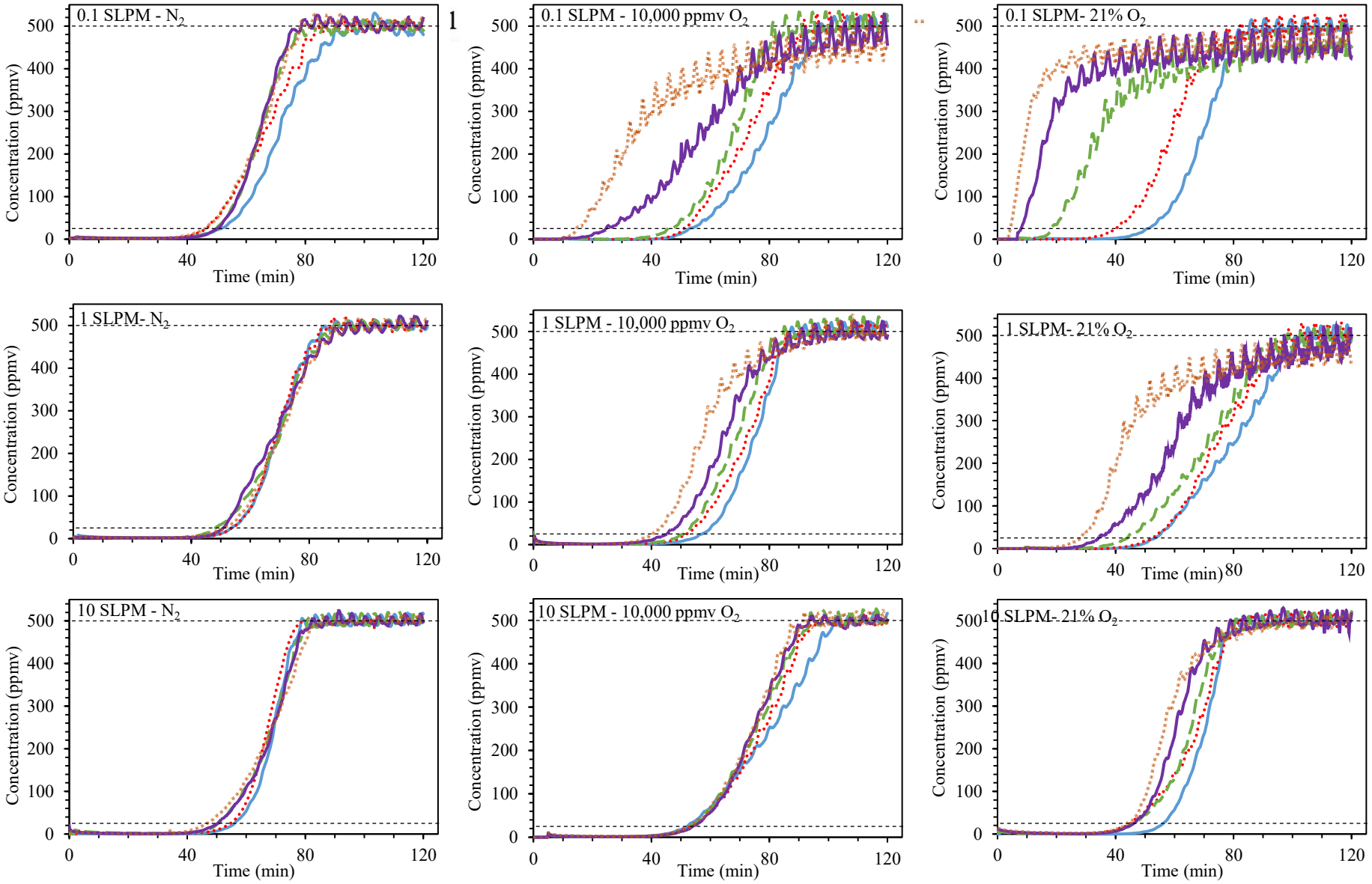

Fig. 3-2. Adsorption breakthrough curves at different desorption purge flow rates and oxygen impurity levels

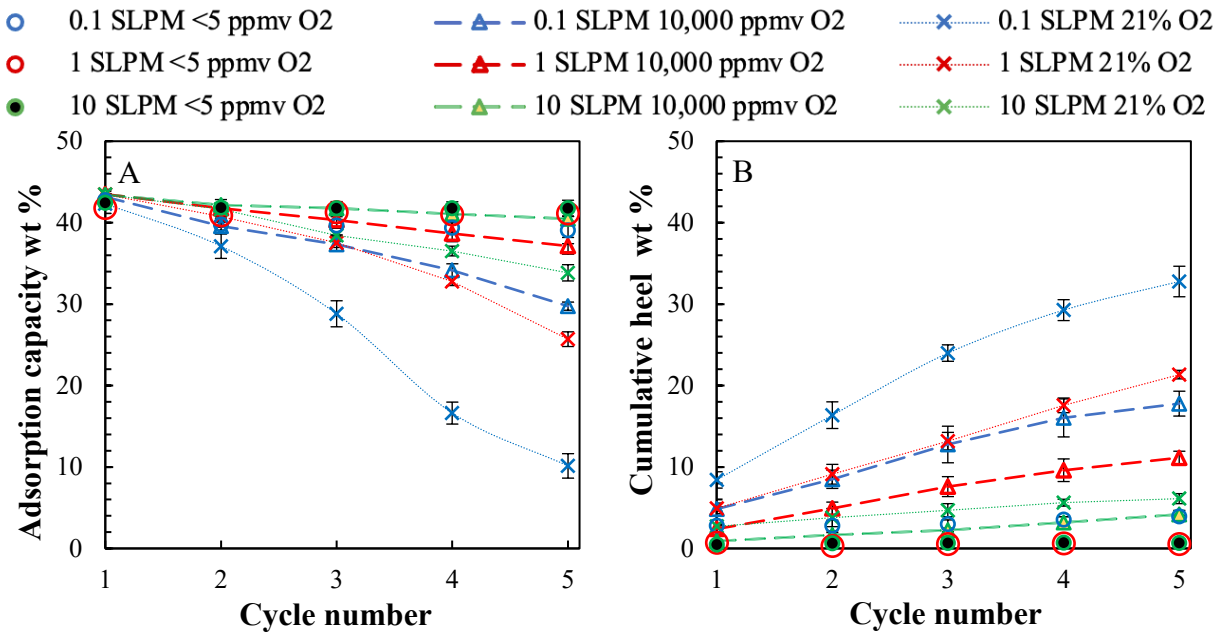

Fig. 3-3. Adsorption capacity (A) and heel formation (B) during cyclic adsorption/regeneration

As expected, the first cycle adsorption capacities in all experiments are similar (42.9 ± 1.7 wt%) since they have not yet experienced different regeneration conditions. It can be deduced that in most of the experiments, the parameters affecting the regeneration of BAC (e.g. temperature, purge gas flow rate and oxygen impurity) were not sufficient to completely desorb the adsorbate resulting in heel buildup on BAC. Subsequently, non-desorbed VOC species may undergo two different pathways :(i) pyrolysis reaction in the absence of oxygen or (ii) thermal oxidation of non-desorbed physiosorbed species [11]. Both paths result in chemically formed heel or chemisorbed species which ultimately transform into char or polymeric species [11].

Thermal regeneration using 1 or 10 SLPM N_2 containing < 5 ppmv O_2 almost completely (97%) recovered the adsorption capacity of BAC during 5-cycle adsorption/regeneration (Fig. 3-3). However, higher heel formation was observed in the BAC samples regenerated in other conditions.

Insufficiently high temperature (T=288 °C) during regeneration, especially at low purge gas flow rates, could be a reason for incomplete removal of VOCs from BAC [15]. Although the boiling point of TMB is only 169 °C, which is less than the applied temperature during thermal regeneration, a higher temperature (T > 288°C) is required to completely desorb TMB from BAC due to diffusion limitation in BAC micropores [21]. Chemisorbed species and adsorbed species in narrower pores are harder to desorb; therefore, a greater driving force for desorption is required [15, 26]. In the absence of oxygen, increasing the desorption temperature reduces the process time and improves the desorption efficiency by facilitating mass transfer and diffusion in micropores specifically for adsorbates with high affinity [21]. However, this increase in temperature can negatively affect BAC lifetime by facilitating pyrolysis of non-desorbed physiosorbed species to form chemisorbed species [11]. On the other hand, in the presence of oxygen, increase in temperature might result in higher heel buildup by facilitating reactions between purge gas oxygen and the adsorbate [21].

3.3.2 Effect of oxygen impurity

The effect of desorption purge gas oxygen impurity on adsorbate breakthrough and adsorption capacity is illustrated in Fig 3-2 and Fig 3-3 A, respectively. The presence of oxygen impurity in the purge gas adversely affected the performance of BAC by contributing to heel formation (Fig 3-2 and Fig 3-3 A). Oxygen molecules can take part in reactions with TMB on the surface of activated carbon, producing species that accumulates as heel [27]. At a constant flow rate, higher concentrations of O_2 in the purge gas led to earlier breakthrough times and decreased the adsorption capacity (Fig. 3-2). The continuous decline in adsorption capacity during cyclic adsorption stems from cumulative heel formation which is accompanied by pore blockage and decrease in adsorbent's available surface area and active sites [11, 18, 21].

Although oxygen impurity clearly exacerbates heel formation on BAC, the magnitude of its negative effect strongly depends on the purge gas flow rate. For instance, at 0.1 SLPM purge flow, by increasing the oxygen impurity in the purge gas from <5 ppmv to 21% (i.e. air), the fifth cycle breakthrough time decreased from 45 to 6 min and the fifth cycle adsorption capacity dropped from 39 to 10 wt%. However, at 10 SLPM purge flow, by increasing the oxygen impurity from < 5 ppmv to 21%, the fifth cycle breakthrough time and adsorption capacity decreased by only 15 min and 8 wt%, respectively.

3.3.3 Effect of desorption purge gas flow rate

A higher purge gas flow rate could desorb more VOCs off BAC surface and recover the adsorption capacity to a greater extent (Fig. 3-3 A). However, the effect of purge gas flow rate on heel formation

is strongly related to the purge gas oxygen impurity. Increasing the purge gas flow rate mitigates the reduction in cyclic adsorption capacity and breakthrough times. This mitigating effect becomes more important when purge gas oxygen impurity increases.

For instance, by increasing the purge gas flow rate from 0.1 to 10 SLPM, the fifth cycle breakthrough time increased by less than 5 minutes for <5 ppmv O_2, while for 21% O_2, the fifth cycle breakthrough time improved by 41 minutes, and the fifth cycle adsorption capacity was enhanced by 2.8 and 26.5 wt% respectively. Evidently, the effect of flow rate on breakthrough time and adsorption capacity becomes more important at high oxygen impurities. Breakthrough curves for samples with cumulative heel greater than 16 wt% could not reach the inlet concentration (500 ppm) after 2h despite their early breakthroughs. It is believed that in these extreme cases (cumulative heel > 16 wt%), heel formation substantially reduced access to micropores and the internal mass transfer rate, preventing complete saturation of the adsorbent in

2h and resulting in the long tail in breakthrough curves shown in Fig 3-2 (0.1 SLPM 21% O_2, 1 SLPM 21% O_2 and 0.1 SLPM 10,000 ppmv O_2). Fig. 3-4 shows the relationship between the cumulative amount of heel in each cycle and the next cycle's adsorption capacity. Regardless of the nature of heel and the pathway it is formed through (non-desorbed physisorption, chemisorption, thermal oxidation, pyrolysis), heel formation results in the loss of BAC active sites on which VOCs can be adsorbed. Based on Fig. 3-4, three important conclusions can be drawn :(i) there is a certain amount of heel after which BAC can be considered fully exhausted and will provide negligible adsorption capacity; (ii) at high cumulative heel (≥16 wt%), the adsorption capacity decreases more sharply with heel formation, likely due to severe pore blockage; and (iii) there is a nonlinear relationship between heel buildup and BAC adsorption capacity in the next cycle, which implies that pore blockage becomes faster as heel buildup increases.

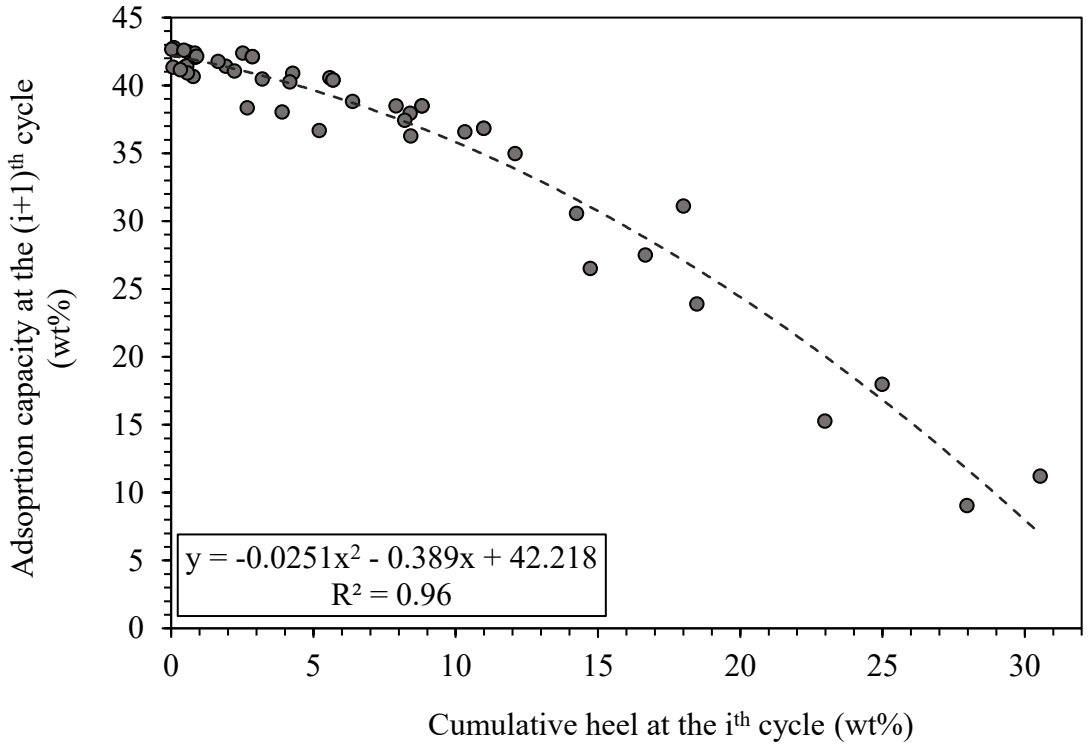

Fig. 3-4. Relationship between cumulative heel for a cycle and the adsorption capacity of the following cycle.

3.4 Heel formation during cyclic adsorption/regeneration

3.4.1 Effect of oxygen impurity

The effect of oxygen impurity on mass balance heel during cyclic adsorption/desorption of TMB on BAC is illustrated in Fig. 3-3 B. Firstly, cumulative heel increases with the cycle number, meaning that heel is being built up over successive cycles and each cycle contributes to the total heel. Moreover, a higher oxygen impurity in the purge gas leads to more heel formation. At 0.1, 1 and 10 SLPM, increasing oxygen impurity from <5 ppmv to 21% increased cumulative heel by approximately 28.85, 20.65 and 5.20 wt%, respectively. This demonstrates that oxygen impurity in the purge gas accelerates heel formation; however, the severity of its impact on heel formation is strongly dependent on the purge gas flow rate. Heating virgin BAC (i.e., no TMB present) with purge gas containing oxygen impurity for 3 hours at 288 °C did not cause heel formation. Therefore, it is reasonable to hypothesize that the interactions between oxygen and TMB molecules on the surface of BAC are the main source of heel formation. In fact, a higher concentration of oxygen in the purge gas during regeneration augments the probability of non-desorbed VOC participation in thermal oxidation reactions, which is one of the major mechanisms in heel formation. The potential by-products of these reactions consist of polymeric species, which are heavier than TMB and more difficult to be desorbed at 288 °C [28, 29].

3.4.2 Effect of flow rate

At a constant oxygen impurity, a lower purge gas flow rate resulted in formation of a larger amount of heel (Fig. 3-3 B). For instance, at 21% oxygen, by decreasing the flow rate from 10 to 0.1 SLPM, cumulative heel in the fifth cycle increased from 5.5 to 32.8 wt%. Thus, increasing the purge gas

flow rate can be used to reduce the negative impact of oxygen impurity on heel formation. Interestingly, at high purge gas flow rate or oxygen impurity, the influence of oxygen impurity concentration on cyclic heel slowly levels off. At 10 SLPM, increasing the oxygen impurity from <5 to 10,000 ppmv increased the fifth-cycle cumulative heel from 0.35 to 4.18 wt%, while its amount at 21% was only 4.55 wt%. Another observation regarding regeneration with nitrogen (<5 ppmv O_2) is that increasing the flow rate from 0.1 to 1 SLPM greatly decreased heel formation, whereas a higher flow rate (i.e. 10 SLPM) brought about minimal improvement to heel formation. This indicates that by increasing the purge gas flow rate, the desorption rate reaches a plateau, after which it will be independent of the flow rate [30].

To understand how increasing purge gas flow rate facilitates TMB desorption, the effect of purge gas flow rate on desorption rate from virgin BAC was investigated in the absence of oxygen (Fig. 3-5). The early stages of desorption are when purge gas flow rate substantively affects desorption rate (Fig. 3-5). During the first ~20 minutes of desorption, the external mass transfer is the rate-determining step, even at high flow rates (i.e., 1 and 10 SLPM), since a considerable amount of adsorbed TMB is being desorbed. After this stage, for 1 and 10 SLPM the internal mass transport resistance will be the dominant factor in desorption [31], which can be verified by the same desorption rate of samples regenerated with 1 and 10 SLPM after t = 20 min. Therefore, in this period, when sufficient purge gas flow rate is applied, desorption rate becomes independent of flow rate.

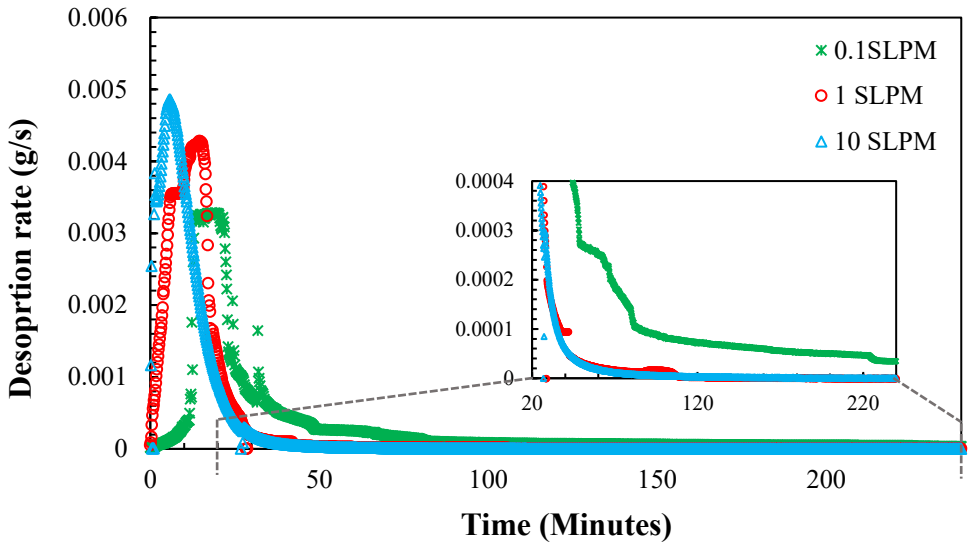

Fig. 3-5. First cycle desorption rate profiles of TMB from virgin BAC with <5 ppmv O_2 at varying purge gas flow rate

3.5 Characterization of regenerated BACs

3.5.1 Nitrogen adsorption analysis

BET surface area, micropore volume, and total pore volume of BAC samples before and after five cycles adsorption/regeneration are listed in Table 3-1. Heel formation substantially decreased BET surface, micropore volume and total pore volume for used BAC samples relative to the virgin BAC. Formed heel blocks the adsorption sites and pores. Comparing the total pore and micropore volumes of virgin and used BAC demonstrates that pore loss mainly occurred in the micropore region, which accounts for greater than 87% of the virgin BAC total pore volume. In the worst regeneration case (0.1 SLPM with 21% O_2), the BET surface area and micropore volume of BAC samples regenerated decreased by 80 and 88 %, respectively. This heel buildup on BAC restricts adsorbate's access to active sites and increases mass transfer resistance in the adsorbent pores resulting in a long tail in the fourth and fifth cycles of adsorption breakthrough. However, with 0.1 SLPM purge gas flow, reducing the oxygen impurity from 21% to <5 ppmv increased the BET

surface area, micropore volume and total pore volume of regenerated samples after 5 cycles by ~ 3.3, 6.2 and 1.5 times, respectively. At 10 SLPM, those values were increased by ~ 32, 30 and 18 %, respectively since high purge gas flow rate mitigated some of the adverse effect of oxygen impurity on BAC regeneration. These results are further supported by the PSD profiles presented in Fig. 3-6. At 5.7, 7.8 and between 10.1 to 13.0 Å, three major peaks are observed for all BAC samples except the one regenerated with 0.1 SLPM air (Fig. 3-6). BAC regenerated with 0.1 SLPM air shows no peaks because of the nearly complete blockage of its pores by non-desorbed adsorbate species and/or species formed during thermal regeneration. For BAC sample regenerated with 1 SLPM air (Fig. 3-6 C), the third peak is shifted to the left relative to virgin BAC and BAC regenerated with 10 SLPM air due to partial blockage of BAC large micropores (10.1-13.0 Å), which made its pores narrower.

Table. 3-1. Physical and chemical characterization of virgin and regenerated BAC samples. Average values are reported.

Carbon description	Pure gas O_2 content (ppmv)	Purge gas flow rate (SLPM)	Physical properties			Chemical properties		
			BET surface area (m^2/g)	Micropore volume (cm^3/g)	Total pore volume (cm^3/g)	O(%) [a]	N(%) [a]	C(%) [a]
Virgin BAC	-	-	1372.0	0.50	0.57	6.0	0.0	94.0
	<5	0.1	1175.9	0.43	0.48	6.6	0.1	93.1
	<5	1	1249.0	0.46	0.50	7.6	0.0	91.9
	<5	10	1279.3	0.47	0.52	6.6	0.0	93.1
BAC after	10,000	0.1	848.6	0.31	0.36	8.5	0.2	91.1
5Ads/Reg.	10,000	1	967.6	0.36	0.39	9.0	0.0	90.8
cycles	10,000	10	1144.3	0.42	0.46	7.8	0.2	91.9
	210,000	0.1	272.3	0.06	0.19	12.9	0.0	86.9
	210,000	1	599.2	0.20	0.30	12.6	0.7	86.4
	210,000	10	980.8	0.36	0.44	10.7	0.4	88.6

[a] Atomic percentage.

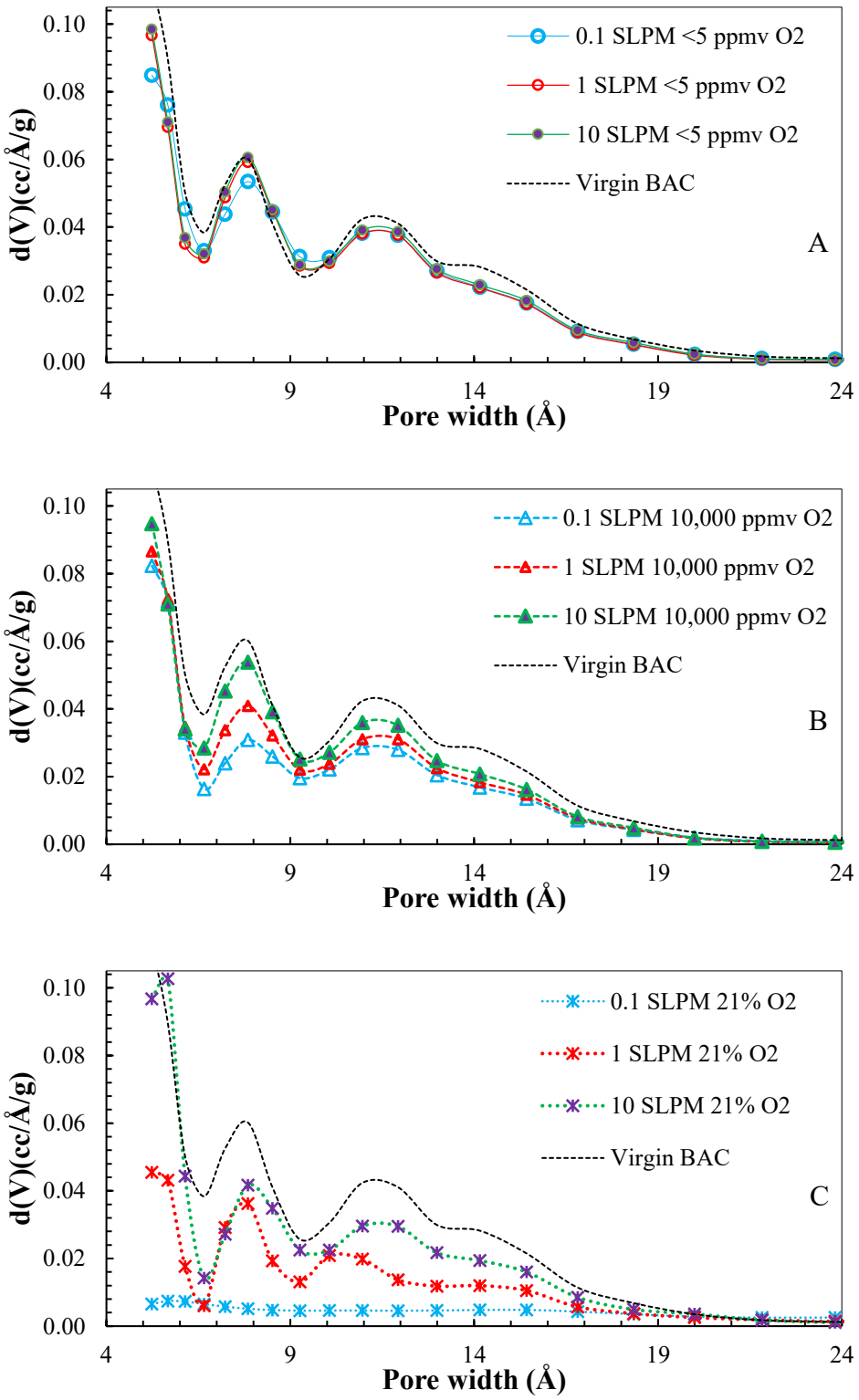

Fig. 3-6. Pore size distributions of BAC samples A) regenerated with < 5 ppmv O_2, B) regenerated with 10,000 ppmv O_2, and C) regenerated with 21% O_2 after five-cycle adsorption/regeneration

3.5.2 XPS

The XPS analysis was conducted to determine the regenerated BAC surface elemental composition and to elucidate the effect of purge gas flow rate and oxygen content on the chemical nature of heel. BAC surface oxygen content increased by increasing the oxygen impurity in the purge gas in all cases, presumably due to thermal oxidation of adsorbed species and heel formation. The oxygen rich heel species are attributed to heavy polymeric products formed as a result of the reactions between TMB and oxygen in the purge gas [29, 32, 33]. The rate of heel formation via thermal oxidation partly depends on the number of collisions between the adsorbed TMB and oxygen molecules in the purge gas. For BAC samples regenerated with purge N_2 containing <5 and 10,000 ppmv oxygen impurity, the use of 1 SLPM purge gas flow rate resulted in the highest surface oxygen content, which could be explained from two points of view. First, at those oxygen concentrations, with 0.1 SLPM purge gas, a very small amount of oxygen enters the adsorbent bed during regeneration; therefore, only a small fraction of the total heel is formed through reactions involving oxygen. Secondly, at 10 SLPM, adsorbed species are desorbed and quickly carried away by air during regeneration due to the high flow rate, leaving fewer TMB molecules available for oxidation reactions. Consequently, it is suggested that under our operating conditions, at <5 and 10,000 ppmv O_2 impurity, 1 SLPM purge gas provides the most suitable conditions for reactions between the adsorbed species and oxygen in the purge gas. As can be seen in Table 3-1, for a particular purge gas flow rate, increasing the concentration of O_2 in the purge gas increases the surface oxygen content on regenerated BAC. This can be attributed to the higher probability of oxidation of TMB as the number of available O_2 molecules increases.

As mentioned above, at <5 and 10,000 ppmv O_2 impurity, using 1 SLPM purge gas results in the maximum reaction between TMB and purge gas oxygen (thermal oxidation); however, the maximum heel (physisorption, chemisorption, polymerization, pyrolysis and thermal oxidation) buildup occurs at 0.1 SLPM. In fact, using lower desorption purge gas flow rate reduces TMB concentration gradient between BAC pores and the purge gas resulting in mass transfer limitation of the desorbed species from the adsorbent to the purge gas, leaving some TMB in the BAC pores. Therefore, at <5 and 10,000 ppmv O_2 impurities, using 0.1 SLPM as purge gas results in the maximum total heel while using 1 SLPM as purge gas results in the highest oxygen induced heel. When air is used as the purge gas, its high oxygen content (21% O_2), even at low flow rates, provides ample oxygen to the BAC bed during regeneration. An increase in purge gas flow rate, however, decreases available TMB on the BAC surface and results in less TMB oxidation during regeneration.

3.5.3 Thermogravimetric analysis

TGA can be used to help understand the nature and potential formation mechanism(s) of heel [56]. Operating condition (e.g., oxic or anoxic) as well as characteristics of adsorbates (boiling point and molecular structure) [34] determine the heel formation mechanism [71]. Therefore, in addition to chemisorbed species, some physiosorbed adsorbates also cannot be fully removed during thermal regeneration due to their high boiling point and large molecular size [17]. These non-desorbed species may be converted into heavier compounds through pyrolysis or thermal oxidation reactions. Ultimately, after repetitive cycles and extended reactions, heel species are converted to char and/or heavy polymeric compounds [11]. DTG results for virgin and regenerated BAC samples are shown in Fig 3-7. Stronger bonds between the adsorbate and adsorbent require higher temperatures to break [3]. Strongly physiosorbed heel is attributed to heel species completely removed by heating to

450 ◦C ($H_{<450}$). The strong DTG peak at around 330-450 °C ($H_{<450}$) can be attributed to the heel formed due to (i) the superposition of wall effect in pores which are similar in size with adsorbate species, and (ii) diffusion limitations in narrow micropores of BAC [15]. Therefore, physiosorbed species trapped in BAC due to low flow rate during regeneration and/or weakly chemisorbed low molecular weight species formed during thermal oxidation could be desorbed at this temperature range. Moreover, chemically formed (chemisorbed) heel is attributed to heel species removed between 450˚C to 850 ˚C (H_{450_850}), and non-desorbable heel made up of chemisorbed heel and char is attributed to heel species that require temperature higher than 850 ˚C ($H_{>850}$) to be removed [21]. As Fig 3-7 indicates, samples began to lose mass at temperatures lower than the regeneration temperature (288 °C) due to adsorption of water vapor after fifth cycle desorption on BAC samples [15].

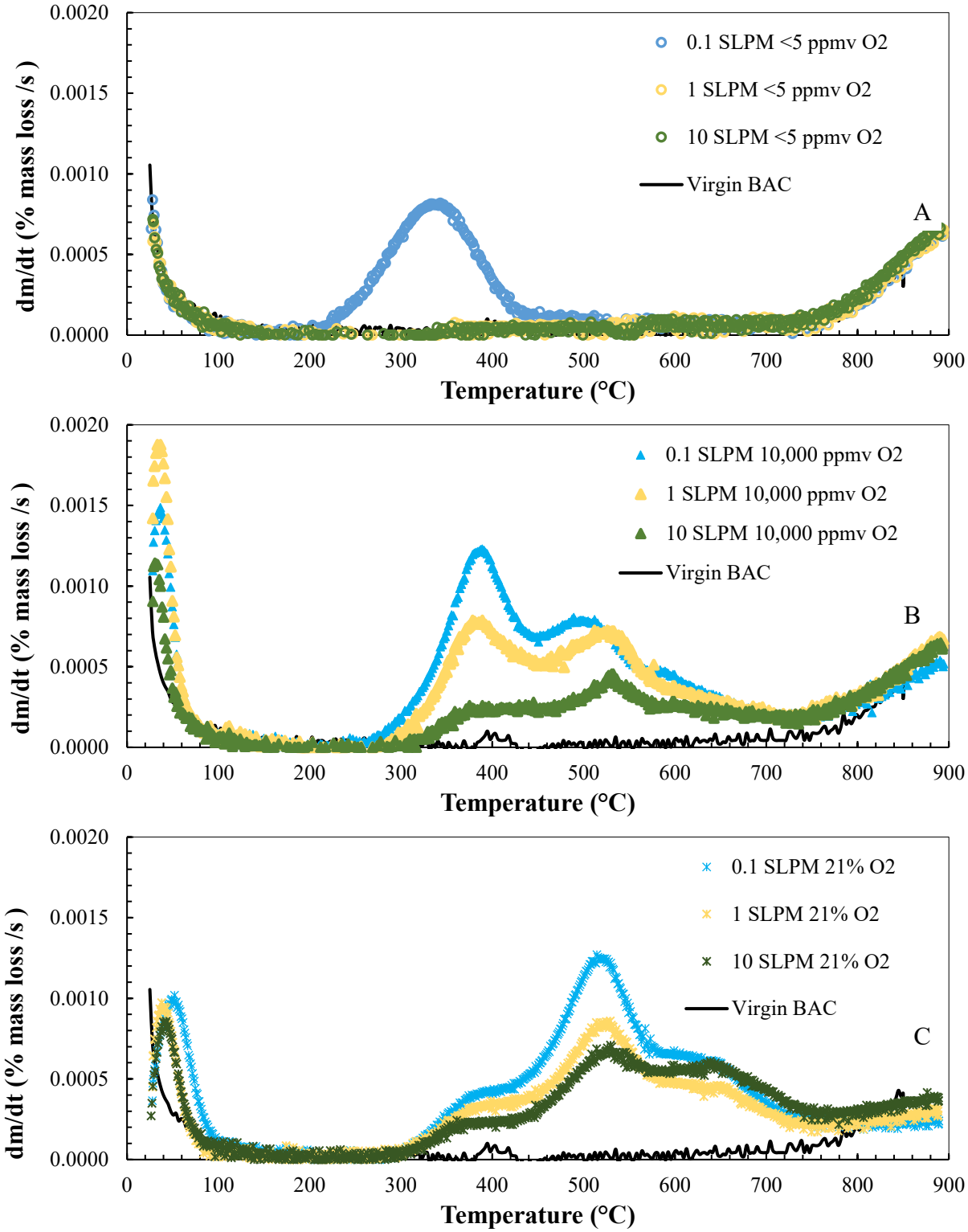

Fig. 3-7. DTG analysis of samples regenerated at A) <5 ppmv, B) 10,000 ppmv and C) 21% oxygen concentrations after five-cycle adsorption/regeneration.

For virgin BAC and BAC regenerated with <5 ppmv O_2 purge gas at 1 and 10 SLPM (Fig 3-7 A), no major peak was observed except the final baseline rise at approximately 800 °C due to carbon loss [16] . Therefore, DTG results further confirm that 1 and 10 SLPM with <5 ppmv O_2 purge gas removed almost all TMB during regeneration.

For the BAC regenerated with <5 ppmv O_2 purge gas at 0.1 SLPM (Fig 3-7 A), the peak at 350 °C ($H_{<450}$) can be only attributed to non-desorbed physiosorbed species as there in no or very little oxygen for thermal oxidation reactions. Higher purge gas flow rate lowers VOC bulk concentration and, therefore, enhances the desorption efficiency by increasing the TMB concentration gradient between the surface of BAC and bulk gas. At 0.1 SLPM, purge gas became saturated with TMB and therefore the concentration gradient was small which resulted in incomplete desorption and accumulation of physiosorbed TMB species. Additionally, as shown in Fig 3-7(A, B and C), an increase in purge gas flow rate during regeneration effectively reduced strongly physiosorbed heel species corresponding to DTG peaks at around 380 °C ($H_{<450}$).

BAC samples regenerated with purge gas containing 10,000 or 21% O_2 show two major peaks at around 380 °C ($H_{<450}$) and 500 °C ($H_{450\text{-}850}$), which were reduced in size with higher purge gas flow rate. At 10,000 ppmv O_2 (Fig 3-7 B), by increasing the flow rate from 0.1 SLMP to 10 SLMP, the ratio of $H_{450\text{-}850}$ to $H_{<450}$ increased, i.e., heel shifts from strongly physiosorbed ($H_{<450}$) to chemisorbed (H_{450_850}), although the total heel amount decreased.

For BAC regenerated with 21% O_2 (Fig 3-7 C), an additional peak is observed at 650°C, which can be attributed to heavy polymeric species formed through thermal oxidation of non-desorbed organic species [11]. For all purge gas flow rates, higher oxygen impurity level led to shifting the DTG peaks to higher temperatures. For all the three oxygen levels, increase in purge gas flow rate reduced heel buildup, and suggests this may be a promising alternative method where greater purge

gas purity is not feasible. However, in the presence of oxygen, higher purge gas flow also resulted in transformation of heel species to heavier compounds which required higher temperature to desorb.

3.5.4 Conclusion

The combined effect of purge gas flow rate and oxygen content on the type and magnitude of heel buildup during 5-cycle adsorption/desorption of TMB on BAC was investigated. Nine different regeneration scenarios corresponding to three flow rates (0.1, 1 and 10 SLPM) and oxygen concentrations (<5 ppmv, 10,000 ppmv and 21%) were considered. Increase in oxygen impurity or decrease in flow rate of the purge gas resulted in higher heel buildup, which in turn led to reduction in adsorption capacity, breakthrough time, and adsorbent surface area and porosity. Thermal regeneration using 1 or 10 SLPM N_2 purge gas (<5 ppm O_2) recovered 97% of its TMB adsorption capacity after 5-cycle adsorption/regeneration. By increasing the purge gas flow rate, the extent of oxygen impurity's effect on heel formation over BAC can be reduced. Higher concentration of oxygen in the purge gas increases the possibility of thermal oxidation of non-desorbed TMB. Utilizing a higher purge gas flow rate reduced the amount of heel formed; however, after a certain purge gas flow rate, increasing purge gas flow rate results in a negligible heel buildup decrease. Comparing the PSDs and micropore volumes of virgin BAC and regenerated BACs indicated that the pore loss due to heel formation mainly occurred in the micropore region. By increasing purge gas flow rate, the PSD of the regenerated BAC approaches that of virgin BAC. On the other hand, at extremely high oxygen impurity (i.e., air), the PSD of regenerated BACs shifted downward indicating blockage of its micropores by heel species. DTG results showed that higher purge gas oxygen impurity alters the nature of heel species from non-desorbed physiosorbed to chemically-formed, heavy organics via consecutive thermal oxidation

reactions. Increase in purge gas flow rate at lower oxygen impurities resulted in lower heel buildup. Although higher flow rate improves desorption efficiency and reduces heel buildup at relatively high oxygen impurities (10,000 ppmv), it transforms the heel into heavier chemically-formed organics.

3.5.5 References

1. Dwivedi, P.; Gaur, V.; Sharma, A.; Verma, N. Comparative Study of Removal of Volatile Organic Compounds by Cryogenic Condensation and Adsorption by Activated Carbon Fiber. *Separation and Purification Technology* **2004,** *39* (1), 23-37; 10.1016/j.seppur.2003.12.016.

2. Wang, H.; Jahandar Lashaki, M.; Fayaz, M.; Hashisho, Z.; Philips, J.H.; Anderson, J.E.; Nichols, M. Adsorption and Desorption of Mixtures of Organic Vapors on Beaded Activated Carbon. *Environmental Science & Technology* **2012,** *46* (15), 8341-8350; 10.1021/es3013062.

3. Patil, K.; Jeong, S.; Lim, H.; Byun, H.; Han, S. Removal of Volatile Organic Compounds from Air Using Activated Carbon Impregnated Cellulose Acetate Electrospun Mats. *Environmental Engineering Research* **2019,** *24* (4), 600-607.

4. Tefera, D.T.; Hashisho, Z.; Philips, J.H.; Anderson, J.E.; Nichols, M. Modeling Competitive Adsorption of Mixtures of Volatile Organic Compounds in a Fixed-Bed of Beaded Activated Carbon. *Environmental Science & Technology* **2014,** *48* (9), 5108-5117; 10.1021/es404667f.

5. Jahandar Lashaki, M.; Atkinson, J.D.; Hashisho, Z.; Phillips, J.H.; Anderson, J.E.; Nichols, M. The Role of Beaded Activated Carbon's Surface Oxygen Groups on Irreversible Adsorption of Organic Vapors. *Journal of Hazardous Materials* **2016,** *317*, 284-294; 10.1016/j.jhazmat.2016.05.087.

6. Tefera, D.T.; Jahandar Lashaki, M.; Fayaz, M.; Hashisho, Z.; Philips, J.H.; Anderson, J.E.; Nichols, M. Two-Dimensional Modeling of Volatile Organic Compounds Adsorption onto Beaded Activated Carbon. *Environmental Science & Technology* **2013,** *47* (20), 11700-11710; 10.1021/es402369u.

7. Rudling, J.; Björkholm, E. Irreversibility Effects in Liquid Desorption of Organic Solvents from Activated Carbon. *Journal of Chromatography A* **1987,** *392*, 239-248; 10.1016/S0021-9673(01)94269-4.

8. Lu, Q.; Sorial, G.A. The Role of Adsorbent Pore Size Distribution in Multicomponent Adsorption on Activated Carbon. *Carbon* **2004,** *42* (15), 3133-3142; 10.1016/j.carbon.2004.07.025.

9. Henning, K.D.; Bongartz, W.; Degel, J. Adsorptive Recovery of Problematic Solvents.

10. Guideline Series, Control of Volatile Organic Compound Emissions from Reactor Processes and Distillation Operations Processes in the Synthetic Organic Chemical Manufacturing Industry; United States Environmental Protection Agency: Research Triangle Park, North Caroline, 1993.

11. Jahandar Lashaki, M.; Hashisho, Z.; Phillips, J.H.; Crompton, D.; Anderson, J.E.; Nichols, M. Mechanisms of Heel Buildup During Cyclic Adsorption-Desorption of Volatile Organic Compounds in a Full-Scale Adsorber-Desorber. *Chemical Engineering Journal* **2020,** *400*, 124937; 10.1016/j.cej.2020.124937.

12. Magne, P.; Walker, P.L. Phenol Adsorption on Activated Carbons: Application to the Regeneration of Activated Carbons Polluted with Phenol. *Carbon* **1986,** *24* (2), 101-107; 10.1016/0008-6223(86)90102-8.

13. Liu, Y.; Li, C.; Peyravi, A.; Sun, Z.; Zhang, G.; Rahmani, K.; Zheng, S.; Hashisho, Z. Mesoporous MCM-41 derived from natural Opoka and its application for organic vapors removal. *Journal of Hazardous Materials* **2021,** *408*, 124911; 10.1016/j.jhazmat.2020.124911.

14. Tanthapanichakoon, W.; Ariyadejwanich, P.; Japthong, P.; Nakagawa, K.; Mukai, S.R.; Tamon, H. Adsorption–Desorption Characteristics of Phenol and Reactive Dyes from Aqueous Solution on Mesoporous Activated Carbon Prepared from Waste Tires. *Water Research* **2005,** *39* (7), 1347-1353; 10.1016/j.watres.2004.12.044.

15. Jahandar Lashaki, M.; Fayaz, M.; Wang, H.; Hashisho, Z.; Philips, J.H.; Anderson, J.E.; Nichols, M. Effect of Adsorption and Regeneration Temperature on Irreversible Adsorption of Organic Vapors on Beaded Activated Carbon. *Environmental Science & Technology* **2012,** *46* (7), 4083-4090; 10.1021/es3000195.

16. Jahandar Lashaki, M.; Atkinson, J.D.; Hashisho, Z.; Phillips, J.H.; Anderson, J.E.; Nichols, M. The Role of Beaded Activated Carbon's Pore Size Distribution on Heel Formation During Cyclic Adsorption/Desorption of Organic Vapors. *Journal of Hazardous Materials* **2016,** *315*, 42-51; 10.1016/j.jhazmat.2016.04.071.

17. Fayaz, M. Adsorption and Microwave Regeneration for Controlling Volatile Organic Compounds Emissions from Automotive Paint Booths. University of Alberta, 2016.

18. Hashemi, S.M.; Jahandar Lashaki, M.; Hashisho, Z.; Phillips, J.H.; Anderson, J.E.; Nichols, M. Oxygen Impurity in Nitrogen Desorption Purge Gas Can Increase Heel Buildup on Activated Carbon. *Separation and Purification Technology* **2019,** *210*, 497-503.

19. Jahandar Lashaki, M.; Atkinson, J.D.; Hashisho, Z.; Phillips, J.H.; Anderson, J.E.; Nichols, M.; Misovski, T. Effect of Desorption Purge Gas Oxygen Impurity on Irreversible Adsorption of Organic Vapors. *Carbon* **2016,** *99*, 310-317; https://doi.org/10.1016/j.carbon.2015.12.037.

20. Carratalá-Abril, J.; Lillo-Ródenas, M.A.; Linares-Solano, A.; Cazorla-Amorós, D. Regeneration of Activated Carbons Saturated with Benzene or Toluene Using an Oxygen-Containing Atmosphere. *Chemical Engineering Science* **2010,** *65* (6), 2190-2198; 10.1016/j.ces.2009.12.017.

21. Feizbakhshan, M.; Amdebrhan, B.; Hashisho, Z.; Phillips, J.H.; Crompton, D.; Anderson, J.E.; Nichols, M. Effects of Oxygen Impurity and Desorption Temperature on Heel Build-up in Activated Carbon. *Chemical Engineering Journal* **2021,** *409*, 128232; 10.1016/j.cej.2020.128232.

22. Compressed Air Best Practices, The Energy Costs Associated with Nitrogen Specifications.; http://www.airbestpractices.com/system-assessments/air-treatment/n2/energy-costs-associated-nitrogen-specifications.

23. Niknaddaf, S.; Atkinson, J.D.; Shariaty, P.; Jahandar Lashaki, M.; Hashisho, Z.; Phillips, J.H.; Anderson, J.E.; Nichols, M. Heel Formation During Volatile Organic Compound Desorption from Activated Carbon Fiber Cloth. *Carbon* **2016,** *96*, 131-138; 10.1016/j.carbon.2015.09.049.

24. J.K.P.j. Barrie *Recent Advances in Zeolite Science.* Elsevier: 1989.

25. Salvador, F.; Martin-Sanchez, N.; Sanchez-Hernandez, R.; Sanchez-Montero, M.J.; Izquierdo, C. Regeneration of Carbonaceous Adsorbents. Part I: Thermal Regeneration. *Microporous and Mesoporous Materials* **2015,** *202*, 259-276; 10.1016/j.micromeso.2014.02.045.

26. Fayaz, M.; Shariaty, P.; Atkinson, J.D.; Hashisho, Z.; Phillips, J.H.; Anderson, J.E.; Nichols, M. Using Microwave Heating to Improve the Desorption Efficiency of High Molecular Weight VOC from Beaded Activated Carbon. *Environmental Science & Technology* **1900,** *49* (7), 4536-4542; 10.1021/es505953c.

27. Feizbakhshan, M. Improving Cyclic Adsorption/Desorption Process of Volatile Organic Compounds in the Presence of Gaseous Phase Oxygen. University of Alberta, 2020.

28. Berndt, B. Reaction of O(3P) Atoms with Benzene. *Zeitschrift für Physikalische Chemie. International Journal of Research in Physical Chemistry and Chemical Physics* **2004,** *218* (4), 391-404.

29. Boocock, G.; Cvetanović, R.J. Reaction of Oxygen Atoms with Benzene. *Canadian Journal of Chemistry* **1961,** *39* (12), 2436-2443; 10.1139/v61-323.

30. Mark A. Waer; Vernon L. Snoeyink Effects of Oxidant on Thermal Regeneration of Granular Activated Carbon. **1994,** *120* (1).

31. Küntzel, J.; Ham, R.; Melin, T. Regeneration of Hydrophobic Zeolites with Steam. *Chemical Engineering & Technology* **1999,** *22* (12), 991-994; 10.1002/(SICI)1521-4125(199912)22:123.0.CO;2-L.

32. S. Sitkiewitz and A. Heller Photocatalytic Oxidation of Benzene and Stearic Acid on Sol-Gel Derived TiO2 Thin Films Attached to Glass. *New Journal of Chemistry* **1996,** *20*, 233-241.

33. D'Hennezel, O.; Pichat, P.; Ollis, D.F. Benzene and Toluene Gas-Phase Photocatalytic Degradation over H2O and HCL Pretreated TiO2: By-Products and Mechanisms. *Journal of Photochemistry and Photobiology. A, Chemistry.* **1998,** *118* (3), 197-204; 10.1016/S1010-6030(98)00366-9.

34. Yun, J.; Choi, D.; Moon, H. Benzene Adsorption and Hot Purge Regeneration in Activated Carbon Beds. *Chemical Engineering Science* **2000,** *55* (23), 5857-5872; 10.1016/S0009-2509(00)00189-5.

4 Prediction of Heel Buildup Using Machine Learning Algorithms (XGBoost and Deep Neural Network)

4.1 Introduction

Adsorptive removal of volatile organic compounds (VOCs) over activated carbon (AC) has been extensively applied at industrial scale [1-4]. In cyclic adsorption processes, used activated carbon (i.e., loaded with VOCs) is regenerated to desorb the organics off the surface and ideally retrieve the original capacity for the subsequent cycle. A common method for regeneration of activated carbon is thermal regeneration using heating elements. In this method, the temperature of adsorbent bed is gradually raised to desorb the adsorbed VOCs while the system is continuously purged by an inert gas (e.g., nitrogen) to remove the desorbed species, improve the desorption efficiency by maintaining a concentration gradient between the purge gas and adsorbent surface, and prevent the adsorbates from participating in reactions on AC. However, a challenge associated with adsorption-based VOC abatement is the accumulation of strongly or irreversibly adsorbed species commonly referred to as a heel. Heel buildup on activated carbon during cyclic adsorption-regeneration results in a progressive decline in AC's adsorption capacity and operation lifetime [5-8]. Heel buildup can be due to: (i) chemisorption of adsorbates or their reaction by-products, (ii) adsorbate decomposition (i.e., char formation) [9], and (iii) accumulation of non-desorbed physiosorbed species due to insufficient regeneration.

Previous studies reported that regeneration operating conditions, adsorbent characteristics and adsorbate properties exert great influence on the magnitude and nature of heel formed on activated carbon [7, 9-22]. In particular, the extensive research by our group on conductive heating regeneration of AC indicated that regeneration temperature [11, 17], heating rate [16], purge gas type [17, 19, 22], and purge gas flow rate [16] significantly affect the desorption efficiency and heel buildup. For instance, it was found that low purge gas flow rate [16] and high oxygen impurity [17, 19, 22] in purge gas [13,23] can accelerate heel buildup. Regeneration temperature can have a negative or positive impact on heel

buildup depending on purge gas oxygen content [17]. On the other hand, with regard to the adsorbent and adsorbate, higher heel buildup values were observed for activated carbons with higher micropore volume [20], non-hierarchical pore structure [14], and higher surface oxygen content [12, 21], and for adsorption of heavy and/or bulky VOCs (i.e., high molecular weight and/or large kinetic diameter) [15]. However, in these works, the effect of one individual parameter [11, 15, 19-22] (or rarely two parameters [16, 17]) on heel buildup was evaluated, limiting one's ability to clearly delineate the interconnections between these parameters and their overall impact on heel buildup.

Machine learning (ML) is one of the most powerful tools to develop non-linear complex models and represent the dependency between output and input values. Machine learning algorithms have shown excellent performance in many chemical engineering problems including adsorption [23-30]. Zhu et al.[30] modeled the adsorption of heavy metals in water on 44 biochars considering the biochar characteristics, metal properties, and process conditions as input variables. Both deep neural network (DNN) and random forest (RF) offered high predictive performance for adsorption efficiency (R^2>0.94). Developed RF models indicated that biochar characteristics, especially cation exchange capacity and pH, have the greatest influence on the adsorption efficiency. In another study, Mendoza-Castillo et al. [31] used DNN to predict the multi-component adsorption of heavy metal ions on char. They suggested that an adsorption capacity-based DNN model would provide better predictions of multi-component adsorption behavior compared to an equilibrium concentration-based one. Toyao et al. [32] developed a ML model to predict adsorption energies of CH_4 related species on Cu-based alloys for methane conversion and compared the predictions with density functional theory (DFT) calculations. The ML model was acceptably accurate and much less time-consuming than first-principles methods, allowing screening of a large number of catalysts.

Knowledge of heel buildup is crucial to assess the long-term performance of an adsorbent in adsorption-regeneration processes. Heel buildup can be experimentally investigated via cyclic adsorption-desorption tests; however, such procedures are time and resource consuming and it is onerous to include all the variables that affect heel formation (i.e., adsorbate/adsorbent properties and adsorption/regeneration conditions) in the experimental design. In this context, machine learning methods can be applied to the data available in the literature to learn/model complex relationships between dependent and independent variables associated with heel formation and predict the rate and extent of heel buildup. In the present work, two ML algorithms, deep neural network (DNN) and extreme gradient boost (XGBoost), that have demonstrated satisfactory results in the field of adsorption [26, 28-30] were applied. A dataset consisting of 411 experimental tests on cyclic adsorption/desorption of VOCs on different ACs conducted by our research group was used for training and testing the selected ML algorithms. The inputs for DNN and XGBoost included adsorbent characteristics (e.g., surface area, pore volume, etc.), adsorbate properties (e.g., boiling point, molecular weight, dipole moment, etc.), desorption conditions, and adsorption capacity while the target variable was heel buildup. The aim is to accurately predict/model heel buildup on different ACs based on relevant parameters, compare the performance of ML algorithms for prediction of heel buildup, and investigate its partial dependency on key parameters to verify the models' reliability.

4.2 Materials and Method

4.2.1 Data Collection and preprocessing

The experimental data (420 tests) used in this study were compiled from our previous published works on single-compound, cyclic adsorption of VOCs on activated carbon [11, 12, 14, 17, 19, 20]. In all these experiments, regeneration of AC was done by conductive heating under a purge gas flow

(most often nitrogen) to desorb adsorbed VOCs. All adsorption tests were conducted at room temperature (21-25°C) and continued until the AC reached full saturation for the given conditions. Afterwards, exhausted AC underwent regeneration (desorption) and then cooling. During regeneration, the adsorbent bed was heated to the desired regeneration temperature and kept at that temperature for three hours, typically, while flowing purge gas through the bed. In the cooling step, heating was stopped but purge gas flow continued for an hour, typically. Schematics of the adsorption-regeneration set-up, details of each stage of the process and characterization of AC, and data analysis can be found elsewhere [12, 14, 19, 22].

Heel buildup refers to the adsorbed species that could not be removed from the adsorbent at the prescribed regeneration conditions. Here, heel buildup, the target variable, is defined as follows:

$$\text{heel buildup (\%)} = \frac{W_{(AD)}^{k} - W_{(BA)}^{k}}{W_{(BA)}^{1}} \times 100 \quad (1)$$

where $W_{(BA)}^{k}$ and $W_{(AD)}^{k}$ respectively denote the weight of adsorbent before adsorption and after desorption in the k^{th} cycle.

The candidate parameters that are considered as the input features in developing the ML models for heel buildup are classified as:

(i) Adsorbent characteristics: mesopore and macropore volume (cm^3/g), micropore volume (cm^3/g), surface oxygen to carbon ratio (molar %), and BET surface area (m^2/g) of virgin AC.

(ii) Regeneration parameters: cycle number, regeneration temperature (°C), purge gas oxygen content (ppm_v), and normalized purge gas flow rate.

$$\text{Normalized purge gas flow rate } \left(\frac{SLPM}{cm^2}\right) = \frac{flow\ rate(SLPM)}{Cross\text{-}sectional\ area\ of\ AC\ bed\ (cm^2)} \quad (2)$$

The adsorbent bed cross sectional area is used here to account for the difference in adsorbent bed cross sectional areas among the tests in the dataset.

(iii) Adsorbate properties: boiling point (°C), molar refraction (MR, $\frac{\mathrm{cm}^3}{\mathrm{mol}}$), and Abraham descriptors [33-35] including the adsorbate's effective H-bonding acidity (A) which represents electron accepting capability, effective H-bonding basicity (B) which represents electron donating capability, dipolarity/polarizability (S), the log of the hexadecane−air partition coefficient (L), and excess molar refraction (E, $\frac{\mathrm{cm}^3}{10\times\mathrm{mol}}$) , which is the difference between adsorbate MR at 20 °C and that of a hypothetical alkane of the same molar volume [36].

MR was calculated using the following equation [35] :

$$MR = \frac{(n^2-1)\mathrm{MW}}{(n^2+2)\,\rho} \quad (3)$$

Where n, MW ($\frac{\mathrm{g}}{\mathrm{mol}}$) and ρ ($\frac{\mathrm{cm}^3}{\mathrm{mol}}$) denote adsorbate refractive index, molecular weight and density, respectively.

The Abraham features have been proven to be useful to describe various physicochemical properties of organic chemicals [37] and are collected from the UFZ-LSER online database [38]. The adsorbent characterization data and adsorption/regeneration operating conditions are reported elsewhere [11, 14, 17, 19-21, 39]. The statistical distribution of input and output variables are depicted in Fig. 4-1.

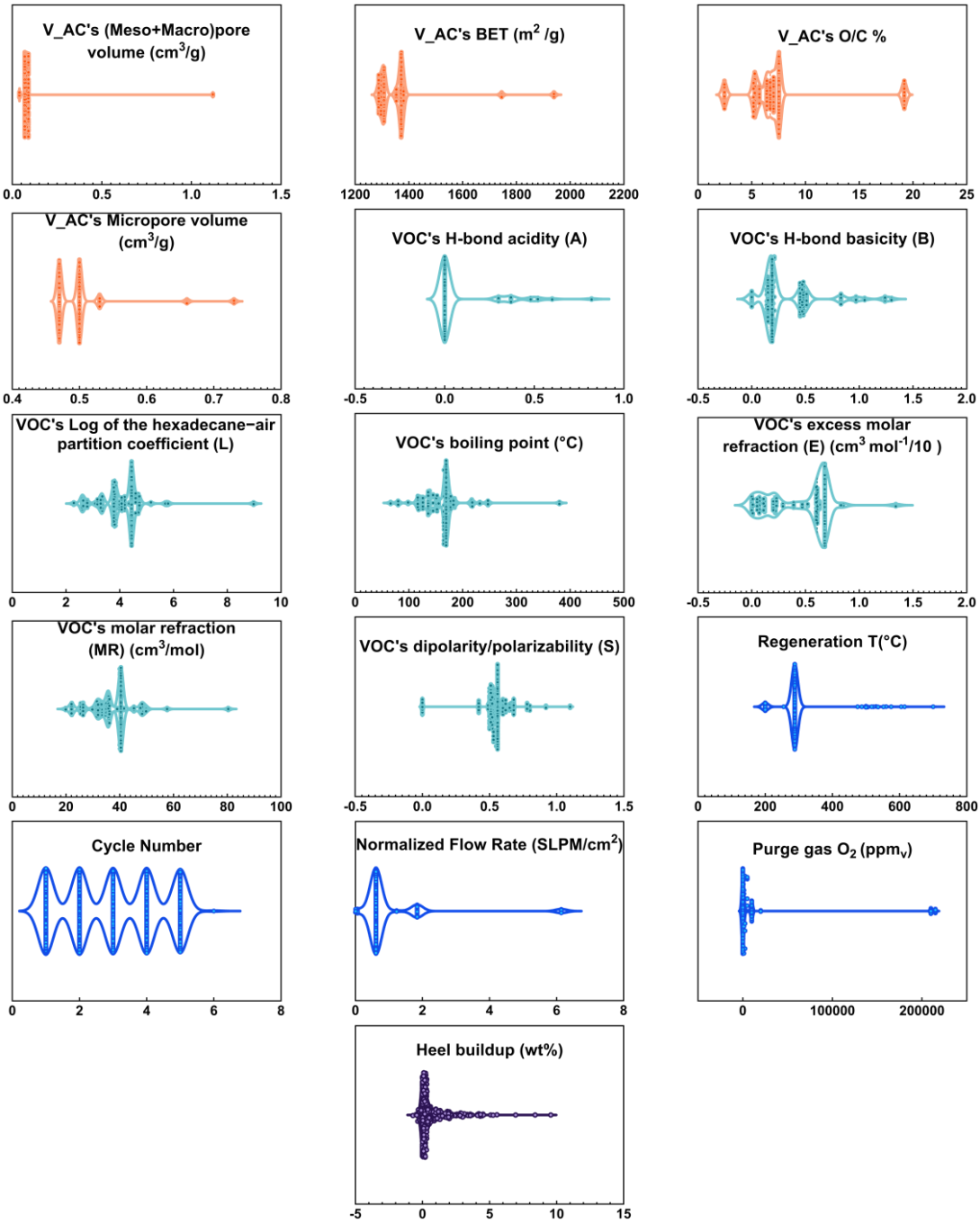

Fig. 4-1. Distribution of target variable (purple) and input features related to regeneration steps (blue), adsorbent characteristics (orange), and adsorbates properties (green). V_AC denotes virgin activated carbon.

Pearson correlation coefficient (PCC) was used to measure linear dependencies between any two features and between any particular feature and the target parameter. PCC varies between -1 and +1, with -1 indicating a strongly negative correlation, +1 a strongly positive correlation, and 0 the absence of a linear correlation. When two features have a PCC close to +1 or -1, one feature can be removed since they both are providing the same information to the model. PCC between two features, α and β, is calculated as follows:

$$PCC_{\alpha\beta} = \frac{\sum_{i=1}^{n}(\alpha_i-\bar{\alpha})\sum_{i=1}^{n}(\beta_i-\bar{\beta})}{\sqrt{\sum_{i=1}^{n}(\alpha_i-\bar{\alpha})^2}\sqrt{\sum_{i=1}^{n}(\beta_i-\bar{\beta})^2}} \quad (4)$$

where $\bar{\alpha}$ and $\bar{\beta}$ represent the average value of α and β among all samples.

The PCCs between any two features used in this study are provided in Fig. 4-2. In training and testing of ML algorithms, two features, virgin AC micropore volume and the hexadecane-air partition coefficient, L, were excluded due to high linear correlation with virgin adsorbent BET surface area ($PCC_{\text{Micropore volume \& BET}} = 0.99$) and MR ($PCC_{\text{L \& MR}} = 0.93$), respectively.

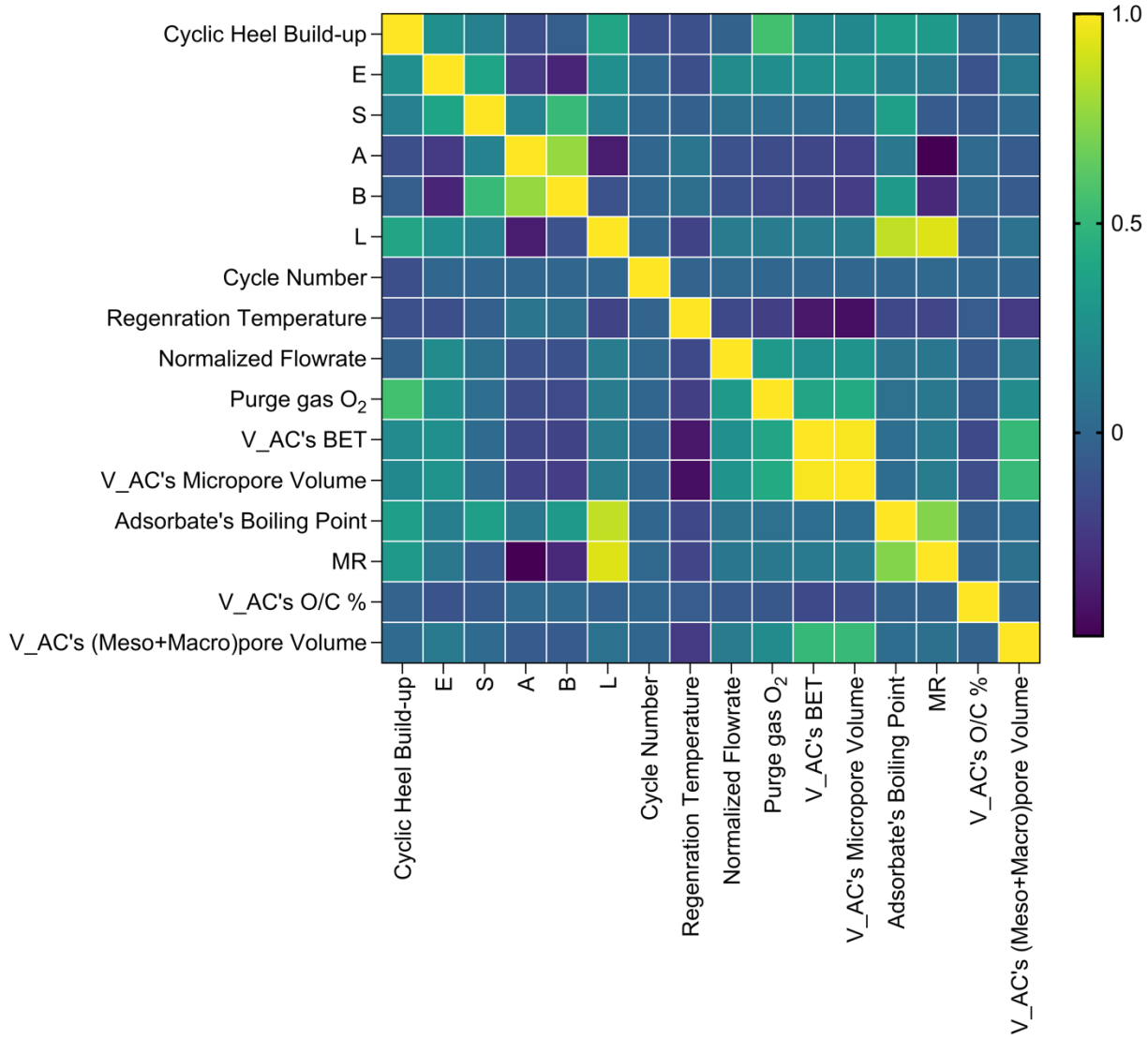

Fig. 4-2. Pearson correlation coefficient between study features and between any particular feature and cyclic heel build-up.

4.2.2 Extreme gradient boosting

XGBoost, developed by Chen et al [40], is a fast, flexible and scalable tree boosting method which has shown promising performance in many machine learning applications. In XGBoost, unlike other tree-based methods, regularization parameters (L1 and L2) can be added to the objective function in order to avoid overfitting. For a dataset with n samples and d features

$D\{(x_i, y_i) \mid i = 1\ to\ n,\ x_i\ \epsilon\ R^d, y_i\ \epsilon\ R\ \}$, $\hat{y}_i^{(t)}$, which is the i[th] predicted value after the model generates the J[th] tree is determined by:

$$\hat{y}_i = \sum_{j=1}^{J} f_j(x_i) \tag{5}$$

where f_j represents the j[th] tree structure.

The relationships between objective function (Φ), loss function (l , a differentiable convex function to measure the difference between prediction and real values) and the regularization terms of the XGBoost method are:

$$\Omega(f_k) = \gamma T + \alpha(\|W\|) + \frac{1}{2}\lambda \|W\|^2 \tag{6}$$

$$\Phi(J) = \sum_{i=1}^{n} l\left(y_i, \hat{y}_i^{(J)}\right) + \sum_{j=1}^{J} \Omega(f_j) \tag{7}$$

where α and λ are the L1 and L2 regularization terms on weights, $\|W\|$ and $\|W\|^2$ denote the L1-norm and L2-norm of the weights respectively, T denotes the number of leaves in the tree and γ determines how to prune XGBoost based on the decrease in loss function associated with adding further branches to an existing tree.

After generating the J[th] decision tree, the predicted value and objective function at $j = J^{th}$ step are as follows:

$$\hat{y}_i^J = \hat{y}_i^{J-1} + f_J(x_i) \tag{8}$$

$$\Phi(J) = \sum_{i=1}^{n} l\left(y_i, \hat{y}_i^{J-1} + f_J(x_i)\ \right) + \Omega(f_J) \tag{9}$$

By applying Taylor expansion, equation (9) is approximated as follows:

$$\Phi(J) \cong \sum_{i=1}^{n} \left[l\left(y_i, \hat{y}_i^{J-1}\ \right) g_i f_J(x_i) + \frac{1}{2} h_i^2 f_J(x_i)\right] + \Omega(f_J) \tag{10}$$

where g_i and h_i are the first and second derivatives of the loss function with respect to the predicted value and are calculated as follows:

$$g_i = \frac{\partial}{\partial \hat{y}^{(J-1)}} \, l(y_i, \hat{y}^{J-1}) \tag{11}$$

$$h_i = \frac{\partial^2}{\partial \hat{y}^{(J-1)}} \, l(y_i, \hat{y}^{J-1}) \tag{12}$$

4.2.3 Deep neural network

Deep neural network can be applied to solve complex machine learning problems. It consists of interconnected neurons in input, hidden and output layers, to non-linearly map input layer parameters to target value(s) in the output layer. Each connection between neurons is associated with a specific weight, which is determined during the training process using the backpropagation algorithm [31]. Neural network consists of two cyclic steps: feed forward and back propagation. In the feed forward step, input connections transmit each layer's neurons output value to the next layer's neurons by multiplying the output value by the connection's attributed weights, and then applying an activation function on the summation of each neuron's input values. For a given dataset with n samples and d features, $\mathrm{D}\{(x_i, y_i) \mid i = 1 \; to \; n, \; x_i \in R^d, y_i \in R\}$, feed forward step in the ith neuron of the qth layer ($q \in \{0, I, Q-1\}$) of a neural network with Q hidden layers, is as follows:

$A^0 = x$ (Input data) (13)

$$z_i^{q+1} = \sum_{k=1}^{n_q - 1} w_{ik}^{q+1} A_k^q \tag{14}$$

$$A_i^{q+1} = f\left(z_i^{q+1}\right) \tag{15}$$

where, w_{ik}^q is the weight of connection between kth neuron in layer q and ith neuron in layer q+1, n_q is the number of neurons in layer q, z_i^{q+1} denotes the input value of ith neuron in layer q+1, A_i^{q+1} denotes the output value of ith neuron in layer q+1 and f is an activation function.

Leaky rectified linear (LReLU) is used as the activation function [41], which is defined as:

$$f(x) = \begin{cases} x, & x \geq 0 \\ \frac{x}{a}, & x < 0 \end{cases} \tag{16}$$

where the best value for a is determined during the hyper parameter tuning process.

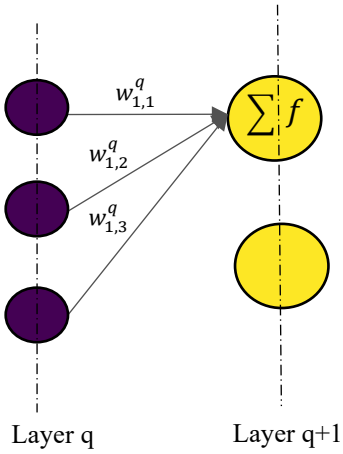

Fig. 4-3. Feed forward in neural network.

The second step is back propagation in which connections' attributed weights are adjusted through gradient descent in order to minimize the objective function:

$$\Phi = \frac{1}{n}\sum_{i=1}^{n}(y_i - \hat{y}_i)^2 + \frac{\lambda}{2n}\sum_{q=1}^{Q}\left\|W^{[q]}\right\|_F^2 \tag{17}$$

where $\left\|W^{[q]}\right\|_F^2$ is calculated as follows :

$$\left\|W^{[q]}\right\|_F^2 = \sum_{i=1}^{n_{q+1}}\sum_{k=1}^{n_q}(w_{ik}{}^{q})^2 \tag{18}$$

To avoid overfitting, L2 regularization (λ) was used. The Keras library[42] was used to build the DNN architecture and implement feed forward and back prorogation algorithms.

4.2.4 Hyper parameter tuning and model performance evaluation

Optuna framework [43], which provides a Bayesian sampling algorithm called Tree-structured Parzen estimator, was coupled with 5-fold cross validation [44] to find the optimum value for hyper parameters. For this purpose, 500 trials on suggested hyper parameters were conducted by Optuna. First, the entire dataset was randomly divided into *train* and *test* sets with an 80-20 split. Then, the *train* set was randomly divided into 5 sub samples, 4 of which serve as the *training set* and the remaining one is used for *validation*. The desired method (XGBoost or DNN) was trained and optimized on the *training* set to achieve the minimum RMSE error on the *validation* set and then was applied to the *test* set to obtain the predicted values. Finally, the predicted values ($\hat{y}$) were compared to the values obtained experimentally (y) in terms of:

$$\text{Regression coefficient } (R^2) = 1 - \frac{\sum_{i=1}^{n}(y_i - \hat{y}_i)^2}{\sum_{i=1}^{n}(y_i - \bar{y}_i)^2} \quad (19)$$

$$\text{Mean absolute error (MAE)} = \frac{\sum_{i=1}^{n}|y_i - \hat{y}_i|}{n} \quad (20)$$

$$\text{Root mean squared error (RMSE): } \sqrt{\frac{1}{n}\sum_{i=1}^{n}(y_i - \hat{y}_i)^2} \quad (21)$$

The hyper parameters that resulted in the lowest average RMSE in 5-fold cross validation were implemented in the modeling. For both XGBoost and DNN, after finding the optimum hyper parameters, the data set was randomly divided into a *training* set (64%), *validation* set (16%) and *test* set (20%). Subsequently, the ML algorithms performance on the *validation* set was monitored during the training step in order to continuously modify the *learning rate* (for DNN) and early stop the training in case of no error reduction on validation set(for XGBoost and DNN). This avoided overfitting for both methods and gradually decreased learning rate in the DNN training process. In

DNN, Adam optimizer was used, and total number of epochs, patience, and reducing factor were set to 200, 30 and 0.9, respectively, which means that, during the training process, the model goes over the entire training data for 200 times, and if in 30 epochs no improvement occurs in the model's performance on the *validation* set, its learning rate will be multiplied by 0.9. In addition, *Model_checkpoint_callback* was used to save the weights that led to minimum loss or error on the *validation* set during training and to avoid overfitting on the *training* set.

Finally, DNN/XGBoost performance was evaluated based on its prediction capability for the *test* set. Since the dataset in this research was relatively small, to ensure the generalizability of each ML method's error and performance on the entire dataset, the above-mentioned procedure was conducted 10 times and the average errors are reported.

4.3 Results and discussion

4.3.1 Comparison of DNN and XGBoost performances

The summary of the hyper parameters tuning process and optimal values of hyper parameters for DNN and XGBoost models are reported in Fig. 4-4 and Table 4-1, respectively. Regarding DNN hyper parameters tuning, as the optimization summary plot shows (Fig. 4-4 B), DNN with two hidden layers architecture outperformed one and three hidden layers DNN during hyper parameter optimization. High numbers of trainable weights in larger DNNs such as 3-layers could lead to overfitting and poor prediction due to the relatively small size of the dataset and the complexity of the underlying phenomena.

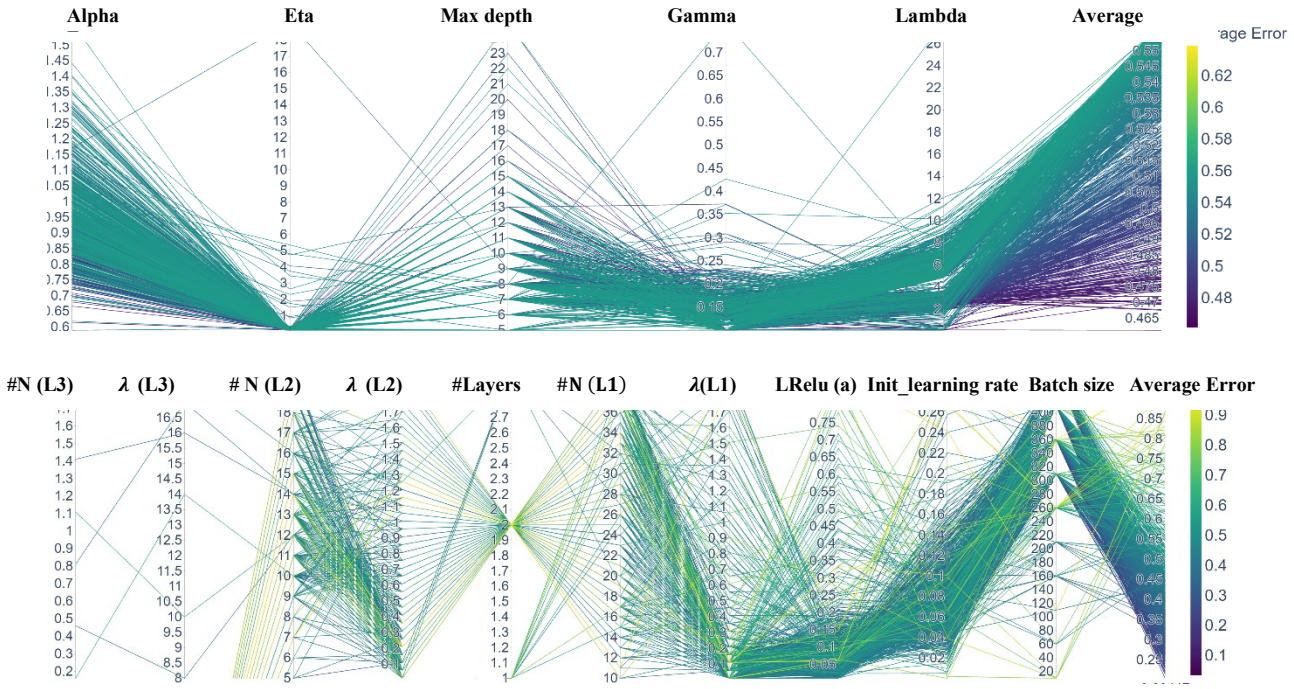

Fig. 4-4. XGBoost (A) and DNN (B) hyperparameters tuning.

Table. 4-1. XGBoost and DNN hyper parameters and their optimum values.

XGBoost		DNN	
Booster	*gbtree*	Number of hidden layers	2
Grow_policy	*depthwise*	Hidden Layers #Neurons	38,13
Alpha	0.43	1st layer λ	0.01
max_depth	9	2nd layer λ	0.01
Eta	0.72	LReLU parameter (a)	0.04
Gamma	0.11	Initial learning rate	0.13
Lambda	2.28	Batch size	460

Using the optimum hyper parameters, XGBoost and DNN algorithms were run (10 times) and the predicted heel buildup values were compared to experimentally measured values (Fig. 4-5). For both models, XGBoost and DNN, the deviations of predicted values from the measured values are relatively small. The performance of XGBoost and DNN were compared based on R^2, MAE, and RMSE values. As can be seen in Fig. 4-6, DNN significantly outperformed XGBoost in terms of prediction accuracy. The average RMSE and MAE for DNN on the test set were 0.08 ± 0.01 and 0.19 ± 0.01, respectively, and for XGBoost were 0.26 ± 0.09 and 0.28 ± 0.04. Similarly, the R^2 values for XGBoost and DNN were 0.81 ± 0.05 and 0.94± 0.03, respectively. In general, the optimized DNN model showed negligible overfitting error while XGBoost performance decreased substantially on the test set relative to the training set, as shown in Fig.4-5.

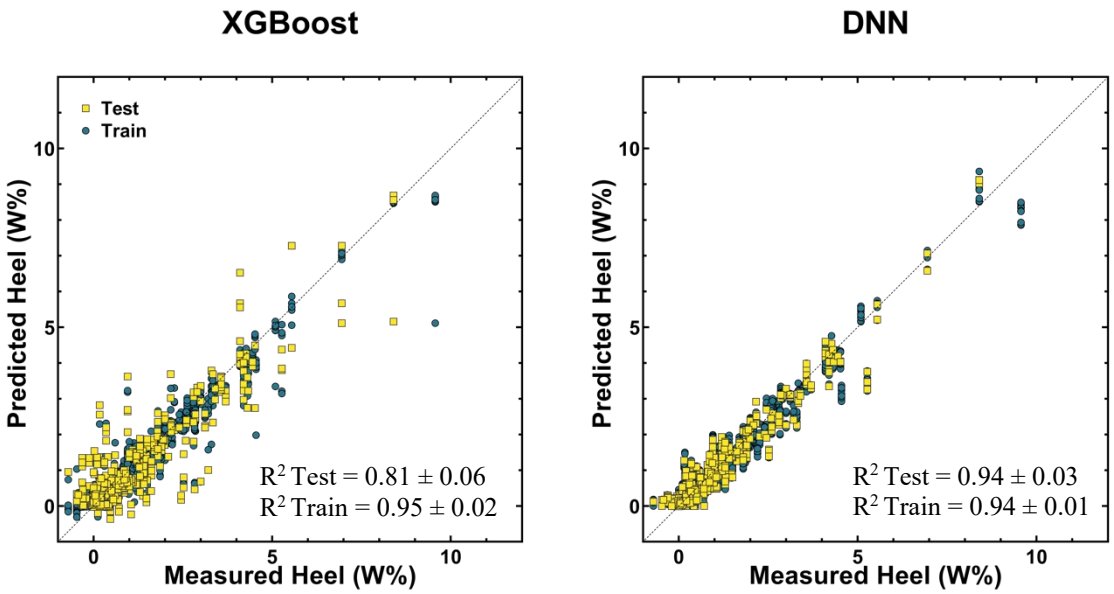

Fig. 4-5. Comparison of predicted and experimentally measured heel buildup values for XGBoost and DNN over 10 runs with random sampling

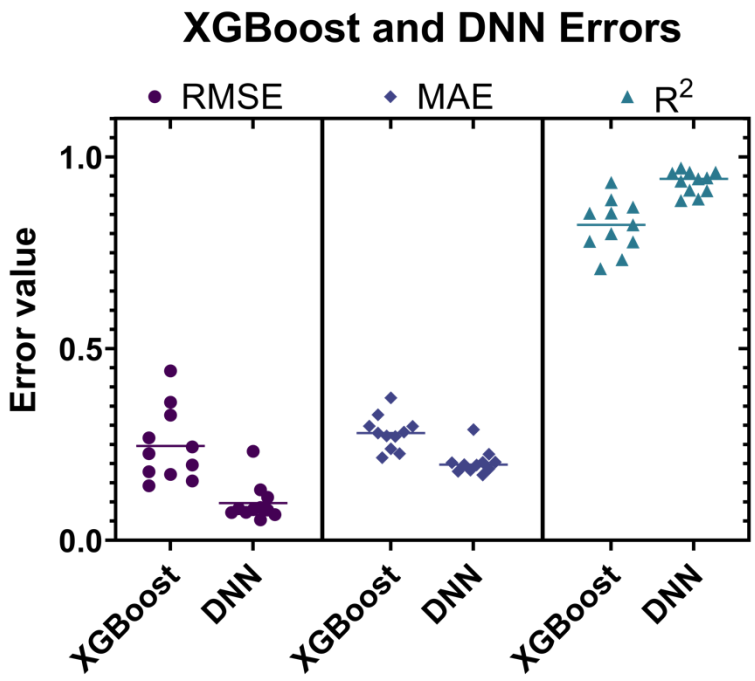

Fig. 4-6. Comparison between DNN and XGBoost models' predictive abilities in 10 different runs with random sampling.

4.3.2 Heel buildup partial dependency on selected parameters

DNN was selected to generate partial dependency plots since it outperformed XGBoost and showed high predictive ability, low variance in different runs and low overfitting error. Heel buildup partial dependency on each individual feature is reported in Supplementary Information (SI). A SHapley Additive exPlanations (SHAP) [45] summary plot (Fig. 7) provides some insight on the impact of each parameter on heel buildup. Features are ordered based on their importance, defined as the average of absolute changes imposed on the predicted values by varying features within their range. Each point represents a single cycle result, its color represents the parameter value, and its X-axis position (SHAP value, wt%) represents the expected change in predicted heel buildup compared to the prediction when a feature has its baseline value.

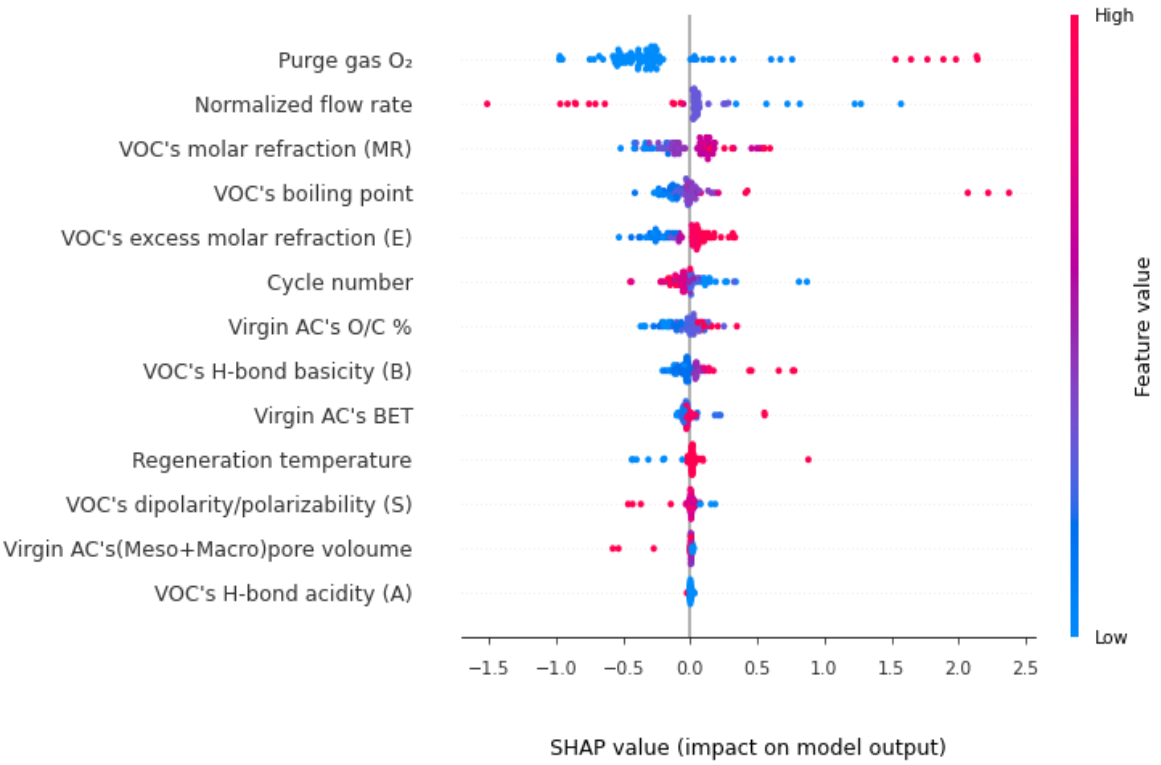

Fig. 4-7. SHAP summary plot of prediction of heel buildup using DNN. Each dot represents an instance, its color represents the feature value and its X-axis position (SHAP value, wt%) represents the expected change in predicted heel buildup compared to the prediction when feature took some baseline value.

Numerous factors were identified that exacerbate heel buildup, including the following: adsorption/regeneration in early cycles (i.e. low cycle number), low purge gas flow rate, high purge gas oxygen impurity, virgin AC with low meso+macro pore volume, and virgin AC with high O/C ratio. Adsorbate properties that contribute to heel building include high boiling point, high excessive and absolute molar refraction, high basicity or electron donating capability, low dipolarity/polarizability and low acidity. Although the data suggest a positive correlation between heel buildup with virgin AC BET surface area (or micropore volume) and virgin AC's O/C % , some of the experimental data were inconsistent suggesting that the depedencies may be affected by other parameters. The same consideration may be true for regeneration temperature. Based on the literature it can be concluded that the AC's "meso+macro" pore volume and the purge gas

oxygen impurity are the most important parameters affecting the impact of BET surface area and regeneration temperature on heel buildup, respectively [14, 17].

To evaluate the reliability of developed DNN algorithm and thoroughly investigate the effect and/or co-effect of adsorbate and adsorbent properties as well as regeneration parameters on heel buildup, the dependency plots shown in Figures 8 a to h were generated. Since the dataset is relatively small, in each run some important samples might not have been in the training set to be learned by the ML algorithm; therefore, the least important features (such as adsorbate's effective H-bonding–A), might show a different partial dependency in some runs. However, the most frequently repeated partial dependency plots are provided here.

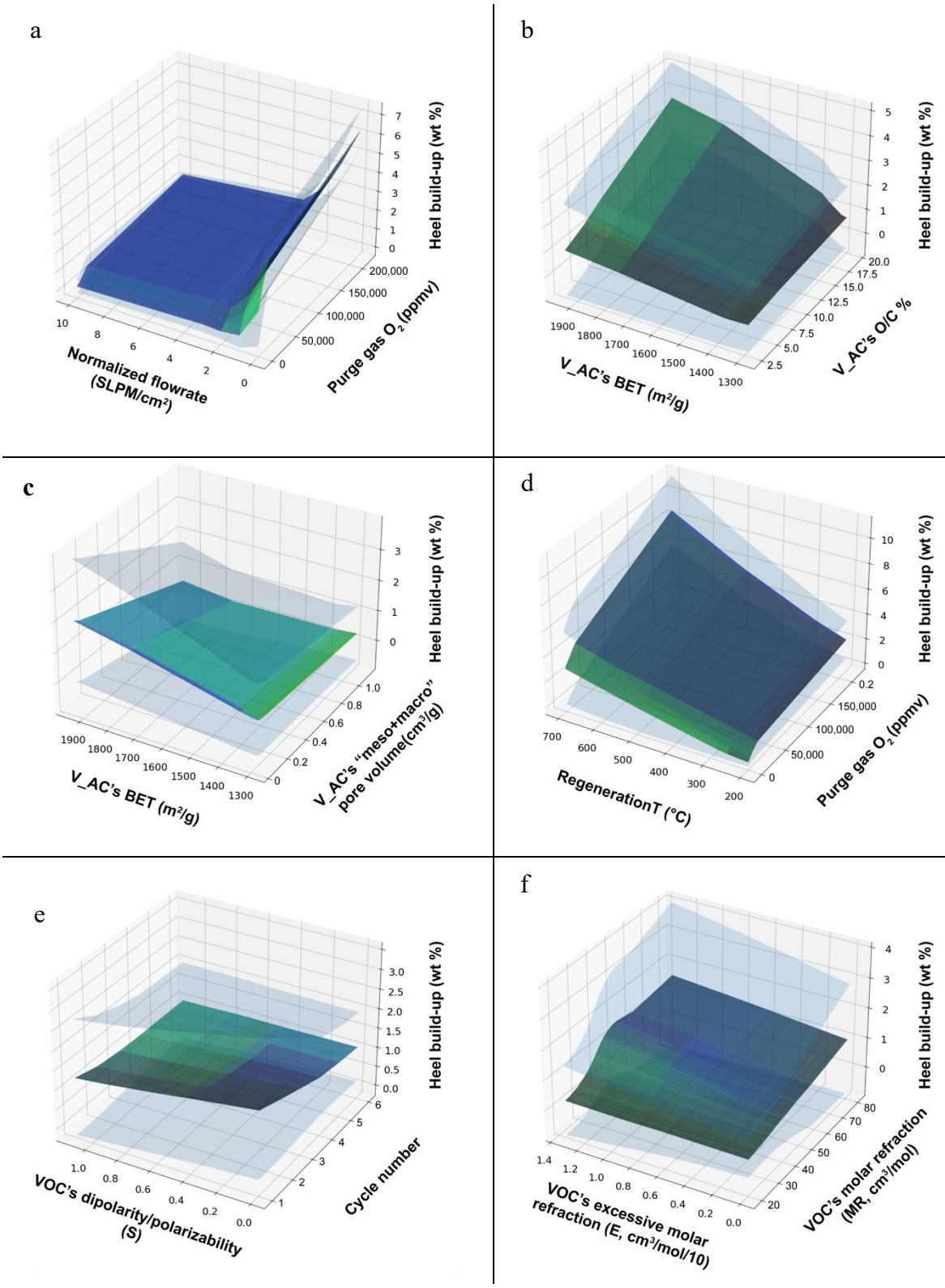
a
Heel build-up (wt %)
Normalized flowrate (SLPM/cm²)
Purge gas O2 (ppmv)
b
Heel build-up (wt %)
V_AC's BET (m²/g)
V_AC's O/C %
c
Heel build-up (wt %)
V_AC's BET (m²/g)
V_AC's "meso+macro" pore volume(cm³/g)
d
Heel build-up (wt %)
RegenerationT (°C)
Purge gas O2 (ppmv)
e
Heel build-up (wt %)
VOC's dipolarity/polarizability (S)
Cycle number
f
Heel build-up (wt %)
VOC's excessive molar refraction (E, cm³/mol/10)
VOC's molar refraction (MR, cm³/mol)

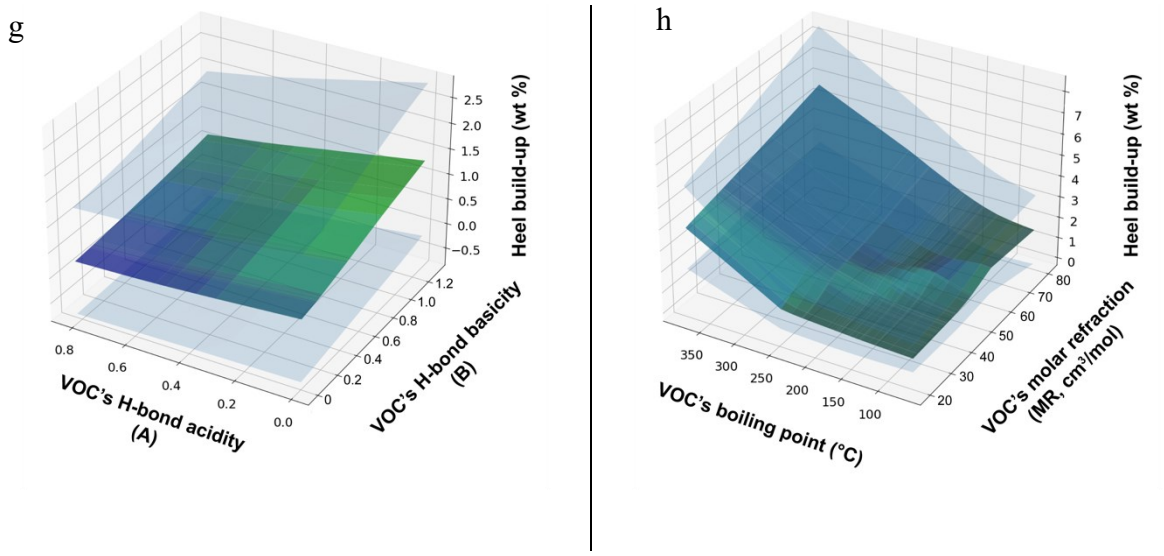

Fig. 4-8. Partial dependency of heel buildup per cycle on a) normalized flow rate (SLPM/cm^2) and purge gas O_2 impurity (ppmv), b) virgin AC' BET surface (m^2/g) and its O/C%, c) Virgin AC's (meso+macro)pore volume (m^3/g) and its BET surface (m^2/g) , d) regeneration temperate (°C) and purge gas O_2 impurity (ppmv) e) cycle number and adsorbate's S-descriptor, f) adsorbate's E-descriptor (cm^3.mol^{-1} /10) and adsorbate's MR (cm^3. mol^{-1}**), g)** adsorbate's A- descriptor and B-descriptor, h) adsorbate's boiling point (°C) and adsorbate's MR (m^3/mol). Gray planes represent variation (upper and lower limit) in the model output.

4.3.2.1 Interaction of oxygen impurity and normalized flow rate

The effect of purge gas oxygen impurity and normalized flow rate on heel buildup is illustrated in Fig. 4-7a. As could be expected from the experimental observations [16, 17, 19, 22], both regeneration parameters have a large impact on the extent of heel buildup on activated carbon during adsorption/desorption of organic compounds. There are also economic and performance trade-off relationships for purge gas purity, purge gas flow rate and heel buildup that must be considered when selecting optimal regeneration conditions [19, 46]. As can be seen in Fig. 4-7a, regardless of the applied normalized flow rate, the heel buildup is more severe on saturated activated carbons that are regenerated with N_2 purge gas containing O_2 impurity. Presence of O_2 in the purge gas induces unwanted chemical reactions between oxygen and adsorbate molecules. It has been found that oxygen reaction with aromatic compounds produces heavy polymeric by-products [47, 48], which

require more energy (i.e., higher regeneration temperature or longer duration) to be removed from the adsorbent. Thermal-oxidation of non-desorbed VOCs during thermal regeneration is a primary mechanism that accounts for the majority of heel buildup in these experiments [19]. Based on the model's outcomes, heel formation is positively correlated with the purge gas oxygen content, meaning that at a certain temperature and flow rate, as the oxygen impurity in the purge gas increases, more non-desorbable species are formed on the activated carbon. The amount of heel buildup and the oxygen impact on heel formation depend on the nature of adsorbate and its reactivity with oxygen[19]. From an economic perspective, the power consumption associated with nitrogen generation rapidly increases with nitrogen purity and with greater flow rate [46]. An increase in the purge gas flow rate during thermal regeneration improves mass transfer and desorption efficiency by shortening VOCs residence time inside AC pores and creating a steep concentration gradient between the AC surface and bulk flow [16]. In Fig. 4-8a, in the high normalized flow rate region (> 4), especially when oxygen concentration is low, an increment in the purge gas normalized flow rate brings about a less significant reduction in the heel buildup compared to a similar change in the low flow rate region. This indicates that there is an optimum flow rate for each specific purge gas oxygen impurity, at which a better trade-off between the activated carbon long-term performance and the regeneration cost can be achieved. Hence, for industrial applications, optimization of the flow rate can be an efficient tool to minimize heel buildup when providing high purity purge gas is not feasible. Likewise, if system down-sizing is desired or operating limitations do not allow high flow rates, purge gas purification should be considered to avoid heel formation.

4.3.2.2 Interaction of of virgin activated carbon BET surface area and surface oxygen groups

The combined effects of activated carbon BET surface area and surface atomic oxygen to carbon ratio on heel buildup are shown in Fig. 4-8b. Since in this dataset BET surface area of virgin activated carbon was linearly correlated with micropore volume, only the BET surface area was used for developing the ML models; however, the information in Fig. 4-8b provides insight on the impact of micropore volume on heel buildup as well. As shown in Fig. 4-8b, for activated carbons with the same O/C ratio, samples with larger BET surface areas (or micropore volumes) exhibit greater heel buildups. The underlying cause is the high adsorption energy of VOCs in micropores which result from the overlapping of attractive forces on adsorbates in narrow channels from the surrounding walls [13, 49]. In addition, diffusional limitations in micropores, particularly when adsorbate molecular size is comparable to that of AC's pores [20, 21, 50], could also account for heel buildup in extremely microporous adsorbents. It has also been suggested that the presence of oxygen groups on AC surface promotes the chemisorption of VOCs during adsorption [21]. On the other hand, surface oxygen groups can participate in reactions with adsorbed VOCs and form high boiling point oxidation by-products [21]. In either case (chemisorption or formation of by-products), activated carbons with higher O/C ratios are more vulnerable to heel buildup because higher energy is required to desorb heavy oxidation by-products and/or chemisorbed VOC molecules. It should be highlighted that the observed trends for heel buildup with variations in activated carbon surface area and O/C ratio are consistent with the experimental data in the literature [12, 14, 20, 21].

4.3.2.3 Interaction of virgin activated carbon BET surface area and mesoo-/macropore volume

Previous experimental investigations of the role of activated carbon's porous structure on heel formation have indicated that activated carbon's meso-macroporosity has a substantial influence on the extent of heel buildup [14]. As shown in Fig. 4-8c, during cyclic adsorption-regeneration, for

adsorbents with the same BET surface area, less heel is formed on activated carbons with greater "meso+macro" pore volumes. This behavior can be justified from different aspects. One reason is that in ACs with very high microporosity, narrow micropore channels hamper the diffusion of adsorbates to the surface during the desorption process, increasing the amount of non-desorbed VOCs (or heel) [14]. On the other hand, the impediment of VOCs diffusion by micropores prolongs the residence time of adsorbates in the AC at elevated temperatures, which in turn increases the probability of VOC polymerization, pyrolysis and/or reaction with purge gas impurities. In the case of oxygen impurity, the oxidation reaction by-products are often large, bulky molecules compared to the original adsorbate and might get trapped in or strongly attached to narrow micropores, causing further heel buildup especially in ACs with high microporosity [20]. It is, therefore, reasonable to propose that to avoid excessive heel formation, microporosity of the adsorbent must not exceed a certain level. At the same time, as the developed ML model clearly indicates, the higher the "meso+macro" pore volume is, the lower the heel buildup will be. High "meso+macro" porosity allows faster mass transfer and diffusion out of the pores. Moreover, in contrast with adsorption in micropores, where superposition of wall effect results in formation of relatively strong bonds, adsorption energy on meso/macro pores is low, and the adsorbate molecules are weakly adsorbed to the BAC surface [20]. Therefore, presence of meso+macro pores can facilitate the desorption process, and adsorption on meso+macro pores is expected to be easier to reverse.

4.3.2.4 Effect of regeneration temperature and purge gas oxygen impurity

The shape of the "regeneration temperature vs. purge gas O_2 content" surface in Fig. 4-8d suggests that at a fixed purge gas O_2 level, the minimum heel could be expected when the applied regeneration temperature is around 200 °C. This is consistent with Feizbakhshan et. al.'s study on

concurrent effects of purge gas oxygen impurity and desorption temperature on heel buildup [17]. As seen in Fig. 4-8d, heel buildup increases with regeneration temperature, except for samples regenerated with low-oxygen purge gas which showed a maximum heel buildup at around 400-500 °C. On one hand, raising the regeneration temperature enhances the desorption efficiency by boosting the mass transfer and diffusion rates, especially for heavy molecules adsorbed in micropores [11, 51, 52]. However, for purge gas with oxygen impurity, higher regeneration temperature increases the rate of the oxidative reactions between O_2 and organic species. Based on Collision theory, reaction rate is directly correlated to frequency of collisions between the reactants [53], and as the kinetic energy increases with increment in the desorption temperature, rate of oxidation reactions on activated carbon rise. Therefore, in the presence of oxygen, high regeneration temperature could have both adverse (more oxidation by-products) and favorable (higher desorption rate) impacts on heel formation, however, with increasing regeneration temperature, the adverse effect becomes dominant. In low-temperature desorption, the driving force is insufficient; consequently, adsorbates, especially the ones in micropores, remain non-desorbed. It is logical to conclude that the heel buildup accruing at low and high temperature is attributable to non-desorbed physisorbed and chemisorbed species, respectively. It should be noted that carbon loss in the TGA of AC samples at very high temperatures (>750 °C) [20], might partially contribute to the decrement in observed and subsequently predicted heel buildup values at these high regeneration temperatures.

4.3.2.5 Effect of cycle number

The effect of cycle number on heel buildup is shown in Fig. 4-8e. For a specific adsorption test set, the virgin activated carbon's surface area is one of the most influential parameters for the prediction of n^{th} cycle (n=1 to 5) heel buildup. As mentioned before (section 3.2.1), there is a

relationship between heel buildup and adsorbent surface area (or micropore volume); a higher heel buildup is expected for adsorbents with larger surface area or micropore volume. On the other hand, it is reported that the adsorbent's surface area and micropore volume linearly decrease with cumulative heel [19]. In cycle 1 (with virgin AC), the highest surface area and the narrowest pores are available, and naturally, maximum heel is formed in comparison with subsequent cycles. Blockage of narrow and accessible micropore channels by non-desorbed species or large molecules produced via oxidation, polymerization and/or pyrolysis reactions during regeneration is the main reason. Fig. 4-8e shows that there is a gradual decrease in cyclic heel buildup as the process proceeds, suggesting that after a certain number of cycles, the heel buildup rate in each adsorption/regeneration cycle would approach a steady value. On the other hand, adsorbate dipolarity/polarizability (S) seems to have a minor negative contribution on heel buildup, as explained in the next section.

4.3.2.6 Effect of adsorbate's properties (A, B, boiling point, MR, and S)

The adsorbate' properties greatly influence the adsorption capacity and desorption efficiency during cyclic operations. Abraham descriptors of the adsorbate can be related to major mechanisms contributing to heel buildup. The adsorbate excess molar refractivity (E), molar refraction (MR), boiling point, basicity (B), dipolarity/polarizability (S), and acidity (A) are shown to contribute to heel build up, in that order (Fig. 4-8). The effect of MR and E on heel build up is shown in Fig. 4-8e. The dominance of MR and E in determining heel buildup among Abraham descriptors (Fig. 4-7), and their positive correlation with heel buildup (Fig. 4-8f) demonstrate that heel buildup proceeds mainly through London dispersive interaction and interaction through π or n electrons, respectively. Interestingly the results of the partial dependency plots produced by DNN are in excellent agreement with the findings of previous studies which conducted derivative

thermogravimetric (DTG) analysis on spent ACs to quantify physiosorbed and chemisorbed heel species. It has been reported that heel buildup is mainly due to accumulation of non-desorbed physiosorbed species [10-12, 16, 17, 19-21], which may further undergo thermal oxidation or pyrolysis based on presence or absence of oxygen in the purge gas [10]. In addition, they considered chemisorbed species and by-products of adsorbed species reactions as the second contributor to heel buildup. Van der Waals interactions described by MR and E-descriptor can be attributed to physiosorbed species while H-bonding interactions described by B- and A-descriptors can be attributed to chemisorbed species. It should be noted that S-descriptor accounts for dipole−dipole and dipole−induced dipole interactions other than H-bonding and hence has some overlap with E and MR.

According to Dubinin-Radushkevich (D-R) model [54] which is commonly used to estimate AC adsorption capacity for VOCs, the adsorption capacity (W) is calculated as follows:

$$W = \frac{W_o}{\rho}\ exp\left(-k\frac{\left(\mathrm{RT}\ ln(-k\frac{P_0}{P})\right)^2}{\beta^2}\right) \tag{22}$$

In this equation, β is affinity coefficient which is determined exclusively based on adsorbate properties. β can be calculated as the ratio of MR of the test adsorbate to that of a reference adsorbate ($MR_{ref,}$)[55]:

$$\beta = \frac{Pe}{Pe_{\ ref}} = \frac{MR}{MR_{\ ref}} \tag{23}$$

Therefore, an increase in MR is associated with an increase in adsorption capacity which contributes to heel buildup. This is understandable because the entrapment of more adsorbates in activated carbon (or a higher adsorption capacity) (i) increases the probability of adsorption on highest energy active sites (e.g., narrow micropores), (ii) necessitates more energy input for

complete regeneration, and (iii) restricts the diffusion/removal of adsorbed species out of AC's pores in a given time (i.e., regeneration duration).

The adsorbate's H-bond basicity (B) is another important adsorbate property (Fig. 4-8g) contributing to heel buildup. Higher heel buildup is expected for VOCs with high electron donation capability, however, acidity among the majority of ACs used in this study were slightly higher than basicity [12, 14, 19, 20]. Therefore, for basic AC's a different correlation might be observed since the acidity of the AC's makes the acid-base interaction with adsorbates more favorable. In contrast with adsorbate basicity, its acidity shows a minor negative impact on heel buildup. Moreover, as shown in Fig. 4-8e, the adsorbate's dipolar type interaction capability (S) has a minor negative impact on heel buildup, and the AC samples of the study have low tendency to form irreversible bonds through the dipole-dipole and dipole-induced dipole interaction with VOC species.

Finally. the DNN model indicates that heel buildup is directly correlated with adsorbate's boiling point (Fig. 4-8h,). Previous studies [15, 39, 56] showed that adsorbates with high boiling point and/or high molecular weight tend to have higher heel buildup at a constant temperature since the regeneration driving force is correlated with the difference between applied temperature and adsorbate's boiling point [17]. The effect of molecular weight has already been considered as a part of MR parameter and hence was not included in this study.

4.4 Conclusion

XGBoost and deep neural network were applied to predict heel buildup for cyclic adsorption/desorption of VOCs on activated carbon based on adsorbent properties, adsorbate characteristics, and adsorption/regeneration parameters. For this purpose, a data set including 411 experimental tests of VOC cyclic adsorption/desorption on activated carbon were collected from the literature. 5-fold cross validation was coupled with Bayesian sampling algorithm to optimize

both algorithms' hyperparameters. Both machine learning algorithms showed reasonable accuracy in predicting the cyclic heel formation, however DNN outperformed XGBoost (e.g., $R^2_{ANN} = 0.94$, $R^2_{XGBoost} = 0.81$). Partial dependency plots between heel buildup and regeneration parameters, adsorbent characteristics and adsorbate describing Abraham parameters were generated to study the simultaneous effects of some of the most important features on heel buildup and to verify the models' reliability.

It was demonstrated that purge gas flow rate and O_2 impurity, cycle number, and the adsorbate's molar refraction (MR, or capability of non-specific dispersive interaction) and excessive molar refraction (E, interactions through π or n electrons) have the most noticeable impacts on the extent of heel buildup. The findings presented in this study can assist in the selection of adsorption/desorption operating conditions to minimize heel buildup over activated carbon in cyclic adsorption/desorption processes. Moreover, the correlations developed between the adsorbent/adsorbate properties and heel buildup can be used to choose suitable adsorbent(s) for a specific application.

4.5 Reference

1. Suzuki, M.; Suzuki, M. *Adsorption Engineering.* Kodansha Tokyo: 1990.

2. Khan, F.I.; Kr. Ghoshal, A. Removal of Volatile Organic Compounds from Polluted Air. *Journal of Loss Prevention in the Process Industries* **2000,** *13* (6), 527-545; https://doi.org/10.1016/S0950-4230(00)00007-3.

3. Ruthven, D.M. *Principles of Adsorption and Adsorption Processes.* John Wiley & Sons: 1984.

4. *Selecting Equipment to Control Air Pollution from Automotive Painting Operations*; SAE Technical Paper Series; https://saemobilus.sae.org/content/920189.

5. Yun, J.; Choi, D.; Moon, H. Benzene Adsorption and Hot Purge Regeneration in Activated Carbon Beds. *Chemical Engineering Science* **2000,** *55* (23), 5857-5872; https://doi.org/10.1016/S0009-2509(00)00189-5.

6. Dąbrowski, A.; Podkościelny, P.; Hubicki, Z.; Barczak, M. Adsorption of Phenolic Compounds by Activated Carbon—a Critical Review. *Chemosphere* **2005,** *58* (8), 1049-1070; https://doi.org/10.1016/j.chemosphere.2004.09.067.

7. Aktaş, Ö; Çeçen, F. Effect of Type of Carbon Activation on Adsorption and Its Reversibility. *Journal of Chemical Technology & Biotechnology: International Research in Process, Environmental & Clean Technology* **2006,** *81* (1), 94-101.

8. Popescu, M.; Joly, J.P.; Carré, J.; Danatoiu, C. Dynamical Adsorption and Temperature-Programmed Desorption of VOCs (Toluene, Butyl Acetate and Butanol) on Activated Carbons. *Carbon* **2003,** *41* (4), 739-748; https://doi.org/10.1016/S0008-6223(02)00391-3.

9. Niknaddaf, S.; Atkinson, J.D.; Shariaty, P.; Jahandar Lashaki, M.; Hashisho, Z.; Phillips, J.H.; Anderson, J.E.; Nichols, M. Heel Formation During Volatile Organic Compound Desorption from Activated Carbon Fiber Cloth. *Carbon* **2016,** *96*, 131-138; 10.1016/j.carbon.2015.09.049.

10. Jahandar Lashaki, M.; Hashisho, Z.; Phillips, J.H.; Crompton, D.; Anderson, J.E.; Nichols, M. Mechanisms of Heel Buildup During Cyclic Adsorption-Desorption of Volatile Organic Compounds in a Full-scale Adsorber-Desorber. *Chemical Engineering Journal* **2020,** *400*, 124937; 10.1016/j.cej.2020.124937.

11. Jahandar Lashaki, M.; Fayaz, M.; Wang, H.; Hashisho, Z.; Philips, J.H.; Anderson, J.E. Effect of Adsorption and Regeneration Temperature on Irreversible Adsorption of Organic Vapors on Beaded Activated Carbon. *Environmental Science & Technology* **2012,** *46* (7), 4083-4090; 10.1021/es3000195.

12. Mosavari Nezamabad, N. Effect of Surface Oxygen Groups on Irreversible Adsorption of Volatile Organic Compounds on Beaded Activated Carbon. University of Alberta, 2017.

13. Yun, J.; Choi, D.; Moon, H. Benzene Adsorption and Hot Purge Regeneration in Activated Carbon Beds. *Chemical Engineering Science* **2000,** *55* (23), 5857-5872; 10.1016/S0009-2509(00)00189-5.

14. Feizbakhshan, M. Improving Cyclic Adsorption/Desorption Process of Volatile Organic Compounds in the Presence of Gaseous Phase Oxygen. University of Alberta, 2020.

15. Fayaz, M. Adsorption and Microwave Regeneration for Controlling Volatile Organic Compounds Emissions from Automotive Paint Booths. University of Alberta, 2016.

16. Niknaddaf, S.; Atkinson, J.D.; Gholidoust, A.; Fayaz, M.; Awad, R.; Hashisho, Z.; Phillips, J.H.; Anderson, J.E.; Nichols, M. Influence of Purge Gas Flow and Heating Rates on Volatile Organic Compound Decomposition during Regeneration of an Activated Carbon Fiber Cloth. *Industrial & Engineering Chemistry Research* **2020,** *59* (8), 3521-3530; 10.1021/acs.iecr.9b06070.

17. Feizbakhshan, M.; Amdebrhan, B.; Hashisho, Z.; Phillips, J.H.; Crompton, D.; Anderson, J.E.; Nichols, M. Effects of Oxygen Impurity and Desorption Temperature on Heel Build-up in Activated Carbon. *Chemical Engineering Journal* **2021,** *409*, 128232; 10.1016/j.cej.2020.128232.

18. Liu, Y.; Li, C.; Peyravi, A.; Sun, Z.; Zhang, G.; Rahmani, K.; Zheng, S.; Hashisho, Z. Mesoporous MCM-41 Derived from Natural Opoka and Its Application for Organic Vapors Removal. *Journal of Hazardous Materials* **2021,** *408*, 124911; 10.1016/j.jhazmat.2020.124911.

19. Hashemi, S.M.; Jahandar Lashaki, M.; Hashisho, Z.; Phillips, J.H.; Anderson, J.E.; Nichols, M. Oxygen Impurity in Nitrogen Desorption Purge Gas Can Increase Heel Buildup on Activated Carbon. *Separation and Purification Technology* **2019,** *210*, 497-503.

20. Jahandar Lashaki, M.; Atkinson, J.D.; Hashisho, Z.; Phillips, J.H.; Anderson, J.E.; Nichols, M. The Role of Beaded Activated Carbon's Pore Size Distribution on Heel Formation During Cyclic Adsorption/Desorption of Organic Vapors. *Journal of Hazardous Materials* **2016,** *315*, 42-51; https://doi.org/10.1016/j.jhazmat.2016.04.071.

21. Jahandar Lashaki, M.; Atkinson, J.D.; Hashisho, Z.; Phillips, J.H.; Anderson, J.E.; Nichols, M. The Role of Beaded Activated Carbon's Surface Oxygen Groups on Irreversible Adsorption of Organic Vapors. *Journal of Hazardous Materials* **2016,** *317*, 284-294.

22. Jahandar Lashaki, M.; Atkinson, J.D.; Hashisho, Z.; Phillips, J.H.; Anderson, J.E.; Nichols, M.; Misovski, T. Effect of Desorption Purge Gas Oxygen Impurity on Irreversible Adsorption of Organic Vapors. *Carbon* **2016,** *99*, 310-317; https://doi.org/10.1016/j.carbon.2015.12.037.

23. Fung, V.; Hu, G.; Ganesh, P.; Sumpter, B.G. Machine learned Features from Density of States for Accurate Adsorption Energy Prediction. *Nature Communications* **2021,** *12* (1), 88; 10.1038/s41467-020-20342-6.

24. Borboudakis, G.; Stergiannakos, T.; Frysali, M.; Klontzas, E.; Tsamardinos, I.; Froudakis, G.E. Chemically Intuited, Large-Scale Screening of MOFs by Machine Learning Techniques. *NPJ Computational Materials* **2017,** *3* (1), 1-7; 10.1038/s41524-017-0045-8.

25. Jäger, M.O.J.; Morooka, E.V.; Federici Canova, F.; Himanen, L.; Foster, A.S. Machine Learning Hydrogen Adsorption on Nanoclusters Through Structural Descriptors. *NPJ Computational Materials* **2018,** *4* (1), 1-8; 10.1038/s41524-018-0096-5.

26. Zhang, Y.; Xu, X. Predictions of Adsorption Energies of Methane-Related Species on Cu-Based Alloys Through Machine Learning. *Machine Learning with Applications* **2021,** *3*, 100010; 10.1016/j.mlwa.2020.100010.

27. Zhu, X.; Wan, Z.; Tsang, D.C.W.; He, M.; Hou, D.; Su, Z.; Shang, J. Machine Learning for the Selection of Carbon-Based Materials for Tetracycline and Sulfamethoxazole Adsorption. *Chemical Engineering Journal* **2021,** *406*, 126782; 10.1016/j.cej.2020.126782.

28. Oliveira, L.M.C.; Koivisto, H.; Iwakiri, I.G.I.; Loureiro, J.M.; Ribeiro, A.M.; Nogueira, I.B.R. Modelling of a Pressure Swing Adsorption Unit by Deep Learning and Artificial Intelligence Tools. *Chemical Engineering Science* **2020,** *224*, 115801; 10.1016/j.ces.2020.115801.

29. Meng, M.; Zhong, R.; Wei, Z. Prediction of Methane Adsorption in Shale: Classical Models and Machine Learning Based Models. *Fuel* **2020,** *278*, 118358; 10.1016/j.fuel.2020.118358.

30. Zhu, X.; Wang, X.; Ok, Y.S. The Application of Machine Learning Methods for Prediction of Metal Sorption onto Biochars. *Journal of Hazardous Materials* **2019,** *378*, 120727; 10.1016/j.jhazmat.2019.06.004.

31. Mendoza-Castillo, D.I.; Reynel-Ávila, H.E.; Sánchez-Ruiz, F.J.; Trejo-Valencia, R.; Jaime-Leal, J.E.; Bonilla-Petriciolet, A. Insights and Pitfalls of Artificial Neural Network Modeling of Competitive Multi-Metallic Adsorption Data. *Journal of Molecular Liquids* **2018,** *251*, 15-27; 10.1016/j.molliq.2017.12.030.

32. Toyao, T.; Suzuki, K.; Kikuchi, S.; Takakusagi, S.; Shimizu, K.; Takigawa, I. Toward Effective Utilization of Methane: Machine Learning Prediction of Adsorption Energies on Metal Alloys. *The Journal of Physical Chemistry C* **2018,** *122* (15), 8315-8326; 10.1021/acs.jpcc.7b12670.

33. Abraham, M.H.; Mcgowan, J.C. The Use of Characteristic Volumes to Measure Cavity Terms in Reversed Phase Liquid Chromatography. *Chromatographia* **1987,** *23* (4), 243-246; 10.1007/BF02311772.

34. Abraham, M.H.; Grellier, P.L.; McGill, R.A. Determination of Olive Oil-Gas and Hexadecane-Gas Partition Coefficients, and Calculation of the Corresponding Olive Oil-Water and Hexadecane-Water Partition Coefficients. *Journal of the Chemical Society, Perkin Transactions 2* **1987,** (6), 797-83; 10.1039/P29870000797.

35. Abraham, M.H.; Ibrahim, A.; Zissimos, A.M. Determination of Sets of Solute Descriptors from Chromatographic Measurements. *Journal of Chromatography A* **2004,** *1037* (1), 29-47; 10.1016/j.chroma.2003.12.004.

36. Abraham, M.H.; Whiting, G.S.; Doherty, R.M.; Shuely, W.J. Hydrogen Bonding. Part 13. A New Method for the Characterisation of GLC Stationary Phases-The Laffort Data Set. *Journal of the Chemical Society, Perkin Transactions 2* **1990,** (8), 1451-146; 10.1039/P29900001451.

37. Endo, S.; Goss, K. Applications of Polyparameter Linear Free Energy Relationships in Environmental Chemistry. *Environmental Science & Technology* **2014,** *48* (21), 12477-12491; 10.1021/es503369t.

38. UFZ-LSER Database V 3.2 [Internet]; Available from http://www.ufz.de/lserd.

39. Jahandar Lashaki, M. Understanding and Improving Gas Phase Capture of Organic Vapors by Carbonaceous Adsorbents. University of Alberta, 2016.

40. Chen, T.; Guestrin, C. XGBoost. Proceedings of the 22nd ACM SIGKDD International Conference on Knowledge Discovery and Data Mining, Association for Computing Machinery, Aug 13, 2016.

41. Xu, B.; Wang, N.; Chen, T.; Li, M. Empirical Evaluation of Rectified Activations in Convolution Network. *CoRR* **2015,** *abs/1505.00853*.

42. Gulli, A.; Pal, S. *Deep Learning with Keras.* Packt Publishing Ltd: 2017.

43. Akiba, T.; Sano, S.; Yanase, T.; Ohta, T.; Koyama, M. Optuna: A Next-generation Hyperparameter Optimization Framework. **2019**.

44. Refaeilzadeh, P.; Tang, L.; Liu, H. Cross-Validation, In *Encyclopedia of Database Systems,* LIU, L.; ÖZSU, M.T., Eds.; Springer US: 2009; pp. 532-538.

45. Lundberg, S.M.; Lee, S. A Unified Approach to Interpreting Model Predictions. Curran Associates Inc, 2017.

46. Compressed Air Best Practices, The Energy Costs Associated with Nitrogen Specifications.; http://www.airbestpractices.com/system-assessments/air-treatment/n2/energy-costs-associated-nitrogen-specifications.

47. Berndt, T.; Böge, O. Reaction of O(3P) Atoms with Benzene. *Zeitschrift Für Physikalische Chemie (Neue Folge)* **2004,** *218* (4), 391-404; 10.1524/zpch.218.4.391.29202.

48. Boocock, G.; Cvetanović, R.J. Reaction of Oxygen Atoms with Benzene. *Canadian Journal of Chemistry* **1961,** *39* (12), 2436-2443; 10.1139/v61-323.

49. Wang, Q.; Liang, X.; Zhang, R.; Liu, C.; Liu, X.; Qiao, W.; Zhan, L.; Ling, L. Preparation of Polystyrene-Based Activated Carbon Spheres and Their Adsorption of Dibenzothiophene. *New Carbon Materials* **2009,** *24* (1), 55-60; 10.1016/S1872-5805(08)60036-0.

50. Hashisho, Z.; Emamipour, H.; Cevallos, D.; Rood, M.J.; Hay, K.J.; Kim, B.J. Rapid Response Concentration-Controlled Desorption of Activated Carbon to Dampen Concentration Fluctuations. *Environmental Science & Technology* **2007,** *41* (5), 1753-1758; 10.1021/es062155y.

51. Ferro-Garcia, M.A.; Joly, J.P.; Rivera-Utrilla, J.; Moreno-Castilla, C. Thermal Desorption of Chlorophenols from Activated Carbons with Different Porosity. *Langmuir* **1995,** *11* (7), 2648-2651; 10.1021/la00007a052.

52. Kim, K.; Kang, C.; You, Y.; Chung, M.; Woo, M.; Jeong, W.; Park, N.; Ahn, H. Adsorption–Desorption Characteristics of VOCs Over Impregnated Activated Carbons. *Catalysis Today* **2006,** *111* (3), 223-228; 10.1016/j.cattod.2005.10.030.

53. Leffler, J.E.; Grunwald, E. *Rates and Equilibria of Organic Reactions.* Wiley: 1963.

54. Long, C.; Li, Y.; Yu, W.; Li, A. Removal of Benzene and Methyl Ethyl Ketone Vapor: Comparison of Hypercrosslinked Polymeric Adsorbent with Activated Carbon. *Journal of hazardous materials* **2012,** *203*, 251-256; 10.1016/j.jhazmat.2011.12.010.

55. Wood, G.O. Affinity Coefficients of the Polanyi/Dubinin Adsorption Isotherm Equations: A Review with Compilations and Correlations. *Carbon* **2001,** *39* (3), 343-356; 10.1016/S0008-6223(00)00128-7.

56. Fayaz, M.; Shariaty, P.; Atkinson, J.D.; Hashisho, Z.; Phillips, J.H.; Anderson, J.E.; Nichols, M. Using Microwave Heating to Improve the Desorption Efficiency of High Molecular Weight VOC from Beaded Activated Carbon. *Environmental Science & Technology* **2015,** *49* (7), 4536-4542; 10.1021/es505953c.

5 Conclusions and Recommendations

5.1 Conclusions

In chapter 3, the simultaneous effect of oxygen impurity and purge gas flow rate on adsorption capacity of and heel build-up on activated carbon during cyclic adsorption-desorption of VOC was studied. 5-cycle adsorption/regeneration experiments were performed with nine different regeneration scenarios by varying purge gas flow (0.1, 1, and 10 SLPM) rate and oxygen impurity (<5 ppmv, 10,000 ppmv, and 21%). The results showed higher heel build-up for samples regenerated with higher oxygen impurity and/or lower flow rate. Furthermore, lower adsorption capacity, BET surface area, breakthrough time were observed for the samples regenerated with high oxygen impurity and/or low flow rate purge gas. In addition, it was found that increasing purge gas flow rate mitigates the extent of oxygen impurity adverse effect on heel build-up. DTG analysis of the regenerated samples showed less heel buildup for samples regenerated with higher flow rates.

In chapter 4, two ML algorithms (XGBoost and DNN) were used to predict heel build-up in cyclic adsorption/desorption of VOCs on activated carbon. Adsorbate's properties (e.g., Abraham descriptors, MR, and boiling point), adsorbent's characteristics (e.g., BET surface area, "meso+macro" pore volume, O/C ratio), and regeneration parameters (e.g., purge gas flow rate, purge gas oxygen impurity, and regeneration temperature) were used as input to predict cyclic heel build-up. DNN (R^2 = 0.94) outperformed XGBoost in prediction of heel buildup (R^2 = 0.81). Partial dependency plots were generated to validate DNN performance and gain insight into the relationship between heel build-up and the input parameters. According to the DNN model and partial dependency plots, purge gas flow rate and O_2 impurity, cycle number, and the adsorbate's

molar refraction (MR, or capability of non-specific dispersive interaction) and excessive molar refraction (E, interactions through π or n electrons) have the most noticeable impacts on the extent of heel build-up.

5.2 Recommendations

In this thesis, the simultaneous effect of the purge gas oxygen impurity and flow rate on heel formation was investigated and heel buildup was predicted using machine learning algorithms. The following recommendations can be made for future research:

· Although increasing the purge gas flow rate and purity reduces heel buildup, they add expenses to the VOC abatement process. Hence, conducting a technoeconomic analysis of the regeneration process can result in finding the optimum regeneration conditions with respect to the purge gas flow rate and its oxygen impurity.

· According to the partial dependency plots provided in chapter 4, the effect of purge gas oxygen impurity on heel buildup is highly dependent on regeneration temperature. Hence, conducting TGA analysis to find the optimum regeneration temperature at which oxygen impurity does not adversely affect heel buildup is strongly recommended.

BIBLIOGRAPHY

Guideline Series, Control of Volatile Organic Compound Emissions from Reactor Processes and Distillation Operations Processes in the Synthetic Organic Chemical Manufacturing Industry; United States Environmental Protection Agency: Research Triangle Park, North Caroline, 1993.

USEPA. Technical Overview of Volatile Organic Compounds; https://www.epa.gov/indoor-air-quality-iaq/technical-overview-volatile-organic-compounds.

U.S. EPA. 2018b. Data from the 2014 National Emissions Inventory, Version 2.Accessed 2021.; https://www.epa.gov/air-emissions-inventories/2014-national-emissions-inventory-nei-data.

Abraham, M.H.; Grellier, P.L.; McGill, R.A. Determination of Olive Oil-Gas and Hexadecane-Gas Partition Coefficients, and Calculation of the Corresponding Olive Oil-Water and Hexadecane-Water Partition Coefficients. *Journal of the Chemical Society, Perkin Transactions 2* **1987,** (6), 797-83; 10.1039/P29870000797.

Abraham, M.H.; Ibrahim, A.; Zissimos, A.M. Determination of Sets of Solute Descriptors from Chromatographic Measurements. *Journal of Chromatography A* **2004,** *1037* (1), 29-47; 10.1016/j.chroma.2003.12.004.

Abraham, M.H.; Mcgowan, J.C. The Use of Characteristic Volumes to Measure Cavity Terms in Reversed Phase Liquid Chromatography. *Chromatographia* **1987,** *23* (4), 243-246; 10.1007/BF02311772.

Abraham, M.H.; Whiting, G.S.; Doherty, R.M.; Shuely, W.J. Hydrogen Bonding. Part 13. A New Method for the Characterisation of GLC Stationary Phases-The Laffort Data Set. *Journal of the Chemical Society, Perkin Transactions 2* **1990,** (8), 1451-146; 10.1039/P29900001451.

Abuzaid, N.S.; Nakhla, G.F. Dissolved Oxygen Effects on Equilibrium and Kinetics of Phenolics Adsorption by Activated Carbon. *Environmental Science & Technology* **1994,** *28* (2), 216-221; 10.1021/es00051a006.

Agranovski, I.E.; Moustafa, S.; Braddock, R.D. Comparison of Fixed and Fluidized Activated Carbon Beds for Removal of Organic Vapors. *Chemical Engineering & Technology* **2004,** *27* (7), 784-789; 10.1002/ceat.200402000.

Akiba, T.; Sano, S.; Yanase, T.; Ohta, T.; Koyama, M. Optuna: A Next-generation Hyperparameter Optimization Framework. **2019**.

Aktaş, Ö; Çeçen, F. Effect of Type of Carbon Activation on Adsorption and Its Reversibility. *Journal of Chemical Technology & Biotechnology: International Research in Process, Environmental & Clean Technology* **2006,** *81* (1), 94-101.

Ania, C.O.; Parra, J.B.; Menéndez, J.A.; Pis, J.J. Microwave-Assisted Regeneration of Activated Carbons Loaded with Pharmaceuticals. *Water Research* **2007,** *41* (15), 3299-3306; https://doi.org/10.1016/j.watres.2007.05.006.

Ania, C.O.; Menéndez, J.A.; Parra, J.B.; Pis, J.J. Microwave-Induced Regeneration of Activated Carbons Polluted with Phenol. A Comparison with Conventional Thermal Regeneration. *Carbon* **2004,** *42* (7), 1383-1387; 10.1016/j.carbon.2004.01.010.

Aydin Berenjian; Natalie Chan; Hoda, J.M. Volatile Organic Compounds Removal Methods: A Review. *American Journal of Biochemistry and Biotechnology* **2012,** *8* (4); 10.3844/ajbbsp.2012.220.229.

Barghi, S.H.; Tsotsis, T.T.; Sahimi, M. Chemisorption, Physisorption and Hysteresis During Hydrogen Storage in Carbon Nanotubes. *International Journal of Hydrogen Energy* **2014,** *39* (3), 1390-1397; 10.1016/j.ijhydene.2013.10.163.

Berndt, T.; Böge, O. Reaction of O(3P) Atoms with Benzene. *Zeitschrift Für Physikalische Chemie (Neue Folge)* **2004,** *218* (4), 391-404; 10.1524/zpch.218.4.391.29202.

Boocock, G.; Cvetanović, R.J. Reaction of Oxygen Atoms with Benzene. *Canadian Journal of Chemistry* **1961,** *39* (12), 2436-2443; 10.1139/v61-323.

Borboudakis, G.; Stergiannakos, T.; Frysali, M.; Klontzas, E.; Tsamardinos, I.; Froudakis, G.E. Chemically Intuited, Large-Scale Screening of MOFs by Machine Learning Techniques. *NPJ Computational Materials* **2017,** *3* (1), 1-7; 10.1038/s41524-017-0045-8.

Burns, T.D.; Pai, K.N.; Subraveti, S.G.; Collins, S.P.; Krykunov, M.; Rajendran, A.; Woo, T.K. Prediction of MOF Performance in Vacuum Swing Adsorption Systems for Postcombustion CO2 Capture Based on Integrated Molecular Simulations, Process Optimizations, and Machine Learning Models. *Environmental Science & Technology* **2020,** *54* (7), 4536-4544; 10.1021/acs.est.9b07407.

Carratalá-Abril, J.; Lillo-Ródenas, M.A.; Linares-Solano, A.; Cazorla-Amorós, D. Regeneration of Activated Carbons Saturated with Benzene or Toluene Using an Oxygen-Containing Atmosphere. *Chemical Engineering Science* **2010,** *65* (6), 2190-2198; 10.1016/j.ces.2009.12.017.

Cecen, F.; Aktas, Ö Activated carbon for Water and Wastewater Treatment; Integration of Adsorption and Biological treatment. *Reference & Research Book News* **2011**.

Chang, C.H.; Savage, D.W. Investigations of Solvent-Regenerable Carbon-Sulfur Surface Compounds for Phenol Removal in a Packed Column. *Environmental Science & Technology* **1981,** *15* (2), 201-206; 10.1021/es00084a005.

Chen, T.; Guestrin, C. XGBoost. Proceedings of the 22nd ACM SIGKDD International Conference on Knowledge Discovery and Data Mining, Association for Computing Machinery, Aug 13, 2016.

Chihara, K.; Oomori, K.; Oono, T.; Mochizuki, Y. Supercritical CO2 Regeneration of Activated Carbon Loaded with Organic Adsorbates. *Water Science and Technology* **1997,** *35* (7), 261-268; https://doi.org/10.1016/S0273-1223(97)00139-X.

Cooney, D.O.; Nagerl, A.; Hines, A.L. Solvent Regeneration of Activated Carbon. *Water Research* **1983,** *17* (4), 403-410; 10.1016/0043-1354(83)90136-7.

Daglar, H.; Keskin, S. Computational Screening of Metal–Organic Frameworks for Membrane-Based CO2/N2/H2O Separations: Best Materials for Flue Gas Separation. *Journal of Physical Chemistry. C* **2018,** *122* (30), 17347-17357; 10.1021/acs.jpcc.8b05416.

Di Natale, F.; Erto, A.; Lancia, A. Desorption of Arsenic from Exhaust Activated Carbons Used for Water Purification. *Journal of Hazardous Materials* **2013,** *260*, 451-458; https://doi.org/10.1016/j.jhazmat.2013.05.055.

Dwivedi, P.; Gaur, V.; Sharma, A.; Verma, N. Comparative Study of Removal of Volatile Organic Compounds by Cryogenic Condensation and Adsorption by Activated Carbon Fiber. *Separation and Purification Technology* **2004,** *39* (1), 23-37; 10.1016/j.seppur.2003.12.016.

Dąbrowski, A.; Podkościelny, P.; Hubicki, Z.; Barczak, M. Adsorption of Phenolic Compounds by Activated Carbon—a Critical Review. *Chemosphere* **2005,** *58* (8), 1049-1070; https://doi.org/10.1016/j.chemosphere.2004.09.067.

Endo, S.; Goss, K. Applications of Polyparameter Linear Free Energy Relationships in Environmental Chemistry. *Environmental Science & Technology* **2014,** *48* (21), 12477-12491; 10.1021/es503369t.

Canada's Air Pollutant Emissions Inventory; Open Data Canada; https://open.canada.ca/data/en/dataset/fa1c88a8-bf78-4fcb-9c1e-2a5534b92131.

Fayaz, M. Adsorption and Microwave Regeneration for Controlling Volatile Organic Compounds Emissions from Automotive Paint Booths. University of Alberta, 2016.

Fayaz, M.; Shariaty, P.; Atkinson, J.D.; Hashisho, Z.; Phillips, J.H.; Anderson, J.E.; Nichols, M. Using Microwave Heating to Improve the Desorption Efficiency of High Molecular Weight VOC from Beaded Activated Carbon. *Environmental Science & Technology* **2015,** *49* (7), 4536-4542; 10.1021/es505953c.

Feizbakhshan, M. Improving Cyclic Adsorption/Desorption Process of Volatile Organic Compounds in the Presence of Gaseous Phase Oxygen. University of Alberta, 2020.

Feizbakhshan, M. Heel Build-up During Thermal Desorption of VOCs in Presence of Oxygen. University of Alberta, 2020.

Feizbakhshan, M.; Amdebrhan, B.; Hashisho, Z.; Phillips, J.H.; Crompton, D.; Anderson, J.E.; Nichols, M. Effects of Oxygen Impurity and Desorption Temperature on Heel Build-up in Activated Carbon. *Chemical Engineering Journal* **2021,** *409*, 128232; 10.1016/j.cej.2020.128232.

Ferro-Garcia, M.A.; Joly, J.P.; Rivera-Utrilla, J.; Moreno-Castilla, C. Thermal Desorption of Chlorophenols from Activated Carbons with Different Porosity. *Langmuir* **1995,** *11* (7), 2648-2651; 10.1021/la00007a052.

Ferro-García, M.A.; Utrera-Hidalgo, E.; Rivera-Utrilla, J.; Moreno-Castilla, C.; Joly, J.P. Regeneration of Activated Carbons Exhausted with Chlorophenols. *Carbon* **1993,** *31* (6), 857-863; 10.1016/0008-6223(93)90185-D.

Foroughi, M.; Ahmadi Azqhandi, M.H.; Kakhki, S. Bio-inspired, High, and Fast Adsorption of Tetracycline from Aqueous Media Using Fe3O4-g-CN@PEI-β-CD Nanocomposite: Modeling by Response Surface Methodology (RSM), Boosted Regression Tree (BRT), and General Regression Neural Network (GRNN). *Journal of Hazardous Materials* **2020,** *388*, 121769; 10.1016/j.jhazmat.2019.121769.

Friday, D.K.; LeVan, M.D. Hot purge gas Regeneration of Adsorption Beds with Solute Condensation: Experimental studies. *AIChE Journal* **1985,** *31* (8), 1322-1328; https://doi.org/10.1002/aic.690310811.

Fung, V.; Hu, G.; Ganesh, P.; Sumpter, B.G. Machine learned Features from Density of States for Accurate Adsorption Energy Prediction. *Nature Communications* **2021,** *12* (1), 88; 10.1038/s41467-020-20342-6.

Grant, T.M.; King, C.J. Mechanism of Irreversible Adsorption of Phenolic Compounds by Activated Carbons. *Industrial & engineering chemistry research* **1990,** *29* (2), 264-271; 10.1021/ie00098a017.

Gulli, A.; Pal, S. *Deep Learning with Keras.* Packt Publishing Ltd: 2017.

Guo, D.; Shi, Q.; He, B.; Yuan, X. Different Solvents for the Regeneration of the Exhausted Activated Carbon Used in the Treatment of Coking Wastewater. *Journal of Hazardous Materials* **2011,** *186* (2), 1788-1793; https://doi.org/10.1016/j.jhazmat.2010.12.068.

Gupta, V.K.; Verma, N. Removal of Volatile Organic Compounds by Cryogenic Condensation Followed by Adsorption. *Chemical Engineering Science* **2002,** *57* (14), 2679-2696; https://doi.org/10.1016/S0009-2509(02)00158-6.

Hashisho, Z.; Emamipour, H.; Cevallos, D.; Rood, M.J.; Hay, K.J.; Kim, B.J. Rapid Response Concentration-Controlled Desorption of Activated Carbon to Dampen Concentration Fluctuations. *Environmental Science & Technology* **2007,** *41* (5), 1753-1758; 10.1021/es062155y.

Hatami, M.; Farmany, A.; Sahraei, R. Physisorption & Chemisorption of Oxygen Molecules on Single- and Multi-walled Carbon Nanotubes. *Fullerenes, Nanotubes, and Carbon Nanostructures* **2014,** *22* (5), 434-453; 10.1080/1536383X.2012.684187.

Helbling, T.; Durrer, L.; Pohle, R.; Stampfer, C.; Goyal, A.; Fleischer, M.; Hierold, C. NO2 Gas Sensors Based on Individual Suspended Single-Walled Carbon Nanotubes. TRANSDUCERS 2007 - 2007 International Solid-State Sensors, Actuators and Microsystems Conference, IEEE, Jun 2007.

Hemphill, L.; Okla, Robert S.Kerr Environmental Research Laboratory, Ada, *Thermal Regeneration of Activated Carbon.* National Technical Information Service: 1978.

Henning, K.D.; Bongartz, W.; Degel, J. Adsorptive Recovery of Problematic Solvents.

Hofelich, T.C.; LaBarge, M.S.; Drott, D.A. Prevention of Thermal Runaways in Carbon Beds. *Journal of Loss Prevention in the Process Industries* **1999,** *12* (6), 517-523; 10.1016/S0950-4230(99)00025-X.

Hu, H.; Xu, K. Chapter 8 - Physicochemical Technologies for HRPs and Risk Control, In *High-Risk Pollutants in Wastewater,* Ren, H.; Zhang, X., Eds.; Elsevier: 2020; pp. 169-207.

Humayun, R.; Karakas, G.; Dahlstrom, P.R.; Ozkan, U.S.; Tomasko, D.L. Supercritical Fluid Extraction and Temperature-Programmed Desorption of Phenol and Its Oxidative Coupling Products from Activated Carbon. *Industrial & Engineering Chemistry Research* **1998,** *37* (8), 3089-3097; 10.1021/ie970936p.

Jahandar Lashaki, M. Understanding and Improving Gas Phase Capture of Organic Vapors by Carbonaceous Adsorbents. University of Alberta, 2016.

Jahandar Lashaki, M.; Atkinson, J.D.; Hashisho, Z.; Phillips, J.H.; Anderson, J.E.; Nichols, M. The Role of Beaded Activated Carbon's Pore Size Distribution on Heel Formation During Cyclic Adsorption/Desorption of Organic Vapors. *Journal of Hazardous Materials* **2016,** *315*, 42-51; 10.1016/j.jhazmat.2016.04.071.

Jahandar Lashaki, M.; Atkinson, J.D.; Hashisho, Z.; Phillips, J.H.; Anderson, J.E.; Nichols, M. The Role of Beaded Activated Carbon's Surface Oxygen Groups on Irreversible Adsorption of Organic Vapors. *Journal of Hazardous Materials* **2016,** *317*, 284-294; 10.1016/j.jhazmat.2016.05.087.

Jahandar Lashaki, M.; Atkinson, J.D.; Hashisho, Z.; Phillips, J.H.; Anderson, J.E.; Nichols, M.; Misovski, T. Effect of Desorption Purge Gas Oxygen Impurity on Irreversible Adsorption of Organic Vapors. *Carbon* **2016,** *99*, 310-317; 10.1016/j.carbon.2015.12.037.

Jahandar Lashaki, M.; Fayaz, M.; Wang, H.; Hashisho, Z.; Philips, J.H.; Anderson, J.E. Effect of Adsorption and Regeneration Temperature on Irreversible Adsorption of Organic Vapors on Beaded Activated Carbon. *Environmental Science & Technology* **2012,** *46* (7), 4083-4090; 10.1021/es3000195.

Jahandar Lashaki, M.; Hashisho, Z.; Phillips, J.H.; Crompton, D.; Anderson, J.E.; Nichols, M. Mechanisms of Heel Buildup During Cyclic Adsorption-Desorption of Volatile Organic Compounds in a Full-Scale Adsorber-Desorber. *Chemical Engineering Journal* **2020,** *400*, 124937; https://doi.org/10.1016/j.cej.2020.124937.

Jäger, M.O.J.; Morooka, E.V.; Federici Canova, F.; Himanen, L.; Foster, A.S. Machine Learning Hydrogen Adsorption on Nanoclusters Through Structural Descriptors. *NPJ Computational Materials* **2018,** *4* (1), 1-8; 10.1038/s41524-018-0096-5.

Kamravaei, S.; Shariaty, P.; Jahandar Lashaki, M.; Atkinson, J.D.; Hashisho, Z.; Phillips, J.H.; Anderson, J.E.; Nichols, M. Effect of Beaded Activated Carbon Fluidization on Adsorption of Volatile Organic Compounds. *Industrial & Engineering Chemistry Research* **2017,** *56* (5), 1297-1305; 10.1021/acs.iecr.6b04165.

Khan, F.I.; Kr. Ghoshal, A. Removal of Volatile Organic Compounds from Polluted Air. *Journal of Loss Prevention in the Process Industries* **2000,** *13* (6), 527-545; https://doi.org/10.1016/S0950-4230(00)00007-3.

Kilduff, J.E.; King, C.J. Effect of Carbon Adsorbent Surface Properties on the Uptake and Solvent Regeneration of Phenol. *Industrial & Engineering Chemistry Research* **1997,** *36* (5), 1603-1613; 10.1021/ie960545v.

Kim, B.; Lee, S.; Kim, J. Inverse Design of Porous Materials Using Artificial Neural Networks. *Science Advances* **2020,** *6* (1), eaax9324; 10.1126/sciadv.aax9324.

Kim, B. VOC Emissions from Automotive Painting and Their Control: A Review. *Environmental engineering research* **2011,** *16* (1), 1-9.

Kim, K.; Kang, C.; You, Y.; Chung, M.; Woo, M.; Jeong, W.; Park, N.; Ahn, H. Adsorption–Desorption Characteristics of VOCs Over Impregnated Activated Carbons. *Catalysis Today* **2006,** *111* (3), 223-228; 10.1016/j.cattod.2005.10.030.

Selecting Equipment to Control Air Pollution from Automotive Painting Operations; SAE Technical Paper Series; https://saemobilus.sae.org/content/920189.

Küntzel, J.; Ham, R.; Melin, T. Regeneration of Hydrophobic Zeolites with Steam. *Chemical Engineering & Technology* **1999,** *22* (12), 991-994; 10.1002/(SICI)1521-4125(199912)22:12<991::AID-CEAT991>3.0.CO;2-L.

Leffler, J.E.; Grunwald, E. *Rates and Equilibria of Organic Reactions.* Wiley: 1963.

Leng, C.-.; Pinto, N.G. An Investigation of the Mechanisms of Chemical Regeneration of Activated Carbon. *Industrial and Engineering Chemistry Research* **1996,** *35* (6), 2024-2031; 10.1021/ie950576a.

Leng, C.-.; Pinto, N.G. Effects of Surface Properties of Activated Carbons on Adsorption Behavior of Selected Aromatics. *Carbon* **1997,** *35* (9), 1375-1385; 10.1016/S0008-6223(97)00091-2.

Li, L.; Liu, S.; Liu, J. Surface Modification of Coconut Shell Based Activated Carbon for The Improvement of Hydrophobic VOC Removal. *Journal of Hazardous Materials* **2011,** *192* (2), 683-690; 10.1016/j.jhazmat.2011.05.069.

Li, Y.; Chang, H.; Yan, H.; Tian, S.; Jessop, P.G. Reversible Absorption of Volatile Organic Compounds by Switchable-Hydrophilicity Solvents: A Case Study of Toluene with N,N-Dimethylcyclohexylamine. *ACS Omega* **2021,** *6* (1), 253-264; 10.1021/acsomega.0c04443.

Lim, J.; Okada, M. Regeneration of Granular Activated Carbon Using Ultrasound. *Ultrasonics Sonochemistry* **2005,** *12* (4), 277-282; https://doi.org/10.1016/j.ultsonch.2004.02.003.

Liu, Y.; Li, C.; Peyravi, A.; Sun, Z.; Zhang, G.; Rahmani, K.; Zheng, S.; Hashisho, Z. Mesoporous MCM-41 Derived from Natural Opoka and Its Application for Organic Vapors Removal. *Journal of Hazardous Materials* **2021,** *408*, 124911; 10.1016/j.jhazmat.2020.124911.

Long, C.; Li, Y.; Yu, W.; Li, A. Removal of Benzene and Methyl Ethyl Ketone Vapor: Comparison of Hypercrosslinked Polymeric Adsorbent with Activated Carbon. *Journal of hazardous materials* **2012,** *203*, 251-256; 10.1016/j.jhazmat.2011.12.010.

Lu, Q.; Sorial, G.A. The Role of Adsorbent Pore Size Distribution in Multicomponent Adsorption on Activated Carbon. *Carbon* **2004,** *42* (15), 3133-3142; 10.1016/j.carbon.2004.07.025.

Lu, Q.; Sorial, G.A. Adsorption of Phenolics on Activated Carbon—Impact of Pore Size and Molecular Oxygen. *Chemosphere* **2004,** *55* (5), 671-679; 10.1016/j.chemosphere.2003.11.044.

Lundberg, S.; Lee, S. A Unified Approach to Interpreting Model Predictions. Proceedings of the 31st International Conference on Neural Information Processing Systems, Curran Associates Inc., May 22, 2017.

Macnaughton, S.J.; Foster, N.R. Supercritical Adsorption and Desorption Behavior of DDT on Activated Carbon Using Carbon Dioxide. *Industrial & Engineering Chemistry Research* **1995,** *34* (1), 275-282; 10.1021/ie00040a029.

Madras, G.; Erkey, C.; Akgerman, A. Supercritical Fluid Regeneration of Activated Carbon Loaded with Heavy Molecular Weight Organics. *Industrial & Engineering Chemistry Research* **1993,** *32* (6), 1163-1168; 10.1021/ie00018a022.

Magne, P.; Walker, P.L. Phenol Adsorption on Activated Carbons: Application to the Regeneration of Activated Carbons Polluted with Phenol. *Carbon* **1986,** *24* (2), 101-107; 10.1016/0008-6223(86)90102-8.

Martin, R.J.; Ng, W.J. Chemical Regeneration of Exhausted Activated Carbon—II. *Water Research* **1985,** *19* (12), 1527-1535; https://doi.org/10.1016/0043-1354(85)90398-7.

Martin, R.J.; Ng, W.J. The Repeated Exhaustion and Chemical Regeneration of Activated Carbon. *Water Research* **1987,** *21* (8), 961-965; 10.1016/S0043-1354(87)80014-3.

McLaughlin, H.S. Regenerate Activated Carbon Using Organic Solvents. *Chemical Engineering Progress* **1995,** *91* (7).

Mendoza-Castillo, D.I.; Reynel-Ávila, H.E.; Sánchez-Ruiz, F.J.; Trejo-Valencia, R.; Jaime-Leal, J.E.; Bonilla-Petriciolet, A. Insights and Pitfalls of Artificial Neural Network Modeling of Competitive Multi-Metallic Adsorption Data. *Journal of molecular liquids* **2018,** *251*, 15-27; 10.1016/j.molliq.2017.12.030.

Meng, M.; Zhong, R.; Wei, Z. Prediction of Methane Adsorption in Shale: Classical Models and Machine Learning Based Models. *Fuel* **2020,** *278*, 118358; 10.1016/j.fuel.2020.118358.

Merchán, M.D.; Salvador, F. Characterization of Solids by Thermal Desorption in Solution. *Studies in Surface Science and Catalysis* **1994,** *87*, 391-400; https://doi.org/10.1016/S0167-2991(08)63100-6.

Compressed Air Best Practices, The Energy Costs Associated with Nitrogen Specifications.; http://www.airbestpractices.com/system-assessments/air-treatment/n2/energy-costs-associated-nitrogen-specifications.

Mojtaba Hashemi, S.; Jahandar Lashaki, M.; Hashisho, Z.; Phillips, J.H.; Anderson, J.E.; Nichols, M. Oxygen Impurity in Nitrogen Desorption Purge Gas Can Increase Heel Buildup on Activated Carbon. *Separation and Purification Technology* **2019,** *210*, 497-503; 10.1016/j.seppur.2018.08.035.

Molhave, L. Volatile Organic Compounds, Indoor Air Quality and Health. *Indoor Air* **1991,** *1* (4), 357-376; 10.1111/j.1600-0668.1991.00001.x.

Montero-Montoya, R.; López-Vargas, R.; Arellano-Aguilar, O. Volatile Organic Compounds in Air: Sources, Distribution, Exposure and Associated Illnesses in Children. *Annals of global health* **2018,** *84* (2), 225-238; 10.29024/aogh.910.

Moreno-Pérez, J.; Bonilla-Petriciolet, A.; Mendoza-Castillo, D.I.; Reynel-Ávila, H.E.; Verde-Gómez, Y.; Trejo-Valencia, R. Artificial Neural Network-Based Surrogate Modeling of Multi-Component Dynamic Adsorption of Heavy Metals with a Biochar. *Journal of Environmental Chemical Engineering* **2018,** *6* (4), 5389-5400; https://doi.org/10.1016/j.jece.2018.08.038.

Mosavari Nezamabad, N. Effect of Surface Oxygen Groups on Irreversible Adsorption of Volatile Organic Compounds on Beaded Activated Carbon. University of Alberta, 2017.

Mubeen, S.; Zhang, T.; Yoo, B.; Deshusses, M.A.; Myung, N.V. Palladium Nanoparticles Decorated Single-Walled Carbon Nanotube Hydrogen Sensor. *Journal of Physical Chemistry. C* **2007,** *111* (17), 6321-6327; 10.1021/jp067716m.

Niknaddaf, S.; Atkinson, J.D.; Gholidoust, A.; Fayaz, M.; Awad, R.; Hashisho, Z.; Phillips, J.H.; Anderson, J.E.; Nichols, M. Influence of Purge Gas Flow and Heating Rates on Volatile

Organic Compound Decomposition during Regeneration of an Activated Carbon Fiber Cloth. *Industrial & Engineering Chemistry Research* **2020,** *59* (8), 3521-3530; 10.1021/acs.iecr.9b06070.

Niknaddaf, S.; Atkinson, J.D.; Shariaty, P.; Jahandar Lashaki, M.; Hashisho, Z.; Phillips, J.H.; Anderson, J.E.; Nichols, M. Heel Formation During Volatile Organic Compound Desorption from Activated Carbon Fiber Cloth. *Carbon* **2016,** *96*, 131-138; 10.1016/j.carbon.2015.09.049.

Oliveira, L.M.C.; Koivisto, H.; Iwakiri, I.G.I.; Loureiro, J.M.; Ribeiro, A.M.; Nogueira, I.B.R. Modelling of a Pressure Swing Adsorption Unit by Deep Learning and Artificial Intelligence Tools. *Chemical Engineering Science* **2020,** *224*, 115801; 10.1016/j.ces.2020.115801.

Ottengraf, S.P.; Van Den Oever, A. H. Kinetics of Organic Compound Removal from Waste Gases with a Biological Filter. *Biotechnology and Bioengineering* **1983,** *25* (12), 3089-3102; 10.1002/bit.260251222.

Pai, K.N.; Prasad, V.; Rajendran, A. Experimentally Validated Machine Learning Frameworks for Accelerated Prediction of Cyclic Steady State and Optimization of Pressure Swing Adsorption Processes. *Separation and Purification Technology* **2020,** *241*, 116651; 10.1016/j.seppur.2020.116651.

Papasavva, S.; Kia, S.; Claya, J.; Gunther, R. Characterization of automotive paints: an environmental impact analysis. *Progress in organic coatings* **2001,** *43* (1), 193-206; 10.1016/S0300-9440(01)00182-5.

Parmar, G.R.; Rao, N.N. Emerging Control Technologies for Volatile Organic Compounds. *null* **2008,** *39* (1), 41-78; 10.1080/10643380701413658.

Patil, K.; Jeong, S.; Lim, H.; Byun, H.; Han, S. Removal of volatile organic compounds from air using activated carbon impregnated cellulose acetate electrospun mats. *Environmental engineering research* **2019,** *24* (4), 600-607.

Popescu, M.; Joly, J.P.; Carré, J.; Danatoiu, C. Dynamical Adsorption and Temperature-Programmed Desorption of VOCs (Toluene, Butyl Acetate and Butanol) on Activated Carbons. *Carbon* **2003,** *41* (4), 739-748; https://doi.org/10.1016/S0008-6223(02)00391-3.

Qin, W.J.; Liu, Q.Y.; Jia, D.W. Multibody System Dynamics Simulation of Loads in Main Bearings of Crankshafts. *Materials Science Forum* **2009,** *628-629*, 55-60; 10.4028/www.scientific.net/MSF.628-629.55.

Refaeilzadeh, P.; Tang, L.; Liu, H. Cross-Validation, In *Encyclopedia of Database Systems,* LIU, L.; ÖZSU, M.T., Eds.; Springer US: 2009; pp. 532-538.

Roelant, G.J.; Kemppainen, A.J.; Shonnard, D.R. Assessment of the Automobile Assembly Paint Process for Energy, Environmental, and Economic Improvement. *Journal of Industrial Ecology* **2004,** *8* (1), 173-191; https://doi.org/10.1162/1088198041269355.

Rudling, J.; Björkholm, E. Irreversibility Effects in Liquid Desorption of Organic Solvents from Activated Carbon. *Journal of Chromatography A* **1987,** *392*, 239-248; 10.1016/S0021-9673(01)94269-4.

Russell, J.; Cohn, R. *Joule Heating.* Bookvika Publishing: 2013.

Ruthven, D. *Principles of Adsorption and Adsorption Processes.* John Wiley & Sons: 1984.

Ruthven, D.M.; Farooq, S.; Knaebel, K.S. *Pressure Swing Adsorption.* VCH: 1994.

Sabio, E.; González, E.; González, J.F.; González-García, C.M.; Ramiro, A.; Gañan, J. Thermal Regeneration of Activated Carbon Saturated with P-Nitrophenol. *Carbon* **2004,** *42* (11), 2285-2293; 10.1016/j.carbon.2004.05.007.

Salvador, F.; Merchán, M.D. Study of the Desorption of Phenol and Phenolic Compounds from Activated Carbon by Liquid-Phase Temperature-Programmed Desorption. *Carbon* **1996,** *34* (12), 1543-1551; https://doi.org/10.1016/S0008-6223(96)00105-4.

Salvador, F.; Merchan, M.D. A Simple Apparatus for Studies of Thermoprogrammed Desorption in Solution. *Langmuir* **1992,** *8* (4), 1226-1229; 10.1021/la00040a034.

Salvador, F.; Sánchez-Montero, M.J.; Salvador, A.; Martín, M.J. Study of the Energetic Heterogeneity of the Adsorption of Phenol onto Activated Carbons by TPD Under Supercritical Conditions. *Applied Surface Science* **2005,** *252* (3), 641-646; 10.1016/j.apsusc.2005.02.090.

Salvador, F.; Martin-Sanchez, N.; Sanchez-Hernandez, R.; Sanchez-Montero, M.J.; Izquierdo, C. Regeneration of Carbonaceous Adsorbents. Part II: Chemical, Microbiological and Vacuum Regeneration. *Microporous and Mesoporous Materials* **2015,** *202*, 277-296; https://doi.org/10.1016/j.micromeso.2014.08.019.

Salvador, F.; Martin-Sanchez, N.; Sanchez-Hernandez, R.; Sanchez-Montero, M.J.; Izquierdo, C. Regeneration of Carbonaceous Adsorbents. Part I: Thermal Regeneration. *Microporous and Mesoporous Materials* **2015,** *202*, 259-276; 10.1016/j.micromeso.2014.02.045.

Salvador, F.; Martin-Sanchez, N.; Sanchez-Montero, M.J.; Montero, J.; Izquierdo, C. Regeneration of Activated Carbons Contaminated by Phenol Using Supercritical Water. *The Journal of Supercritical Fluids* **2013,** *74*, 1-7; 10.1016/j.supflu.2012.11.025.

Schirmer, W. *Physical Adsorption: Forces and Phenomena.* De Gruyter Oldenbourg: 1999.

Sigmund, G.; Gharasoo, M.; Hüffer, T.; Hofmann, T. Deep Learning Neural Network Approach for Predicting the Sorption of Ionizable and Polar Organic Pollutants to a Wide Range of Carbonaceous Materials. *Environmental Science & Technology* **2020,** *54* (7), 4583-4591; 10.1021/acs.est.9b06287.

Sutikno, T.; Himmelstein, K.J. Desorption of Phenol from Activated Carbon by Solvent Regeneration. *Industrial & Engineering Chemistry Fundamentals* **1983,** *22* (4), 420-425; 10.1021/i100012a011.

Suzuki, M.; Suzuki, M. *Adsorption Engineering.* Kodansha Tokyo: 1990.

Tamon, H.; Okazaki, M. Desorption Characteristics of Aromatic Compounds in Aqueous Solution on Solid Adsorbents. *Journal of Colloid and Interface Science* **1996,** *179* (1), 181-187; 10.1006/jcis.1996.0200.

Tamon, H.; Saito, T.; Kishimura, M.; Okazaki, M.; Toei, R. Solvent Regeneration of Spent Activated Carbon in Wastewater Treatment. *Journal of Chemical Engineering of Japan* **1990,** *23* (4), 426-432; 10.1252/jcej.23.426.

Tan, C.S.; Liou, D.C. Supercritical Regeneration of Activated Carbon Loaded with Benzene and Toluene. *Industrial & Engineering Chemistry Research* **1989,** *28* (8), 1222-1226; 10.1021/ie00092a015.

Tanthapanichakoon, W.; Ariyadejwanich, P.; Japthong, P.; Nakagawa, K.; Mukai, S.R.; Tamon, H. Adsorption–Desorption Characteristics of Phenol and Reactive Dyes from Aqueous Solution on Mesoporous Activated Carbon Prepared from Waste Tires. *Water Research* **2005,** *39* (7), 1347-1353; 10.1016/j.watres.2004.12.044.

Taylor, P.N.; Lester, J.N. Rapid Extraction of Isoproturon and Diuron from Granular Activated Carbon. *Chemosphere* **1996,** *33* (7), 1227-1240; 10.1016/0045-6535(96)00261-5.

Tefera, D.T.; Hashisho, Z.; Philips, J.H.; Anderson, J.E.; Nichols, M. Modeling Competitive Adsorption of Mixtures of Volatile Organic Compounds in a Fixed-Bed of Beaded Activated Carbon. *Environmental Science & Technology* **2014,** *48* (9), 5108-5117; 10.1021/es404667f.

Tefera, D.T.; Jahandar Lashaki, M.; Fayaz, M.; Hashisho, Z.; Philips, J.H.; Anderson, J.E.; Nichols, M. Two-Dimensional Modeling of Volatile Organic Compounds Adsorption onto Beaded Activated Carbon. *Environmental Science & Technology* **2013,** *47* (20), 11700-11710; 10.1021/es402369u.

Toyao, T.; Suzuki, K.; Kikuchi, S.; Takakusagi, S.; Shimizu, K.; Takigawa, I. Toward Effective Utilization of Methane: Machine Learning Prediction of Adsorption Energies on Metal Alloys. *The Journal of Physical Chemistry C* **2018,** *122* (15), 8315-8326; 10.1021/acs.jpcc.7b12670.

UFZ-LSER Database V 3.2 [Internet]; Available from http://www.ufz.de/lserd.

Uranowski, L.J.; Tessmer, C.H.; Vidic, R.D. The Effect of Surface Metal Oxides on Activated Carbon Adsorption of Phenolics. *Water Research* **1998,** *32* (6), 1841-1851; 10.1016/S0043-1354(97)00479-X.

Verstraete, S.; Hermia, J.; Vigneron, S. VOC Separation on Membranes: A Review. *Studies in Environmental Science* **1994,** *61*, 359-373; https://doi.org/10.1016/S0166-1116(08)72068-5.

Vidic, R.D.; Suidan, M.T. Role of Dissolved Oxygen on the Adsorptive Capacity of Activated Carbon for Synthetic and Natural Organic Matter. *Environmental Science & Technology* **1991,** *25* (9), 1612-1618; 10.1021/es00021a013.

Vidic, R.D.; Suidan, M.T.; Brenner, R.C. Oxidative Coupling of Phenols on Activated Carbon: Impact on Adsorption Equilibrium. *Environmental Science & Technology* **1993,** *27* (10), 2079-2085; 10.1021/es00047a013.

Waer, M.A.; Snoeyink, V.L. Effects of Oxidant on Thermal Regeneration of Granular Activated Carbon. *Journal of Environmental Engineering* **1994,** *120* (1), 190-201; 10.1061/(ASCE)0733-9372(1994)120:1(190).

Wang, H.; Jahandar Lashaki, M.; Fayaz, M.; Hashisho, Z.; Philips, J.H.; Anderson, J.E.; Nichols, M. Adsorption and Desorption of Mixtures of Organic Vapors on Beaded Activated Carbon. *Environmental Science & Technology* **2012,** *46* (15), 8341-8350; 10.1021/es3013062.

Wang, Q.; Liang, X.; Zhang, R.; Liu, C.; Liu, X.; Qiao, W.; Zhan, L.; Ling, L. Preparation of Polystyrene-Based Activated Carbon Spheres and Their Adsorption of Dibenzothiophene. *New Carbon Materials* **2009,** *24* (1), 55-60; 10.1016/S1872-5805(08)60036-0.

Wilcox, J. Adsorption, In *Carbon Capture,* Wilcox, J., Ed.; Springer: 2012; pp. 115-175.

Wood, G.O. Affinity Coefficients of the Polanyi/Dubinin Adsorption Isotherm Equations: A Review with Compilations and Correlations. *Carbon* **2001,** *39* (3), 343-356; 10.1016/S0008-6223(00)00128-7.

Xiao, J.; Li, C.; Fang, L.; Böwer, P.; Wark, M.; Bénard, P.; Chahine, R. Machine learning–Based Optimization for Hydrogen Purification Performance of Layered Bed Pressure Swing Adsorption. *International Journal of Energy Research* **2020,** *44* (6), 4475-4492; 10.1002/er.5225.

Xu, B.; Wang, N.; Chen, T.; Li, M. Empirical Evaluation of Rectified Activations in Convolution Network. *CoRR* **2015,** *abs/1505.00853*.

Yonge, D.R.; Keinath, T.M.; Poznanska, K.; Jiang, Z.P. Single-Solute Irreversible Adsorption on Granular Activated Carbon. *Environmental Science & Technology* **1985,** *19* (8), 690-694; 10.1021/es00138a006.

Yun, J.; Choi, D.; Moon, H. Benzene Adsorption and Hot Purge Regeneration in Activated Carbon Beds. *Chemical Engineering Science* **2000,** *55* (23), 5857-5872; 10.1016/S0009-2509(00)00189-5.

Zhang, K.; Zhong, S.; Zhang, H. Predicting Aqueous Adsorption of Organic Compounds onto Biochars, Carbon Nanotubes, Granular Activated Carbons, and Resins with Machine Learning. *Environmental Science & Technology* **2020,** *54* (11), 7008-7018; 10.1021/acs.est.0c02526.

Zhang, Y.; Xu, X. Predictions of Adsorption Energies of Methane-Related Species on Cu-Based Alloys Through Machine Learning. *Machine Learning with Applications* **2021,** *3*, 100010; 10.1016/j.mlwa.2020.100010.

Zhu, L.; Shen, D.; Luo, K.H. A Critical Review on VOCs Adsorption by Different Porous Materials: Species, Mechanisms and Modification Methods. *Journal of Hazardous Materials* **2020,** *389*, 122102; https://doi.org/10.1016/j.jhazmat.2020.122102.

Zhu, X.; Wan, Z.; Tsang, D.C.W.; He, M.; Hou, D.; Su, Z.; Shang, J. Machine Learning for the Selection of Carbon-Based Materials for Tetracycline and Sulfamethoxazole

Adsorption. *Chemical Engineering Journal* **2021,** *406*, 126782; 10.1016/j.cej.2020.126782.

Zhu, X.; Wang, X.; Ok, Y.S. The Application of Machine Learning Methods for Prediction of Metal Sorption onto Biochars. *Journal of Hazardous Materials* **2019,** *378*, 120727; 10.1016/j.jhazmat.2019.06.004.

Appendix A: Supplementary Information for Chapter 4

A.1 DNN architecture

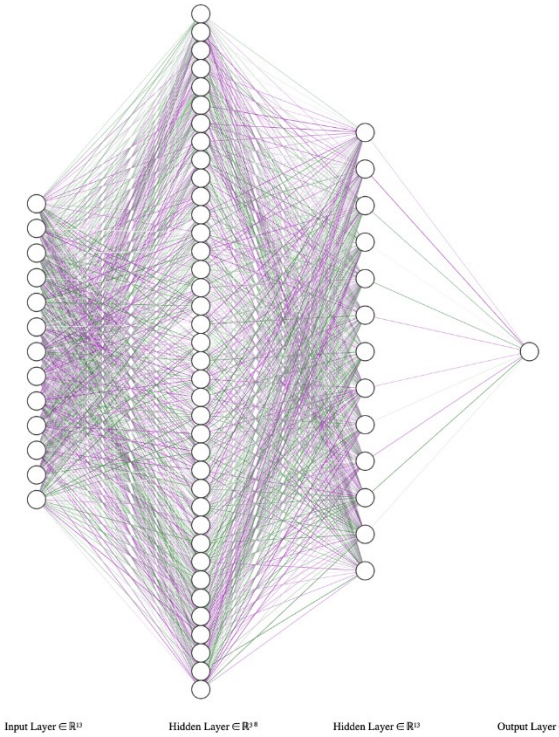

Fig. A-1. Architecture of DNN model used in the study

A.2 Partial dependency plots

The y axis illustrates the difference between predicted heel and what would be predicted at the baseline or leftmost value. Specifically,

Δ Heel (W%) = Heel (W%) (at X = x) – Heel (W%) (at X = x_0)

where x can be any value within the feature domain and x_0 is the minimum observed value of that feature in data set. For example, as shown in Fig S.3, Δ Heel at T = 300 °C is about 0.2 W%

which means that by increasing the temperature from $X=x_0$ = 200 °C to X = 300 °C, 0.2 W% increase in average cyclic heel buildup would be expected.

The blue shaded area indicates confidence level. Hence, greater shaded area represents larger uncertainty in the reported average value.

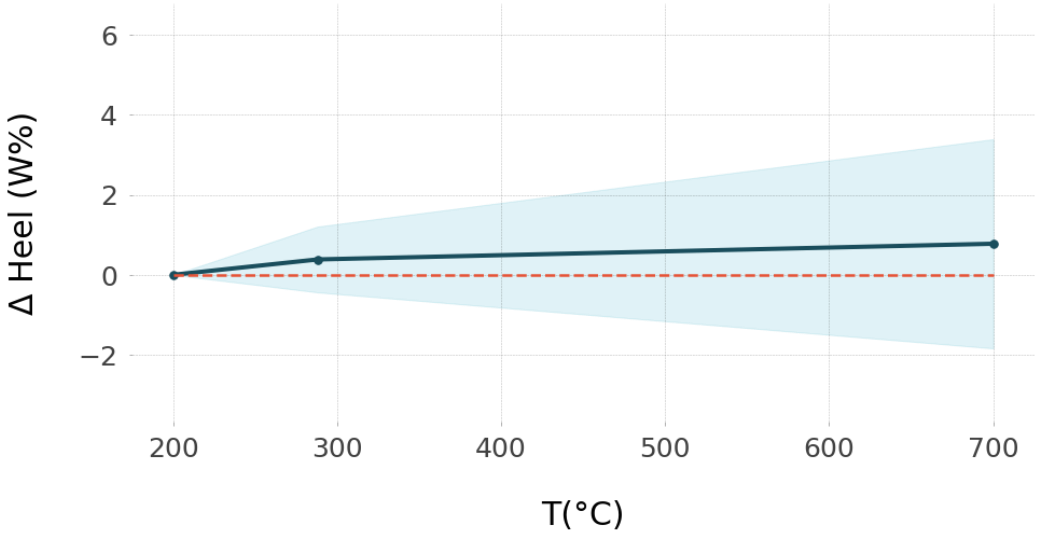

Fig. A-2. Heel partial dependency on regeneration temperature (°C)

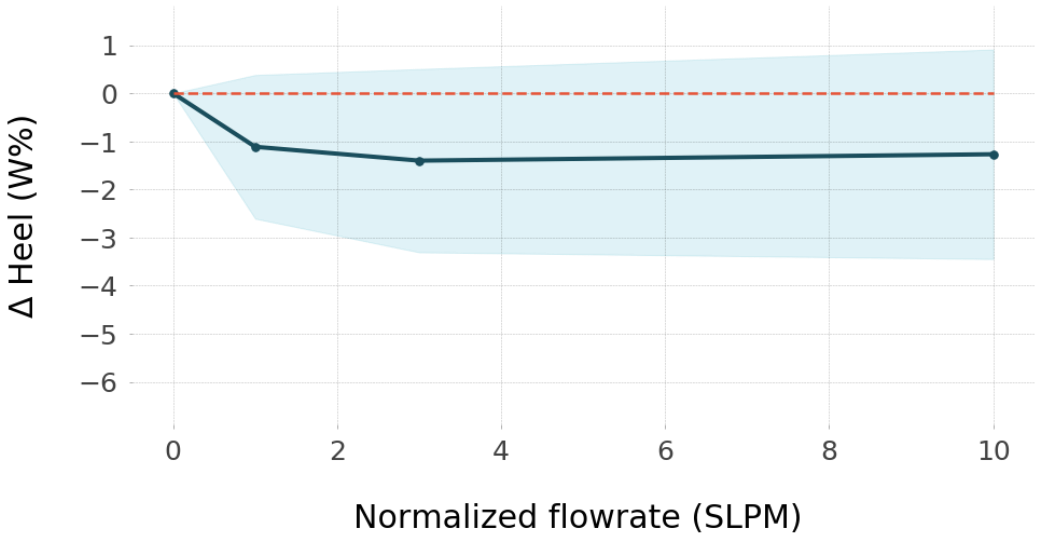

Fig. A-3. Heel partial dependency on purge gas normalized flow rate (SLPM)

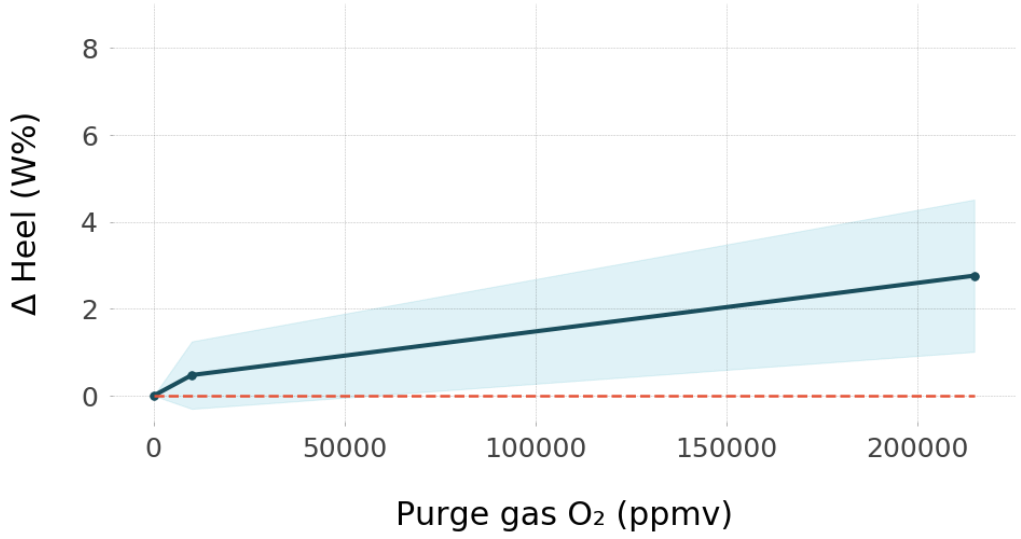

Fig. A-4. Heel partial dependency on purge gas oxygen content (ppmv)

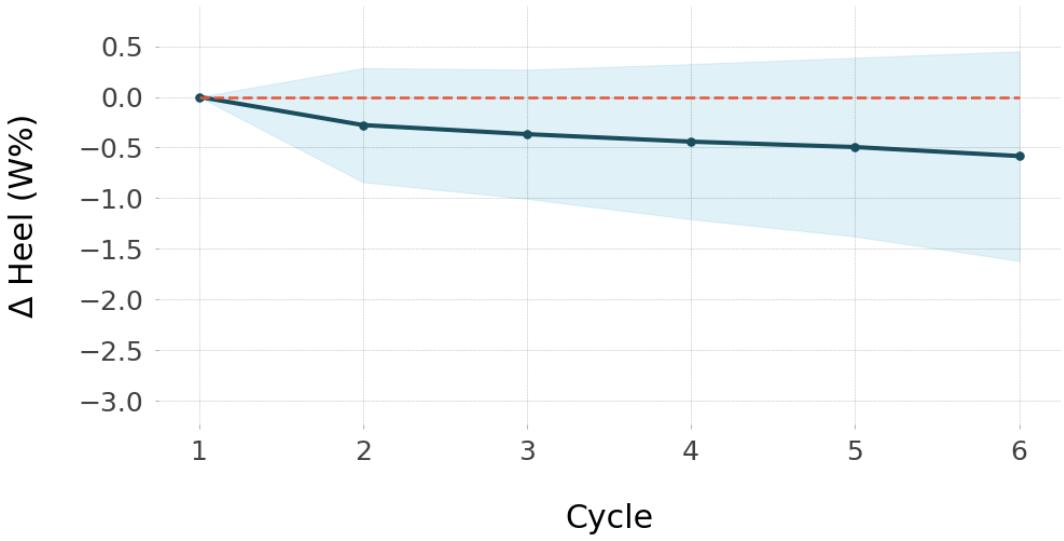

Fig. A-5. Heel partial dependency on cycle number

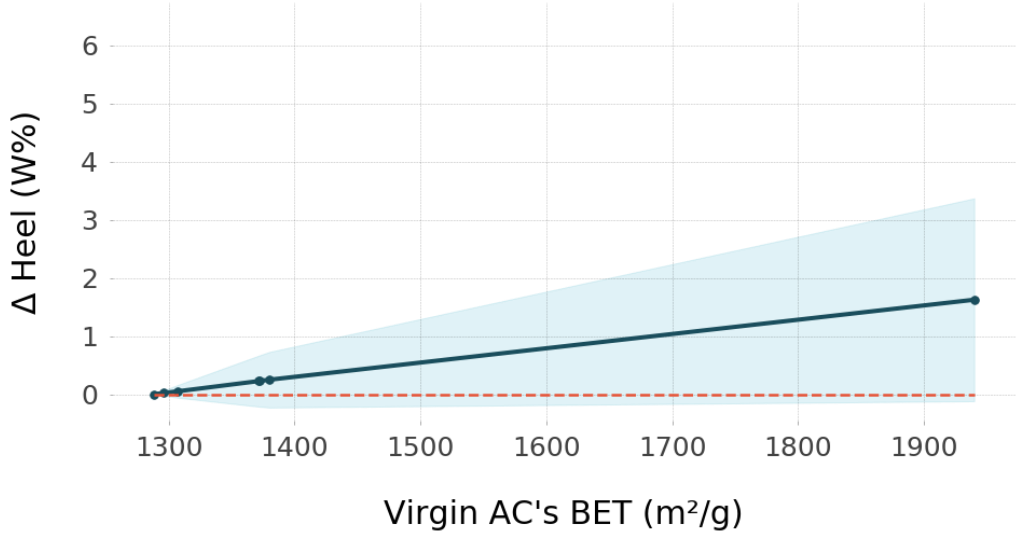

Fig. A-6. Heel partial dependency on virgin activated carbon's BET surface area ($\frac{m^2}{g}$)

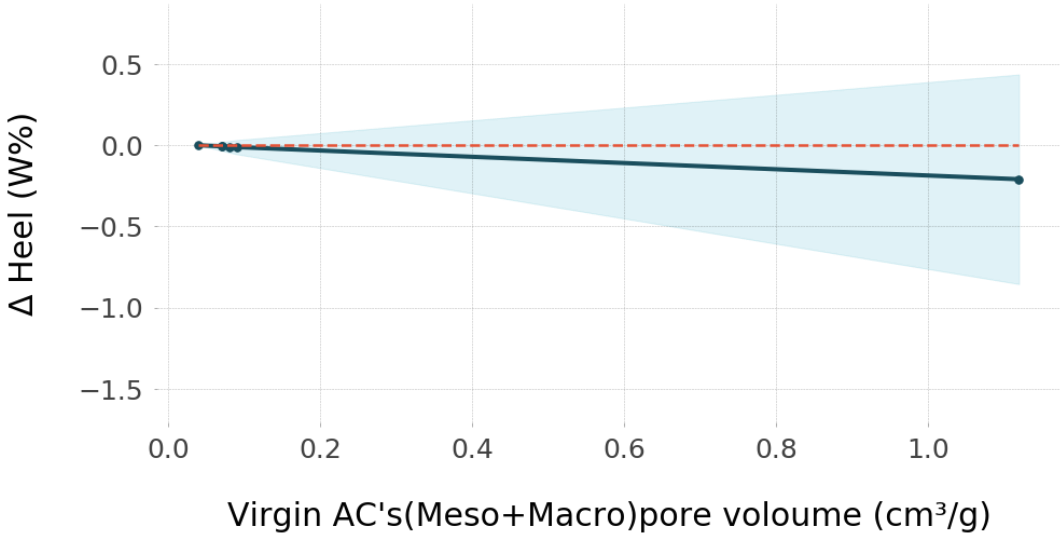

Fig. A-7. Heel partial dependency on virgin activated carbon's "mesoo+macro" pore volume ($\frac{cm^3}{g}$).

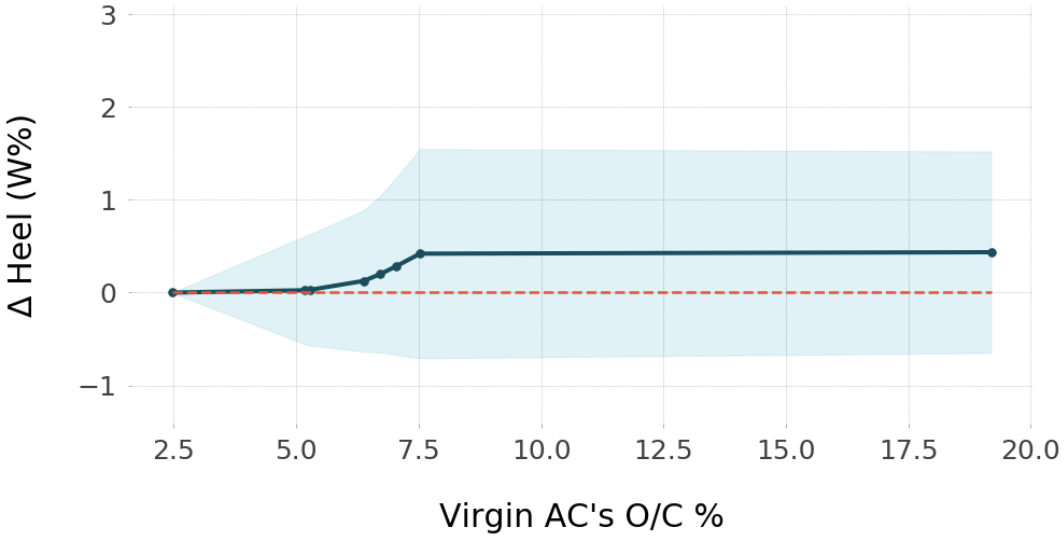

Fig. A-8. Heel partial dependency on virgin activated carbon's O/C %

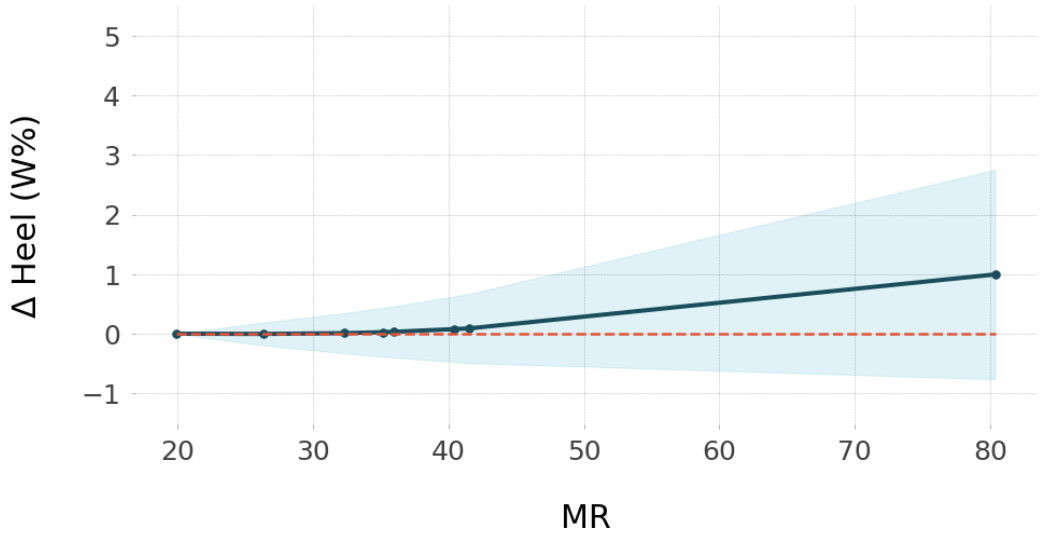

Fig. A-9. Heel partial dependency on adsorbate's molar refraction (MR, $\frac{cm^3}{mol}$)

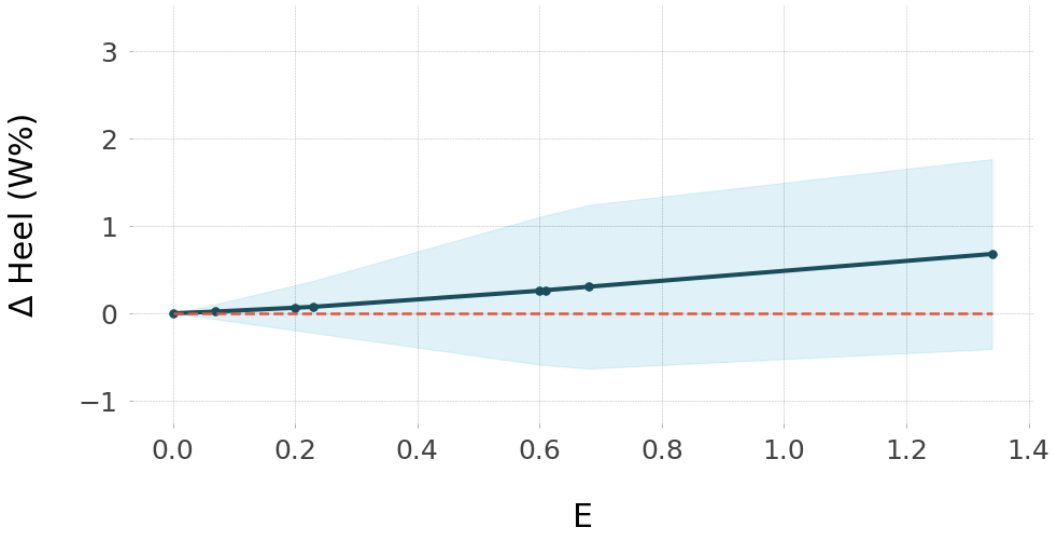

Fig. A-10. Heel partial dependency on adsorbate's excessive molar refraction (E, $\frac{cm^3}{10\times mol}$)

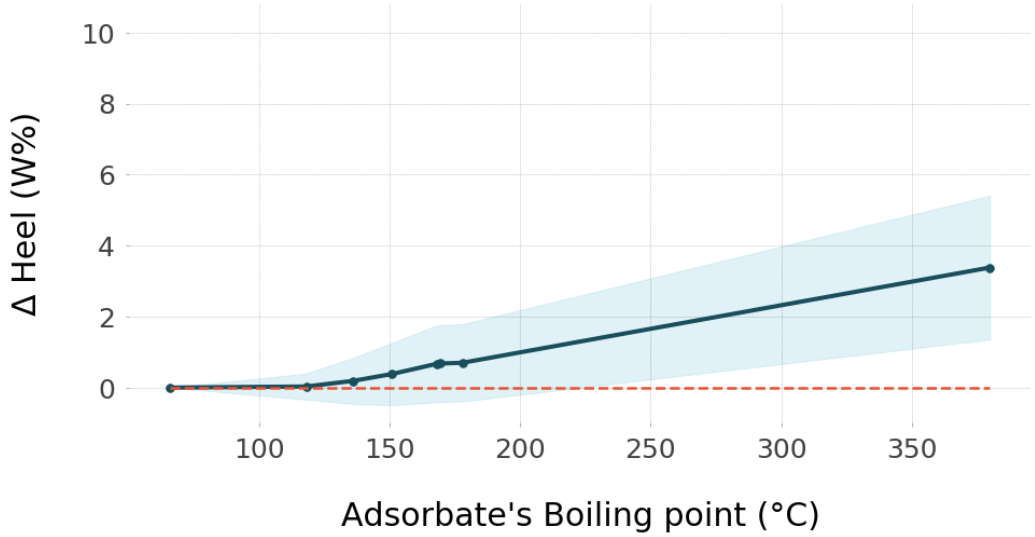

Fig. A-11. Heel partial dependency on adsorbate's boiling point (°C)

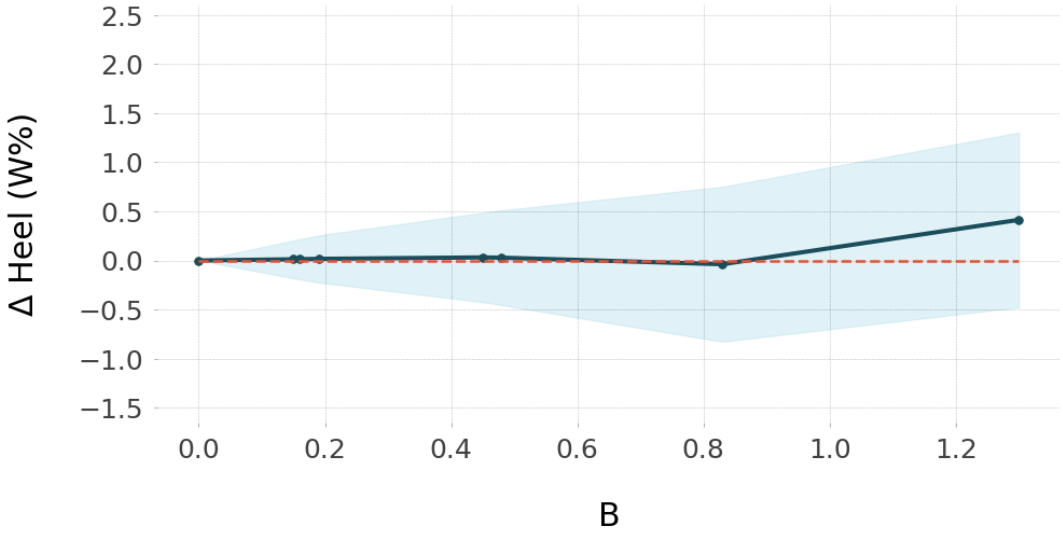

Fig. A-12. Heel partial dependency on adsorbate's effective H-bonding basicity (B)

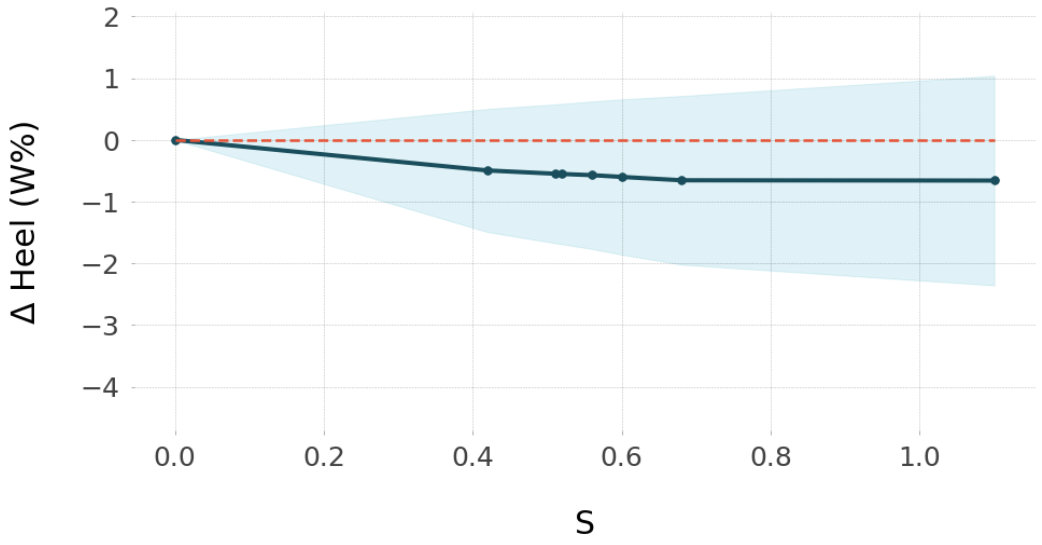

Fig. A-13. Heel partial dependency on adsorbate's dipolarity/polarizability (S)

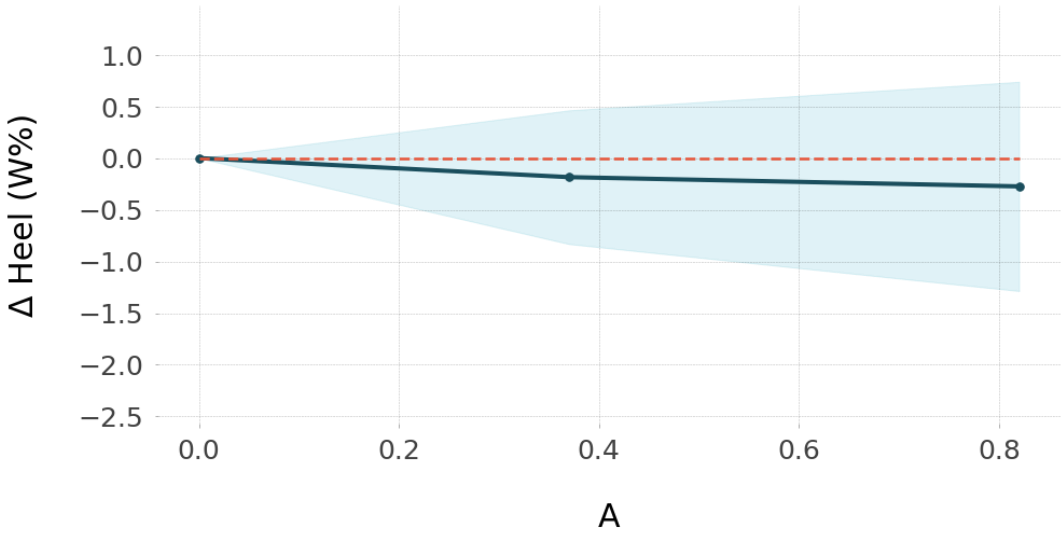

Fig. A-14. Heel partial dependency on adsorbate's effective H-bonding acidity (A)